



Technische Universität München  
Fakultät für Chemie

# **Visualization of structural intermediates in an E3-E3 ligase ubiquitylation cascade via cryo-EM**

Daniel Horn-Ghetko

Vollständiger Abdruck der von der Fakultät für Chemie der Technischen Universität München zur Erlangung des akademischen Grades eines Doktors der Naturwissenschaften (Dr. rer. nat.) genehmigten Dissertation.

Vorsitzender: Prof. Dr. Matthias Feige

Prüferinnen der Dissertation: 1. Hon.- Prof. Brenda Schulman, Ph.D.

2. Prof. Dr. Cathleen Zeymer

3. Prof. Dr. Kathrin Lang

Die Dissertation wurde am 26.01.2022 bei der Technischen Universität München eingereicht und durch die Fakultät für Chemie am 28.04.2022 angenommen.



# Acknowledgements

First and foremost, I would like to thank Brenda for the opportunity to conduct my PhD research in her laboratory. I could not have imagined what great journey I would be going through. You are a wonderful mentor and I could not have wished for a better person to guide me through my PhD. Thank you for lifting my spirits up in bad times and teaching me how even the tiniest little details can make a big difference in science. I had a wonderful time here and am very thankful for all the good memories I could make.

Sebi, if I would need to describe the perfect colleague it certainly is be you! You are one of the most generous persons I have ever met. You are a hard worker and always up for fun. Thank you for all the great times we had - I will always remember the football game against the Contis, in which we scored this amazing goal with combined efforts. I also very much enjoyed the last part of our PhDs, in which we worked together on several projects and had the best time ever. However, the one good thing about you leaving is that my pipettes will stay on my bench!

Big thanks to Asia, Ishita and Laura for all the fun we had inside and outside of the lab. Shout-out to Ishi for having an amazing husband and introducing him to me! Your wonderful wedding in India was one the highlights of my PhD even though Sebi, Margot and me got lost in the New Delhi military area.

Rajan, thank you for your endless help and effort when it came to processing the cryo-EM data or building the awfully complicated three-way crosslinks. I also enjoyed every little chat we had throughout the course of the time.

Josie and Jiale, you two are such kind and positive human beings. It is always a pleasure to be around you and talk with you about anything.

Dawa, Jakub and Linus, thank you for being always up to help and discuss scientific ideas and results.

Khee, we had a great time when things got started in the lab. In hindsight, it was fun to struggle with the scope and samples together. Thank you for getting this project and me on track.

Sepp, du bist eine Marke für sich und ohne dich würde hier im Labor nichts laufen. Danke für all den Einsatz, den du jeden Tag zeigst- dieser ist ganz und gar nicht selbstverständlich.

Gary, thank you so much for making this piece of work so much better with your amazing skills. I thrived from the scientific discussions we had when you were or weren't here. Cheers, bud!

To all the technicians in the lab- you are wonderful people and your work made my daily lab life so much easier. Thank you for all your efforts- Susanne, Maren, Judith, Ronald, Viola, Susanne and Sabine.

Thanks to Arno for the wonderful scientific discussions we had and the curiosity you show for all projects that are going on.

David, Randy, Kirby, Danny- You guys are scientists by heart and have taught me so much about many different aspects of science. Thank you for that.

To all other new and old people from the lab- thank you for being a great bunch of people!

Shout-out to the amazing facility services at the MPI, especially Daniel Bollschweiler and Tillman Schäfer for doing an excellent job at the Cryo-EM facility and Stefan Pettera who has synthesized a bucket load of great peptides for me.

Natürlich möchte ich auch meiner Familie für Ihre unendliche und unerschöpfbare Unterstützung danken. Ich könnte mir keine bessere Familie vorstellen und ich bin extrem dankbar, dass es euch gibt. Ich liebe euch!

Das Beste kommt wie immer zum Schluss: Lea, du hast mich durch deine unglaubliche Energie und Liebe zu mir extrem unterstützt - auch wenn du das nicht wahrhaben willst. Ich bin sehr dankbar, dass du ein großer Teil meines Lebens bist und freue mich auf alles was da kommen mag.

# Table of Contents

<b>LIST OF PUBLICATIONS</b>	9
<b>ABSTRACT</b>	10
<b>ZUSAMMENFASSUNG</b>	11
<b>CHAPTER 1 – Introduction</b>	
1.1 Ubiquitin	13
1.1.2 Deubiquitinases	15
1.1.3 Post-translational modifications of ubiquitin	16
1.1.4 Ubiquitin-like proteins	17
1.2 Ubiquitin E3 ligases	17
1.2.1 HECT E3 ligases	19
1.2.2 RING E3 ligases	20
1.2.2.1 Cullin-RING E3 ligases	21
1.2.3 RBR E3 ligases	23
1.2.3.1 ARIH1	24
1.2.4 RCR E3 ligase MYCBP2	25
1.2.5 RZ-finger E3 ligase RNF213	26
1.2.6 CRL-RBR E3-E3 ligases	27
1.3 Activity-based probes	29
1.4 Strategy to stabilize and visualize ubiquitin transfer intermediates of the E3-E3 ubiquitylation mechanism	30
<b>CHAPTER 2 – A suite of activity-based probes to conquer the structures and concerted mechanism of the RBR E3 ligase ARIH1 and the RING E3 CUL1-RBX1</b>	
2.1 Generation of a TS1 activity-based probe to stably mimic ubiquitin transfer from E2 to E3	34
2.1.1 Verification and comparison of native CRL-RBR E3-E3 reaction requirements with TS1 ABP conjugation	36
2.2 Generation of an activity-based probe to stably mimic ubiquitin transfer from E3-E3 to F-box protein-bound substrate	37
2.2.1 Verification and comparison of native CRL-RBR E3-E3 reaction requirements with TS2 ABP conjugation	39

## **CHAPTER 3 – Cryo-EM studies of chemically stabilized Transition State 1 and intermediates enable new insights into transfer from E2 to E3-E3 superassembly**

3.1 Cryo-EM sample preparation & processing	42
3.2 Cryo-EM structure of Transition State 1- transfer of ubiquitin from E2 to E3-E3	43
3.2.1 Formation of an E3-E3 <sup>act</sup> superdomain is the basis for Ubiquitin transfer by the E3 duo	45
3.2.2 Transfer of Ubiquitin from E2 to E3-E3 depends on release of autoinhibition by NEDD8 and RBX1	46
3.3 Cryo-EM structures of Transition State 1 intermediates	48

## **CHAPTER 4 – Cryo-EM of chemically stabilized Transition State 2 and biochemical assays reveal mechanism for E3-E3-catalyzed ubiquitylation of SCF substrates**

4.1 Cryo-EM structures of Transition State 2	52
4.1.1 Ubiquitin transfer from E3-E3 to substrate involves relocation of the ubiquitin transferase module	52
4.1.2 Other SCF systems	54
4.1.3 Cryo-EM structures of a Transition State 2 intermediate	56
4.2 Determination of kinetic ubiquitylation parameters and comparison to the E2-E3 mechanism	57
4.3 Comparison of ARIH1-CRL1 and ARIH2-CRL5 E3-E3s	58

## **CHAPTER 5 – Discussion**

5.1 A suite of ABPs to tackle structural endeavors and open up new routes	60
5.2 Structural insights and principles of the E3-E3 ubiquitylation cascade.	61
5.3 Generalizable Cullin-RING ligase substrate specificity	63
5.4 New and old paradigms for E3 ligase mechanism	64
5.5 Future perspectives	65

## **CHAPTER 6 – Material & Methods**

6.1 Material	
6.1.1 DNA - Primers & Plasmids	67
6.1.2 Experimental models- Organisms & Strains	68
6.1.3 Buffers	69
6.1.4 Media & Antibiotics	71
6.1.5 Peptides	72

6.2 Methods	
6.2.1 Molecular biology	73
6.2.1.1 DNA isolation & purification	73
6.2.1.2 Cloning	73
6.2.1.3 Transformation of Chemo-competent <i>E. coli</i>	74
6.2.2 Protein expression & purification	
6.2.2.1 Protein expression in <i>E. coli</i>	75
6.2.2.2 Protein expression in insect cells	75
6.2.2.3 Protein purification	76
6.2.2.4 Ubiquitin-MESNa purification	76
6.2.3 Generation of activity-based probes	
6.2.3.1 Generation of a Transition State 1 ABP	77
6.2.3.2 Formation of an unreacted UBE2L3-ABP	77
6.2.3.3 Conjugation of ubiquitin to UBE2L3	78
6.2.3.4 Generation of UbVME	78
6.2.3.5 Generation of TS2 ABPs	78
6.2.4 Biochemical assays	
6.2.4.1 Pulse-chase assays	79
6.2.4.2 TS1 UBE2L3-ABP assays	80
6.2.4.3 TS2 ABP assays	81
6.2.5 Enzyme kinetics	
6.2.5.1 Rapid-quench flow kinetics to dissect the E3-E3 ubiquitin transfer mechanism	80
6.2.5.2 Estimating the $K_m$ of ARIH1 and UBE2D for various SCF-substrate complexes	81
6.2.5.3 Estimating the rate of ubiquitin transfer ( $k_{obs}$ ) from ARIH1 and UBE2D to substrate	82
6.2.6 Cryo-EM	
6.2.6.1 Sample preparation	83
6.2.6.2 Data collection	83
6.2.6.3 Data processing	84
6.2.6.4 Model building	84
References	85
Abbreviations	94
Appendix	98

## List of publications

Parts of this thesis were published as follows:

### Research articles (peer reviewed):

**Horn-Ghetko, D.**, Krist, D.T., Prabu, J.R., Baek, K., Mulder, M.P.C., Kluegel, M., Scott, D.C., Ovaa, H., Kleiger, G., Schulman, B.A. Ubiquitin ligation to F-box protein targets by SCF–RBR E3–E3 super-assembly. *Nature* **590**, 671–676 (2021).

Kostrhon, S., Prabu, J.R., Baek, K., **Horn-Ghetko, D.**, von Gronau, S., Kluegel, M., Basquin, J., Alpi, A.F., Schulman, B.A. CUL5-ARIH2 E3-E3 ubiquitin ligase structure reveals cullin-specific NEDD8 activation. *Nature Chemical Biology* **17**, 1075–1083 (2021).

### Review article (peer reviewed):

**Horn-Ghetko, D.**, Schulman, B.A. New classes of E3 ligases illuminated by chemical probes. *Current Opinion in Structural Biology* **73**, (2022)

## Abstract

Immense eukaryotic cellular regulation depends on E3 ligase-catalyzed ubiquitylation of proteins. E3 ligases are molecular machines able to covalently attach the 76-amino acid small protein ubiquitin onto target substrates, thereby signaling for a multitude of cellular outcomes such as their proteasomal degradation. The majority of E3 ligases are bearing hallmark domains, such as HECTs and RINGs, which specifies their ubiquitylation mechanism and consequently enables their categorization. However, NEDD8-activated cullin-RING-type and ARIH-family RBR-type E3s, coordinately ubiquitylate substrates in E1-E2-E3-E3 tetra-enzymatic pathways. The cooperative effort of these two E3 ligase families is essential for the homeostasis of a plethora of substrates in virtually every cellular pathway.

Here, through development of activity-based chemical probes generating stable mimics of fleeting E3-E3 transition states, we report cryo-EM structures visualizing the catalytic configurations of the multistep E3-E3 ubiquitylation cascades. Extraordinary structural remodeling accompanies amalgamation of the two different types of E3s into a singular E3-E3 ligase that switches between radically different catalytic configurations mediating stepwise E3-E3 ubiquitylation. Studying several distinct CRLs in the SKP1-CUL1-Fbox family and their different F-box protein-bound substrates (SCF<sup>SKP2</sup> with substrate p27, SCF<sup>FBXW7</sup> with its substrate Cyclin E and SCF<sup>β-TRCP</sup> with substrate IκBα) showed common catalytic assemblies, irrespective of the identity of the F-box protein-substrate pairing. Our data establish fundamental principles whereby two distinctive E3 types unite for specific substrate ubiquitylation and demonstrate how the autoinhibited RBR E3 is activated to receive ubiquitin. Additionally, we propose that the mechanism of the neddylated SCF/ARIH1 E3-E3 assembly is perfectly suitable for the ubiquitylation of the vast amount of substrate receptor shapes and sizes that are defining features of the mix-and-match cullin-RING ligase system. Taken together with previous structures showing the inactive individual E3s, the structures suggest how neddylated SCF/ARIH1 ubiquitylation succeeds stepwise- with ubiquitin progressively changing its C-terminal linkage, starting its cycle at the E2 enzyme UBE2L3 and ending it at the SCF substrate's lysine.

# Zusammenfassung

Ein enormer Anteil eukaryotischer, zellulärer Regulation unterliegt der E3 Ligase-katalysierten Ubiquitylierung von Proteinen. E3 Ligasen sind molekulare Maschinen, die Zielsubstrate kovalent mit dem 76-Aminosäuren kleinen Protein Ubiquitin verknüpfen und damit das Signal für eine Vielzahl an zellulären Ausgängen, wie zum Beispiel deren proteosomalen Abbau, setzen. Ein Großteil der E3 Ligasen besitzt kennzeichnende Domänen, wie HECTs oder RINGs, die den Mechanismus der Ubiquitylierung bestimmen und daher ihre Kategorisierung ermöglichen. NEDD8-aktivierte Cullin-RING und die zur Ariadne-Familie zugehörigen RBR E3 Ligasen, ubiquitylieren Substrate in vierfach-enzymatischen Reaktionsketten. Der kooperative Einsatz dieser zwei E3 Ligase Familien ist essentiell für das physiologische Gleichgewicht von einer Fülle an Substraten in praktisch jedem Signalweg.

Durch die Entwicklung von Aktivitäts-basierten chemischen Sonden, die stabile Nachahmungen von sonst schnellen Übergangszuständen generieren, berichten wir hier von Cryo-EM Strukturen, die katalytische Konfigurationen der mehrschrittigen E3-E3 Ubiquitylierung visualisieren. Eine außergewöhnliche Umstrukturierung wird dabei begleitet von einer Verschmelzung der beiden E3 Ligasen in eine einzige E3-E3 Einheit, die zwischen radikal unterschiedlichen, katalytischen Konformationen wechselt. Die Untersuchung von mehreren unterschiedlichen Cullin-RING-Ligasen in der **SKP1-CUL1-F**box Familie und deren Substrate (SCF<sup>SKP2</sup> mit dem Substrat p27, SCF<sup>FBXW7</sup> mit dem Substrat Cyclin E und SCF<sup>β-TRCP</sup> mit dem Substrat IκBα) ergab übereinstimmende katalytische Konformationen unabhängig von der Identität des Substratrezeptor-Substrat Paares. Unseren Daten etablieren fundamentale Prinzipien bei der Zusammenarbeit von zwei unterschiedlichen E3 Ligasen und demonstrieren wie die RBR E3 Ligase aktiviert wird um Ubiquitin annehmen zu können.

Zusätzlich schlagen wir vor, dass die strukturellen Prinzipien der zwei E3 Ligasen perfekt für die Vielzahl an Formen und Größen der Substratrezeptoren gemacht ist, die das Kennzeichen von Cullin-RING Ligasen sind. Zusammengenommen mit den bestehenden Strukturen der inaktiven E3 Ligasen lassen unsere Strukturen auf einen kompletten Kreislauf der Ubiquitylierung schließen, in welchem sich die C-terminale Verlinkung Ubiquitins ständig ändert, beginnend mit dem E2 Enzym UBE2L3 und endend an dem Lysin des Substrates.

# Chapter 1 – Introduction

How 76 amino acids dictate the cellular fate of thousands of proteins in eukaryotic cells.

In this chapter, parts of the following publications were integrated:

**Horn-Ghetko, D.**, Schulman, B.A. New classes of E3 ligases illuminated by chemical probes. *Current Opinion in Structural Biology* (accepted January 2022).

**Horn-Ghetko, D.**, Krist, D.T., Prabu, J.R., Baek, K., Mulder, M.P.C., Kluegel, M., Scott, D.C., Ovaa, H., Kleiger, G., Schulman, B.A. Ubiquitin ligation to F-box protein targets by SCF–RBR E3–E3 super-assembly. *Nature* **590**, 671–676 (2021).

Display items and text were reprinted with permission from Springer Nature and Elsevier.

# 1. Introduction

The human genome is predicted to encode for only around 21,000 proteins[15]. Even though modification on DNA and RNA level with events like alternative splicing are adding variety to the pool of proteins, the real spice in the soup of life stems from post-translational modifications (PTMs). There are hundreds of post-translational modifications, each with its distinct chemical properties[16]. After proteins are synthesized by the ribosome, PTMs are covalently attached to a multitude of sites on them. Among the many types of post-translation modifications, one of them steals the show- because it does not include substrate modification with a single functional group but rather a whole protein.

## 1.1 Ubiquitin

*Ubique (Latin) – everywhere.* The 76-amino acid small protein ubiquitin lives up to its name as it is found in all eukaryotes and regulates almost every intracellular process- it is ubiquitous. Ubiquitin is one of the most stable proteins and adopts its characteristic beta-grasp fold terminated by a flexible, six amino acid long C-terminal tail[17]. This tail can be covalently attached to several residues on proteins: serine, threonine, cysteine and lysine- the latter representing the most frequent location of attachment[18]. In recent years, new types of ubiquitin modification have been uncovered, which include the ubiquitylation of the free, N-terminal  $\alpha$ -amino groups in proteins as well as hydroxyl groups of sugars or sugar-modified lipids[13,19,20]. Ubiquitin can also serve as its own substrate- targeting one out of seven lysine residues (K6, K11, K27, K29, K33, K48, K63) generates polyubiquitin chains with a variety of topologies. These chains can contain more than ten ubiquitin molecules and are either linked via the same residue to obtain homogenous chains or connected on alternating residues to generate branched chains. The complexity of this system is often referred as the “ubiquitin code”[21,22].

The complexity is undermined by the fact that more than 1000 proteins control the ubiquitylation process in human cells[23-25]. Ubiquitylation requires a three-step catalytic cascade: activation, conjugation and ligation. In the first step ubiquitin is activated in an ATP-dependent two-step reaction by the E1 ubiquitin-activating enzyme. This reaction yields a thioester-linked ubiquitin-E1 intermediate.

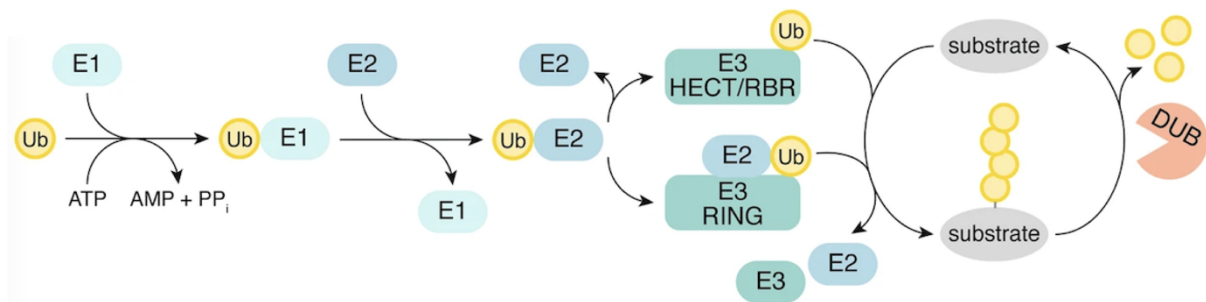


**Figure 1 – The ubiquitin cascade.** In human cells, two E1 ubiquitin-activating enzymes (UBA1 and UBA6) catalyze the transfer of ubiquitin to ~40 E2 ubiquitin-conjugating enzymes solely dedicated to ubiquitin. These E2 enzymes then transfer ubiquitin to over 600 E3 ubiquitin-ligating enzymes. E3 ligases modify their specific substrates with ubiquitin and/or ubiquitin chains, which then- in the case of K48-linked ubiquitin chains signals for their degradation via the 26S proteasome. Deubiquitylating enzymes are able to antagonize E3 activity by cleaving of ubiquitin from substrates. *Adapted from and reprinted by permission from Springer Nature: Damgaard, R.B. The ubiquitin system: from cell signalling to disease biology and new therapeutic opportunities. Cell Death Differ 28, 423–426 (2021).*

Through trans-thioesterification, ubiquitin is then attached to yet another catalytic cysteine in the active center of an E2 ubiquitin-conjugating enzyme, forming another covalent enzyme-ubiquitin complex. E3 ubiquitin ligases then ultimately mediate the generation of an isopeptide bond between ubiquitin’s C-terminal glycine and the substrate’s lysine  $\epsilon$ -amino group. Once attached to a protein, ubiquitin is able to alter its cellular location, change structure and function or mediate binding to ubiquitin-binding domain (UBD)-bearing proteins[26,27].

Decryption of the ubiquitin code into signals by UBD-containing proteins, also referred as “readers”, is most often determined by the type of ubiquitin chains. Some chain types preferentially signal for one outcome, while others have multiple ones. K48-linked ubiquitin chains on proteins signal for their proteolytic degradation via the 26S proteasome, which displays high affinity towards K48-linked chains with four or more ubiquitin building blocks[28-30]. Another function of K48-linked chains is their association with the AAA+ ATPase p97, which has an important role in the Endoplasmic reticulum-associated degradation (ERAD). Hereby, p97 recognizes polyubiquitinated (K11- or K48-linked), misfolded ERAD substrates and dislocates them to the cytosol in an ATP-driven manner where substrates can be subjected to the degradation via the proteasome[31,32]. The second most abundant chain type are K63-linked chains and -together with K48-linked chains - account for up to 80% of total

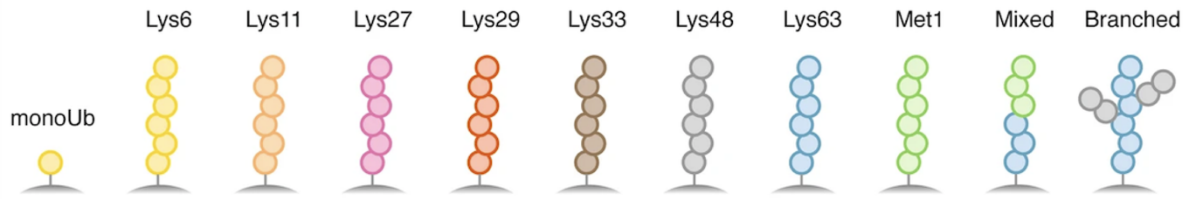


**Figure 2 – The ubiquitin code.** Cartoon representing the possible linkage types of ubiquitin. In addition to the two canonical ubiquitin chain types (K48 and K63), six atypical (M1, K6, K11, K27, K29, K33) chains types can be assembled. Further diversification of the ubiquitin code is achieved with mixed or branched ubiquitin chains. *Adapted from and reprinted by permission from Springer Nature: Damgaard, R.B. The ubiquitin system: from cell signalling to disease biology and new therapeutic opportunities. Cell Death Differ 28, 423–426 (2021).*

linkages in mammalian cells[33]. The function of K63-linked chains has been extensively studied and predominantly serves for inflammatory signaling and consequent NF- $\kappa$ B activation[34]. In this signaling pathway, K63-linked chains are mixed up with Linear Ubiquitin Chain Assembly Complex (LUBAC)-generated M1-linked ubiquitin chains to activate kinase complexes[35]. M1- along with K6, K11, K27, K29 and K33-linked chains are categorized as atypical ubiquitin chains. With the advent of tools to specifically study ubiquitin chains, highly linkage-specific enzymes and their signaling pathways have been uncovered. For example, the heterodimeric BRCA1/BARD1 RING E3 ligase assembles K6-linked chains on a variety of substrates. It is best characterized for its function to promote homologous recombination in order to repair double-stranded breaks in DNA[36-38]. Another linkage type comes into play upon DNA damage- K27-linked chains. Here, RNF168 was characterized to assemble K27-linked chains upon DNA damage, which act as a platform to recruit DNA damage repair enzymes[39].

### 1.1.2 Deubiquitinases

Deubiquitinases (DUBs) are able to break the isopeptide linkage between ubiquitin and its substrates or disassemble polyubiquitin chains. Thus, DUBs are regulating the abundance of ubiquitin substrates by preventing proteasomal degradation or reverse other outcomes of ubiquitylation. The approximately 100 deubiquitinases in human cells are categorized into seven major classes[40]. Four of the seven classes employ an active site cysteine (Cys<sup>cat</sup>), similarly to E3 ligases. Ubiquitin C-terminal hydrolases (UCHs), ubiquitin specific proteases (USPs), ovarian tumor proteases (OTUs) and

Machado-Joseph Domain (Josephin domain)-containing proteins (MJD) are able to sever the isopeptide bond with a nucleophilic attack of the active site cysteine. The other three classes of DUBs consist of the JAB1/MPN domain-associated metalloproteases and two more recently discovered families including the Motif interacting with Ubiquitin (MIU)-containing DUB family MINDY, and the zinc finger with UFM1-specific peptidase domain-containing ZUFSP family[41]. All DUBs bear minimally one ubiquitin binding domain, the S1 site. The S1 site acts as ubiquitin binding platform to orchestrate its C-terminal cleavage by positioning the C-terminus into the DUB active site. Many DUBs are linkage-specific as exemplified by the K63-specific JAMM metalloprotease or the K48-specific MINDY DUB family[42,43].

### 1.1.3 Post-translation modifications of Ubiquitin

Ubiquitin demonstrates its versatility by employing several patches on its surface to interact with UBD-containing proteins, whether it serves as reader or eraser. Its most frequently contacted interaction site is the hydrophobic patch centered around Ile44, especially utilized by the proteasome and UBDs[44]. The hydrophobic patch centered around Ile36 is important for interaction between ubiquitin in chains and recognition by UBDs and HECT E3 ligases. Other interaction sites include the TEK box (K6, K11, Thr12, Thr14, Glu34) and the Phe4 patch[21]. The most important residues in Ubiquitin include the seven lysines to assemble ubiquitin chains as discussed in the previous chapter. These lysines and other residues such as Ser65 can be targets of other post-translational modification to create a vast amount of possible ubiquitin and ubiquitin chain variations in addition to the canonical and non-canonical types of ubiquitylation[45]. Six out of seven lysines residues on ubiquitin can be targets of acetylation. Acetylation can have a widespread impact as it not only counteracts ubiquitylation to stabilize proteins such as Histone2B in cells but also possibly prevents ubiquitin chain formation[45]. One of the most prominent non-protein post-translational modifications on ubiquitin is the phosphorylation of Ser65 by the PTEN-induced kinase1, which will be discussed in context in the RBR E3 ligase Parkin[46-49]. Most intriguingly, ubiquitin is not only able to mixed and branched chains with itself but with ubiquitin-like proteins (Ubls), too.

### 1.1.4 Ubiquitin-like proteins

Ubiquitin-like proteins are ubiquitin twins with some of them more identical than others. Structurally, they are adopting the same beta-grasp fold and are also able to act as molecular tag, albeit with their very own cascading machinery. While displaying the same architecture, some Ubls like NEDD8 contain around 60% sequence identity. There are approximately 12 Ubls namely NEDD8, SUMO1/2/3, ISG15, FAT10, MNSF $\beta$ , ATG8/12, URM1 and HUB1[50]. Many of them like FAT10 and MNSF $\beta$  are poorly studied and their function remains elusive. SUMOylation and its conjugation machinery, however, is well explored and regulates many DNA-dependent pathways including transcription, DNA repair and chromatin remodeling[51]. Consequently, SUMO substrates are mainly found in the nucleus with rare exceptions in other compartments of the cell. One prominent SUMO1 substrate is the Ran GTPase-activating protein, that binds to RanBP2 with increased affinity after it is sumoylated[52].[51,53] Another Ubl, Interferon-stimulated gene 15 (ISG15), is expressed after stimulation by type I interferons and plays a key role in the host defense by targeting proteins of invading pathogens[54].

## 1.2 Ubiquitin E3 ligases

Coming back to the key players of the ubiquitin system - E3 ligases. With their vast number, E3 ligases add specificity to the system by determining the final destination of ubiquitin- the E3 substrates. E3s ordinarily use one of two major mechanisms to ligate Ub to the target/substrate and are classified based on their hallmark domains. Members of the RING E3 ligase family (**R**eally **I**nteresting **N**ew **G**ene) comprise the largest E3 family, and function by bridging an activated E2~Ubl intermediate and a target. RING E3s promote Ubl transfer directly from the E2 Cys<sup>cat</sup> to a primary amino group on the target protein, which could also be one of seven lysines or the N-terminus of Ub itself[55]. RING E3s have a protein interaction domain or subunit that recruits substrates for Ub/Ubl modification, and a zinc-binding RING domain that catalyzes Ub ligation without donating any residues directly to the ligation active site. Instead, a RING domain binds both E2 and Ub distal from the thioester linkage between them, and aligns the E2~Ub intermediate to strain the thioester bond for nucleophilic attack. Other E3s, such as members of the HECT (**H**omologous to **E**6AP **C**-Terminus) or RBR families (**R**ING1-**I**BR-**R**cat), function via a two-step mechanism involving an E3

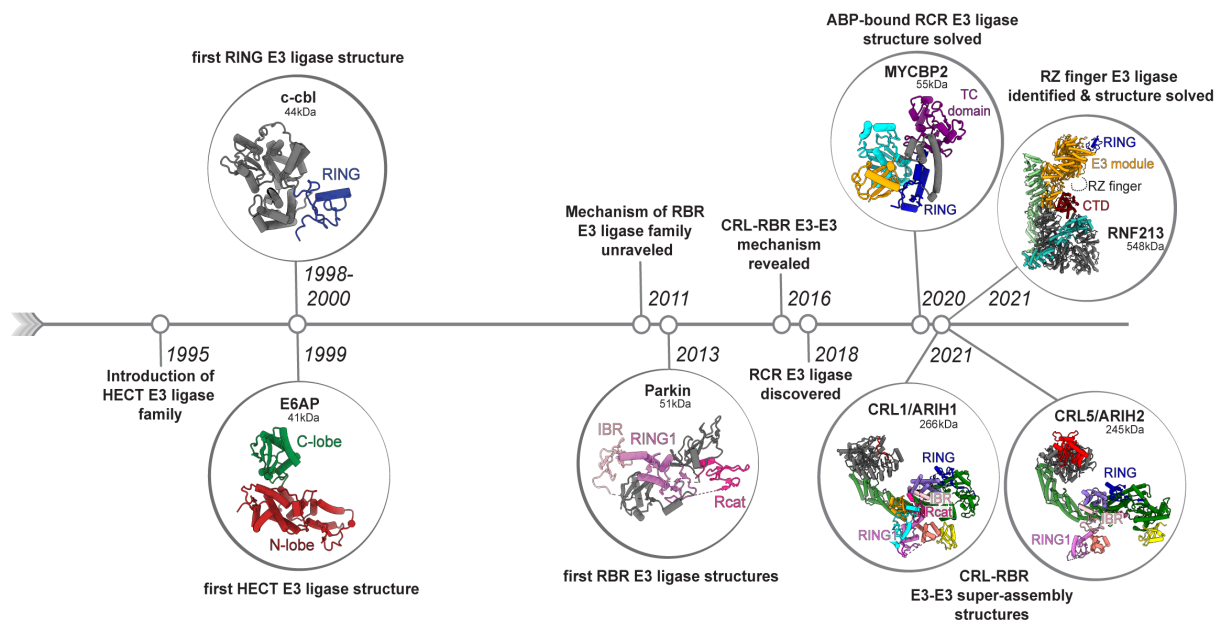


**Figure 3 – Historical timeline of E3 ubiquitin ligase research.** 1995- Huibregtse et al. define the first E3 ligase family- the Homologous to E6-AP C-Terminus (HECT) E3 ligases[1]. 1998-2000- Together with the identification of the RING E3 ligase family, a burst of crystal structures heralds a new age of E3 ligase research[3,4]. Two milestone crystal structures of the Pavletich lab demonstrate the architecture of the family-defining E6-AP HECT ligase (PDB ID: 1C4Z, E2 not shown) as well as the first RING E3 ligase structure of c-cbl bound to E2 and substrate peptide (PDB ID: 1FBV, E2 and substrate peptide not shown)[3,5]. More than a century later, another family of E3 ligases was discovered- RING1, IBR and Rcat- (RBR) ligases[6]. Only two years later several crystal structures of RBR ligases including Parkin (PDB ID: 4K95) have shed light on their intricate mechanism[7,8]. In 2016 it was demonstrated how the RBR ligase ARIH1 is activated by Neddylated CRLs and ubiquitylates their substrates, showing how two distinct types of E3 ligases can work together[9]. The RCR ligase MYCBP2, another type of E3 ligase, was identified with activity-based proteomic profiling and the E2-ABP-bound structure solved two years later (PDB ID: 5O6C)[10,11]. In the following year, yet another type of E3 ligase has been uncovered- the RZ-finger ligase RNF213[13,14]. Around the same time, several structures of CRL RBR E3-E3 super-assemblies display the full cycle of ubiquitin transfer for ARIH1 (PDB ID: 7B5L) and demonstrate how the highly homologous ARIH1-CRL5 super-assembly (PDB ID: 7ONI) deviates in its way of being activated by NEDD8[2]. Adapted from [12].

catalytic Cysteine that participates in catalysis. Here, Ub is transferred from the E2 Cys<sup>cat</sup> to the E3 Cys<sup>cat</sup>, and then from the E3 Cys<sup>cat</sup> to the target[5,6].

For all classes of E3, repeated cycles of Ubiquitin transfer between the enzymes active sites generate polyubiquitin chains. It seems likely that the size of Ub and Ubls, which are proteins rather than small chemical post-translational modifications such as phosphates, methyl or acetyl groups, constrains the organization of reactants and products in E1>E2>E3 enzyme cascades. It is an entire protein that must move between enzyme active sites, to the substrate's acceptor site, and to a specific Lys at the end of a growing polyubiquitin chain. It has been shown E3 enzymes are often

multifunctional and display different assemblies and conformations for different functions. In order to do so, E3s may interconvert between a range of inactive and active complexes and conformations to achieve regulation. Thus, specificity and regulation come from the combination of molecular recognition and conformational control, as different factors harness flexible E3s into specific architectures for diverse activities. Even though there are two types of E3 operationally—from E2 Cys<sup>cat</sup> to substrate (or Ub) or from E2 to E3 to substrate (or Ub) - we now start to realize that there are many more types, different reaction trajectories and different types of active sites altogether.

### 1.2.1 HECT E3 ligases

The roots of E3 ligase research goes back to when HECT E3 ligases were first discovered in the 1990s[1]. They are regulating a vast number of important pathways by ubiquitylating target substrates in a two-step reaction: first, the E2 enzyme transfers ubiquitin to the catalytic cysteine to form a covalent thioester-linked HECT~Ub intermediate. Second, ubiquitin is transferred onto the substrate's lysine to form a covalent isopeptide bond. HECT ligases are composed of a N-terminal and C-terminal lobe. The N-terminal lobe acts as E2 binding site while the C-terminal lobe bears the catalytic cysteine. The transfer of ubiquitin between these two lobes is enabled by a flexible tether connecting both lobes. The NEDD4-family (including NEDD4, NEDD4L, Smurf2, and Itch among others) of HECT ligases are one of the most intensively studied and characterized E3 ligases[56].

NEDD4-family members are involved in the regulation of trafficking and/or endocytosis of substrates such as EGFR, HIV Gag, TGFb-R, and JNK, as well as many other non-degradative functions such as proteasomal processing of specific transcription factors[57-59]. In order to recognize and bind their substrates, NEDD4-family members typically compromise several WW domains. In contrast to this, the HERC-family of HECT ligases features regulator of chromatin condensation 1-like domains (RLD), defining them as second HECT E3 ligase class[60]. Since the remaining HECT E3 ligases do not share specific domains, no classification is made. NEDD4-family E3s display distinctive specificity by which they modify substrates with mono-ubiquitin or K63 chains, unlike some other HECT E3s such as E6AP that synthesizes K48-linked poly-ubiquitin chains. Furthermore, NEDD4-family E3s are autoinhibited through intramolecular interactions. HUWE1 for example, is only activated upon disruption of

its native homo-dimerization that keeps its HECT domain inaccessible[61]. Other than intrinsically autoinhibited E3s, other forms by which activity can be modulated include adaptor proteins such as SMAD7 for SMURF1 and SMURF2[62].

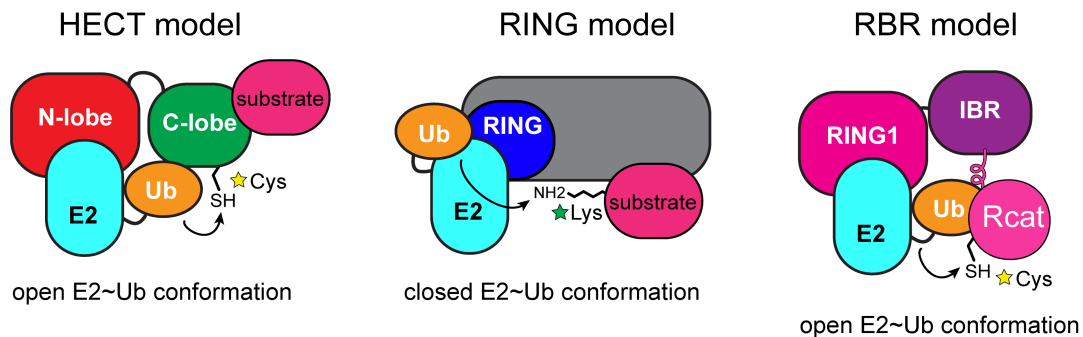


**Figure 4 – Model mechanism of E3 ubiquitin ligases.** Schematic representation of ubiquitin transfer from E2 enzyme to E3 ligase or substrate. Left- HECT E3 ligases bind E2 enzymes with their N-lobe and stimulate the discharge of ubiquitin to their catalytic cysteine containing C-lobe. Middle- working model for ubiquitin transfer from an E2 bound to a RING E3. A closed, canonical conformation, in which the E2, ubiquitin, and the RING domain all contact each other, promotes ubiquitin transfer to a substrate's lysine residue. Ultimately, the closed arrangement catalyzes discharge from E2 to lysine. Right- working model for ubiquitin transfer to RBR E3 ligase. The RING1 domain binds E2~ubiquitin in an open conformation and then transfers ubiquitin to the Rcat domain, which contacts ubiquitin via its ubiquitin-guided helix. Figure adapted from [12].

### 1.2.2 RING E3 ligases

RING E3 ligases comprise the largest E3 family, and function by bridging an activated E2~Ubl intermediate and a target substrate. RING E3s promote Ubl transfer directly from the catalytic cysteine of the E2 enzyme to a primary amino group, normally sitting on the lysine side chain, on the target protein. Hereby, ubiquitin can also be coupled to one of the seven lysines or the N-terminus of ubiquitin itself during polyubiquitination. The hallmark domain of RING E3s is the zinc-coordinating RING domain that catalyzes Ub ligation without donating any residues directly to the ligation active site. Additionally, they comprise a protein interaction domain or subunit that recruits substrates for ubiquitin or Ubl modification. The RING domain binds E2 and its distal ubiquitin in a closed conformation to align them perfectly for a nucleophilic attack of the target's amino group to generate the covalent isopeptide linkage.

### 1.2.2.1 Cullin-RING E3 ligases

The largest class of the RING E3 ligases consists of the modular, multisubunit **Cullin-RING Ligase** (CRL) family, with approximately 250-300 members in humans[63,64]. CRL E3s collectively mediate 20% of 26S proteasomal degradation and much non-degradative ubiquitylation as well. Mutations of CRL subunits can lead to cancer and neurodegenerative as well as cardiovascular diseases including hypertension[65-70]. Furthermore, many pathogenic bacteria and viruses hijack or inactivate CRLs to promote infection[69]. Various CRLs mediate ubiquitination of key regulators of cell division, circadian rhythms, development, and many more important biological processes[71-73]. This vast impact is rationalized from the assembly of CRLs and their mix-and-match architecture based on related but distinct swappable modules: a core cullin-RBX complex, and a variable cullin- and substrate-specific receptor complex.

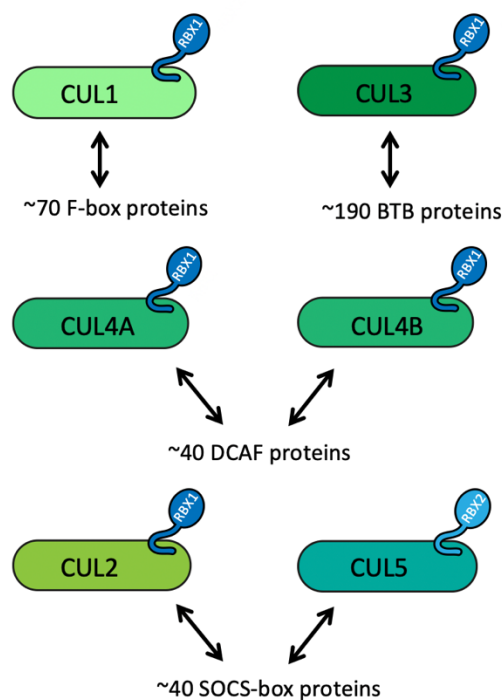


**Figure 5 – Cullin-RING ligases and their cognate substrate receptor family.** Schematic representation of Cullin (shades of green) RING (shades of blue) ligases. CRL1 to CRL4 partner up with RBX1 to mediate substrate ubiquitylation while CRL5 is specifically teaming up with RBX2.

For example, the prototypic CRLs in the human SCF (SKP1-CUL1-Fbox protein) family are based on CUL1, which forms its characteristic elongated banana-like shape with its three Cullin repeats[74,75]. One end, CUL1 associates interchangeably with  $\approx 70$  substrate-binding Fbox protein-SKP1 complexes, and the other binds RBX1, which

features the hallmark E3 ligase RING domain. Under any given cellular condition, dozens of different Fbox proteins are assembled into SCFs that are licensed for E3 ligase activity through site-specific modification of CUL1 with the ubiquitin-like protein NEDD8[63,76-78]. Post-translation modification of CRLs greatly increases ubiquitin transfer from E2 to target substrates and simultaneously hinders recognition by CAND1. CAND1 initiates the assembly of CRLs and their cognate substrate receptors in the first place. NEDD8 modification occurs on a conserved lysine residue in the winged helix-B (WHB) domain of the CRL C-terminus[79]. Other subdomains in the C-terminus include the four helix-bundle (4HB) and the CUL-RBX domain (C/R domain-former alpha-beta domain). RBX1's N-terminal strand is hereby integrated into a beta-sheet of the C/R domain and therefore essential for proper folding of the whole domain. RBX1's catalytic RING domain is connected its N-terminal strand via a linker and is contacting CUL1's WHB domain in the unneddylated crystal structure but was shown to be able to adopt different conformations for different functions[74].

No other Ubl intervenes as much with the ubiquitin system as NEDD8. It is the gatekeeper of Cullin-RING ligases (CRLs) since -once modified with NEDD8- it increases their ubiquitylation activity tremendously[80]. NEDD8 brings its own neddylation machinery with it: (1) the NEDD8-activating enzyme (NAE), a heterodimeric protein that comprises APP-BP1 and UBA3, (2) the two E2-conjugating enzymes UBE2M and UBE2F. NAE maintains high specificity for NEDD8 dictated by a single residue in NEDD8, Ala72. Conversion of Ala72 to Arg72 allows binding to Uba1 and vice versa. Furthermore, a specific groove in Uba3 determines specificity for the two NEDD8-conjugating E2 enzymes[81].

As already mentioned, members of the CRL family are typically modified with NEDD8 on a conserved lysine, enabling CRL-dependent ubiquitylation. Because UBE2M specifically interacts with RBX1, it determines conjugation of NEDD8 to CRLs 1-4. Oppositely, UBE2F neddylates CRL5 with high efficiency[82]. To complete the cycle, the eight protein COP9 signalosome complex (CSN) is responsible for the removal of NEDD8 from CRLs and switches off CRL activity. More precisely, the CSN5 subunit comprises a metalloprotease to sever the NEDD8 isopeptide bond[83-85]. Lastly, CAND1 bind the non-neddylated form of CRLs and promotes substrate adaptor/substrate receptor exchange[86-88]. Taken together, NEDD8-modified and substrate-bound Cullin-RING ligases are hallmarks for their activity in an ever-

changing cycle of neddylation, ubiquitylation, deneddylation and substrate receptor exchange[89].

### 1.2.3 RBR E3 ligases

The mechanism of **R**ING-**I**n-Between-**R**ING (RBR) E3 ligases remained elusive for much longer than for RING or HECT E3s. However, the reactivity profile of the E2 enzyme UBE2L3 revealed its inability to discharge ubiquitin onto lysine residues and thus rationalized its strong preference to cooperate with RBR E3 ligases[6]. RBR E3s utilize a hybrid approach to ubiquitylate their substrates: (1) binding of their cognate E2 enzyme with their RING1 domain (similarly to RING E3s), (2) transfer of ubiquitin to its catalytic cysteine, located in the Rcat domain (similarly to HECT E3s), (3) ubiquitin transfer from Cys<sup>cat</sup> to substrate.

The best-characterized RBR E3s are the Parkinson's disease associated protein Parkin, the Linear Ubiquitin Chain Assembly Complex (LUBAC) that contains the two RBR E3s HOIP and HOIL-1L as well as Sharpin, and members of the Ariadne family. LUBAC is implicated in Nf- $\kappa$ b signaling and is the only E3 ligase to assemble linear polyubiquitin chains by connecting Ubiquitins C-terminus with the alpha-amino group of Met1[90]. One of the best characterized substrates of LUBAC is NEMO, which is accumulating upon linear ubiquitination caused by the high affinity of the UBAN domain of NEMO towards linear ubiquitin. Thereafter, IKK induces phosphorylation-mediated activation of IKK $\beta$ , which in turn phosphorylates I $\kappa$ B $\alpha$  to trigger the activation of Nf- $\kappa$ b[91-93].

A common trend for RBR E3s is their natural autoinhibition. Full-length HOIP is inactive and only becomes activated within LUBAC to mediate the generation of linear chains[94]. Parkin plays an important role in Parkinson's Disease, as mutations in the PARK2 gene cause early forms of this neurodegenerative disorder and is only activated upon phosphorylation of its ubiquitin-like domain as well as binding to phosphorylated ubiquitin[95-97]. In both cases, phosphorylation is mediated by PTEN-induced kinase (PINK1) on Serine 65[98]. Not all RBR E3s require posttranslational modifications on themselves to be activated but instead require partner proteins to modulate their activity like ARIH1 and ARIH2. ARIH1, ARIH2 (TRIAD1), Cullin-9 and ANKIB1 belong to the largest subgroup of RBR E3 ligases- the Ariadne family[99-101]. Ariadne-family RBR E3s are represented in eukaryotes as well as yeast. Members of this subgroup include ARIH1 and ARIH2, which are highly homologous E3 ligases,

CUL9 - a linear fusion between a CRL (CUL7) and a RBR E3 (ARIH1) and ANKIB1 bears N-terminal Ankyrin repeats[102]. Genetic studies have demonstrated how the drosophila gene *ariadne-1* is essential for differentiation and thus development[103].

### 1.2.3.1 ARIH1

As a member of the Ariadne-subfamily, ARIH1 is a prime example of how RBR E3s can be autoinhibited. ARIH1s crystal structure revealed its general architecture: it adopts an extended conformation leading with a UBA domain and the E2-binding RING1[104]. Together with a RING1-to-IBR (RTI) helix, the IBR domain connects the N-terminal domains with the C-terminal, catalytic cysteine-bearing Rcat domain that is tightly packed against the autoinhibitory, four-helix bundle Ariadne domain. The N-

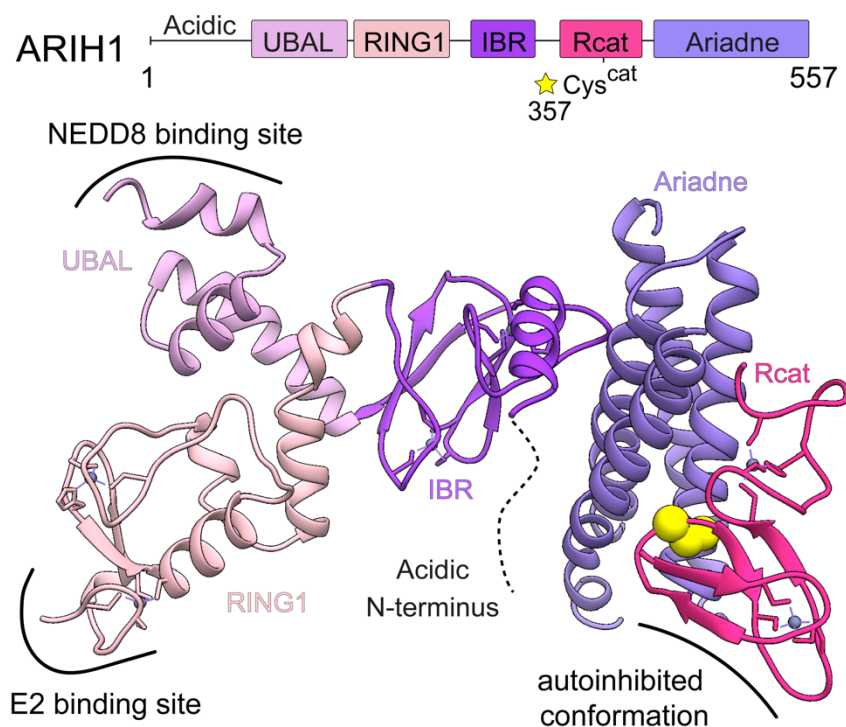


**Figure 6 – Structural architecture of ARIH1.** Top- Schematic of ARIH1 color-coded by domains. Bottom- Crystal structure of ARIH1 (apo structure- PDB ID: 4KBL). ARIH1s acidic and glycine-rich N-terminus is not visible in the crystal structures. Residues 99-105 are termed the IBR-interacting strand as it folds into a three-stranded beta sheet with the central IBR domain. This strand is followed by the three-helix UBAL domain, that has been shown to be binding NEDD8 and Ubiquitin. The RING1 domains is anchor for the E2 enzyme, while the IBR domain connects ARIH1s N-terminal portion with its C-terminus. The Rcat domain bears the catalytic cysteine 357 (indicated as yellow spheres), which is enwrapped by ARIH1 autoinhibitory, 4-helix bundle Ariadne domain.

terminal acidic/glycine-rich region is presumably flexible and not visible in any crystal structure.

Unlike the canonical RING1 domain, the Rcat domain adopts an unusual zinc-binding motif. Two of its zinc atoms are coordinated by seven of the eight cysteine residues in the Rcat domain. While one of the zincs is coordinated by four cysteines in two anti-parallel beta sheets, the other one is coordinated by a loop-like assembly with three cysteines and one histidine facing inward. The remaining uncoordinated cysteine is ARIH1s conserved, catalytic cysteine 357 and responsible for accepting ubiquitin. In its native conformation, the catalytic cysteine is tightly packed against the Ariadne domain and consequently inaccessible. However, autoinhibition can be artificially released by introducing mutations in the Ariadne domain that disrupt the molecular latch between Ariadne and Rcat domains. This is achieved by substitution of three residues for alanine, namely Phe430, Glu431, Glu503 (ARIH1\* or ARIH1 open). Several studies have shown UBE2L3 (Ubch7) to be ARIHs cognate E2 while E2 enzymes of the UBE2D-family show much less activity towards ARIH1[105]. UBE2L3~ubiquitin-bound structures revealed multiple important interaction sites of UBE2L3 with ARIH1s RING1 domain, however, no major structural rearrangements occur in comparison to the apo structure. UBE2L3~Ubiquitin engages ARIH1 in an open conformation as it is consistent with the hybrid-like RBR mechanism to transfer Ubiquitin. ARIH1s catalytic cysteine is still more than 50 Å away from the catalytic cysteine of UBE2L3 and ubiquitin is shown to be present in multiple locations, possibly owed due to the absence of the Rcat domain[105,106].

#### 1.2.4 RCR E3 ligase MYCBP2

Recently, a RING domain containing, neuron-associated E3 without known HECT or RBR catalytic domain, was identified via activity-based proteomic profiling-MYCBP2[10]. Extensive biochemical characterization revealed the modification of hydroxyl groups with ubiquitin via an unprecedented RING-Cys-Relay (RCR) mechanism. Two essential cysteine residues in the RING-neighboring TC domain govern the transfer of Ubiquitin to threonine (and serine). While the RING domain engages the E2~Ub intermediate in the archetypal closed conformation, ubiquitin is unorthodoxically passed to the upstream Cysteine in the mediator loop[10,11]. While canonical RING E3s promote E2 discharge to Lysine in a linchpin driven-manner, it

turns out ubiquitin is undergoing a slight rotation during transthiolation thus destabilizing hallmark features required for aminolysis activity of the closed confirmation. The absence of a linchpin and Ub Ile36 interactions could diminish the activity-level to a sweet spot, in which transthiolation is favored and ultimately secured by Asn77. Once the upstream cysteine is transthiolated, Ub relay to the downstream cysteine is steered by an entropically driven helix-coil transition of the mediator loop, finally leading to the esterification of substrate hydroxyl groups[11].

At this point it is unclear but it is speculated that E2s and traditional active sites are suboptimally reactive towards threonine, which is why new active sites with improved reactivity towards hydroxyl nucleophiles have evolved. The relay could also allow additional regulation. Ubiquitylation of Threonine residues on native targets in vivo by MYCBP2 has yet to be demonstrated and makes us wonder what advantage E3 ligase esterification activity has over classical aminolysis.

### 1.2.5 RZ-finger E3 ligase RNF213

Speaking of atypical E3 ligases with esterification activity, another remarkable variation was identified recently, embodied in RNF213[13,14,107]. Retrospectively, the distinct chemical features of RNF213 could have been portended by this RING-domain containing E3 reacting with the E2 ABP from Pao *et al*[10]. Three publications in the last 12 months have shed light on the extraordinary structural mechanism and function of this Moyamoya disease-associated, giant E3 ligase[13,14,107]. But besides its role as major susceptibility factor of this cerebrovascular disorder, it also serves as first line of defense mechanism against cytosol-invading Salmonella. Surprisingly, the ubiquitin acceptor is non-proteinaceous and instead hydroxyl groups on the lipid A of bacterial lipopolysaccharide (LPS) are esterified with ubiquitin. The exact sites of ubiquitylation, however, have yet to be identified since there are several hydroxyl groups in the lipid A. On top of this, the RING domain is not required for its basal E3 autoubiquitylation as well as LPS esterification activity[13,107].

Unexpectedly, a 27-residue small RZ finger with a highly conserved catalytic cysteine, located at the C-terminal lobe of the E3 shell, is responsible for its ubiquitylation activity. This RING-independent mechanism was confirmed when a UBE2L3 ABP was utilized as suicide substrate in a cryo-EM structure to mimic the transient E2-E3 transthiolation intermediate. The ABP-guided approach demonstrated UBE2L3 binding

to the CTD of RNF213 and displayed additional density compared to the apo structure that can be assigned to the RZ finger. By employing UBE2L3 as E2, RNF213 joins the HECT and RBR E3 ligase-family that use UBE2L3 to govern the transthiolation of their respective catalytic cysteines in an open E2~Ub conformation. In addition to the elusive role of the RING domain, the importance of the dynein-like ATPase module for E3 ligase activity has been unclear. However, there is now striking evidence that E3 ligase activity is dependent on ATP binding, suggesting it to function as a metabolic sensor, thereby altering its activity in response to the cellular energy state[13,14,107].

### 1.2.6 CRL-RBR E3-E3 ligases

There were early indications that some E3s function either in complexes or synergistically. Ubr1 functions in a pathway with Ufd4, depicting the collaboration of a RING and HECT E3 ligase[108,109]. Subsequently, LUBAC was found to be a complex containing two RBR-type E3s[90]. The RBR ligase ARIH1 is known to associate with more than 45% of all cellular SCFs, therefore establishing a huge pool of E3s[9]. Remarkably, the NEDD8 modification of SCFs alone causes a major fraction of cellular SCFs, as well as CUL2- and CUL3-based CRLs, to associate with ARIH1. The resultant neddylated SCF/ARIH1 E3-E3 ligases utilize a distinctive ubiquitylation mechanism, whereby the ARIH1 E3 rather than a RING-bound E2 is the direct mediator of ubiquitin ligation to substrates recruited to the F-box proteins. Moreover, whereas knocking down or deleting CRL partner E2s may impact selected substrates, including the I $\kappa$ B $\alpha$  substrate of SCF $^{\beta$ TRCP, ARIH1 knockdown stabilizes several CRL substrates, including phosphorylated p27 and Cyclin E substrates of SCF $^{SKP2}$  and SCF $^{FBXW7}$ , respectively[99].

Indeed, CRISPR screens showed widespread ARIH1 essentiality paralleling that of CUL1 and NEDD8. For many CRLs and structurally diverse substrates, E3-E3 catalyzed ubiquitylation is strikingly more efficient than conventional cullin-RING-dependent ubiquitin transfer from an E2, with the notable exception of UBE2D-mediated ubiquitylation of substrates recruited to the F-box protein  $\beta$ -TRCP explained by the ideal structural arrangement this particular neddylated SCF-E2 assembly[110]. In a landmark study, a mutational survey of ARIH1 was carried out to dissect key residues in the ARIH1/CRL1 interaction[9]. By profiling mutants via their activity profile signature, important residues required for activation of ARIH1 by neddylated CRLs

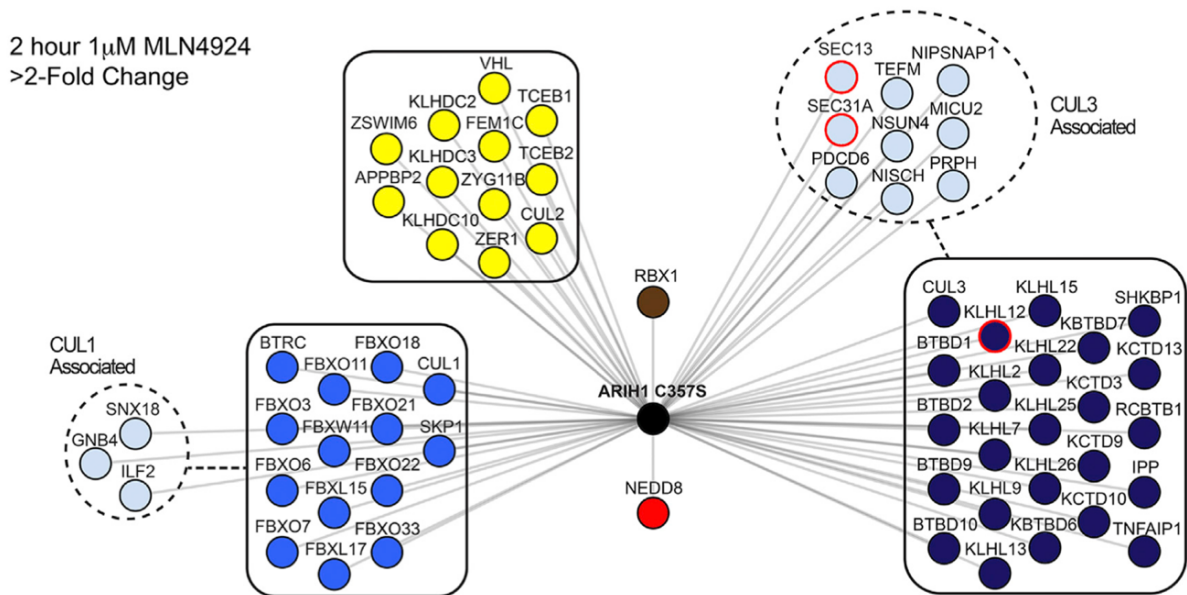


**Figure 7 – ARIH1 interactome upon neddylation inhibitor treatment.** Scheme displaying high-confidence candidate interacting proteins (HCIPs) of ARIH1 C357S that decreased two-fold upon MLN4924 (neddylation inhibitor) treatment. Decreasing HCIPs of ARIH1 are based on CRL family members and their matching substrate adaptors/substrate receptors. Additionally, the two CRL hallmark proteins RBX1 and NEDD8 significantly decrease upon MLN treatment. *Adapted and reprinted from Two Distinct Types of E3 Ligases Work in Unison to Regulate Substrate Ubiquitylation. Cell 2016, 166:1198-1214 e1124., with permission from Elsevier.*

have been identified e.g residues Phe150 and Val123 that are essential for NEDD8 binding to ARIH1s UBAL domain. The strong dependence on neddylated CRLs for activation of ARIH1 implies the need for tight regulation of ARIH1s activity in a cellular environment. Furthermore, it was shown how ARIH1 multi-monoubiquitylates CRL substrates in a two step-reaction. First, Ubiquitin is transferred from UBE2L3 to ARIH1s catalytic cysteine in a neddylated CRL-dependent manner. Then, Ubiquitin is lifted to the F-box protein-bound substrate. For each individual step of the transfer cascade, different residues seem to play varying roles suggesting large conformational rearrangements.

Another Ariadne-family E3, ARIH2, specifically binds neddylated CUL5, which in turn teams with RBX2. Despite the high sequence homology of ARIH1 and ARIH2 of approximately 40%, ARIH2 copurifies exclusively with neddylated CRL5-based CRLs. ARIH2 mediates degradation of a virally-directed CUL5-based CRL substrate in infected cells. Structurally and functionally homologous CRL5<sup>BC-box</sup> assemblies are formed by substrate-bound BC-box proteins complexed with the two-protein ElonginB-ElonginC adaptor and CUL5-RBX2[111,112].

### 1.3 Activity-based probes

The ubiquitin system cascades ubiquitin from one active site to the other. Since this system relies on thiol chemistry in order to transfer ubiquitin, catalytic cysteines of E1, E2, E3 (HECT, RBR, RCR and RZ-finger E3 ligases) or DUB enzymes are targetable by activity-based probes. Activity-based probes describe molecules with three building blocks: a recognition group of the target (herein ubiquitin), an affinity handle (often used for purification purposes) as well as a reactive group (to covalently attach to the target)[113-115]. The most straight-forward approach includes installing electrophilic warheads at the C-terminus of ubiquitin- either synthesizing ubiquitin from scratch or relying on semi-synthetic strategies to generate ubiquitin-based ABPs[116].

Early approaches included modification of ubiquitin C-terminal Gly76 with a vinyl sulfone warhead that readily reacted with deubiquitylating enzymes[117]. Soon after, this strategy was adapted to integrate a variety of thiol-reactive electrophiles with varying reactivity towards ubiquitin-processing enzymes. Ubiquitin ABPs have been used to study the activity of enzymes as only conformations with exposed active sites are covalently attached to the ABP. Consequently, reaction of ARIH1 with Ubiquitin-vinylmethylester does not occur in the absence of its activator neddylated CRL. In addition to screening reactivity of enzymes in vitro, Ubiquitin-based ABPs are able to provide deep insights into global DUB or E3 enzyme activity with chemoproteomic approaches in cells[117-119]. Another way to exploit ubiquitin ABPs is to utilize them in high-throughput screens against small molecule compound libraries possibly acting as modulators of activity. Here, the traditional E1-E2-E3 cascade can be bridged by installing a mercaptoethanesulfonate (MES) handle in ubiquitin C-terminus, which generates thiol-linked E3 complexes[120]. Alternatively, ubiquitin-MES is most often used as an activated ubiquitin-species and basis for the conjugation of additional chemical handles. This is exemplified by conjugating fluorescein-thiol with ubiquitin-MES to obtain a ubiquitin-ABP that provides a fluorescent readout in high-throughput screens for inhibitors[121].

With increased knowledge about the ubiquitin system, ABPs have evolved to target enzymes more selectively. A new generation of ABPs incorporates a second recognition element by creating fusions between ubiquitin and a second ubiquitin, a peptide or E2 enzymes. In the first case, di-ubiquitin ABPs can be generated by several different approaches. One is the expression of a linear di-ubiquitin fusion, in which the latter ubiquitin bears an N-terminal cysteine. This cysteine can then be converted to

dehydroalanine (dha) with 2,5-dibromohexanediamide, resulting in a reactive electrophile[122]. The linear di-ubiquitin probe was shown to form a covalent complex with the deubiquitinase OTULIN, which is dedicated to process linear ubiquitin chains[123]. To generate Di-ubiquitin probes with alternative linkages, Li et al. describe an approach in which Ub-MES is coupled with BmDPA resulting in a reactive Ubiquitin species[124]. This species can then form covalent adducts with cysteine residues on proteins. Mutation of any lysine residue of ubiquitin to cysteine allows to generate chain linkages of any type. Even though it has not been explored so far, this technique can also be utilized to generate ubiquitin-E2 enzyme or ubiquitin-peptide fusions to mimic the transfer of ubiquitin from E2 to E3 ligase or from E3 ligase to peptidyl substrate. An alternative method that has proven to be successful, is the total synthesis of a ubiquitin species harboring a C-terminal click chemistry handle that allows for triazole coupling between ubiquitin and E2 enzyme in a copper-catalyzed azide-alkyne cycloaddition[119,125]. It is also possible to synthesize both, ubiquitin and the E2 enzyme from scratch[126]. These ABPs were used to study active E3 ligases in whole cell systems and structure-based approaches. When applied to cell extracts, E1 and the suite of E3 ligases known to have an active site cysteine that receives Ubiquitin were identified.

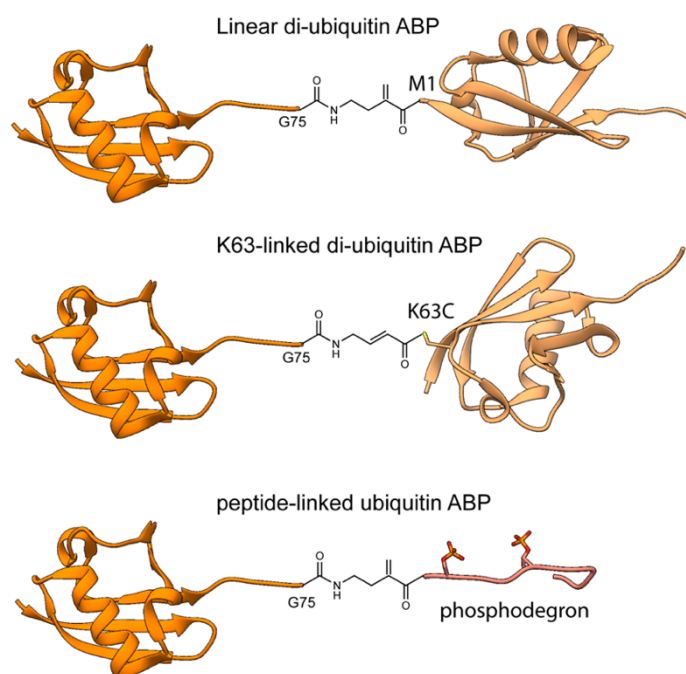


**Figure 8 – Ubiquitin-derived activity-based probes.** Top- M1-linked di-ubiquitin ABP with a central electrophilic dehydroalanine. Di-ubiquitin was generated by conjugating Ub-MES with another ubiquitin carrying a N-terminal cysteine. Middle- K63-linked di-ubiquitin ABP derived by coupling K63C-ubiquitin with Ub-MES, that was modified with Ub-BmDPA and deprotected afterwards. Bottom- peptide-linked ubiquitin ABP with a central electrophilic dehydroalanine.

## 1.4 Strategy to stabilize and visualize ubiquitin transfer intermediates of the E3-E3 ubiquitylation mechanism

The goal of this study is to unravel the concerted E3-E3 ubiquitylation mechanism of the cullin-RING-ligase CUL1-RBX1 and the RBR ligase ARIH1. Cryo-EM structures of the tandem interplay in action should reveal how ubiquitin is transferred all the way from ARIH1's cognate E2 UBE2L3 to any native CRL substrate. One challenge to visualize the E3-E3 mechanism is that an entire ubiquitylation cycle occurs in less than one second (Figure 9). The E3-E3-dependent ubiquitylation is a two-step reaction: first ubiquitin is transferred from the E2 UBE2L3 to ARIH1 in a neddylated CRL-dependent manner. Then ARIH1 delivers ubiquitin to the substrate's target lysine, followed by the disassembly of the E3-E3 ligase. We are hypothesizing that the E3-E3-dependent ubiquitylation depends on stabilization of fleeting transition states, resulting from interconverting protein conformations.

These transition states are occurring on a millisecond time scale as auto-ubiquitylation as well as substrate ubiquitylation is an extremely efficient reaction when ARIH1 is activated by neddylated CRLs.

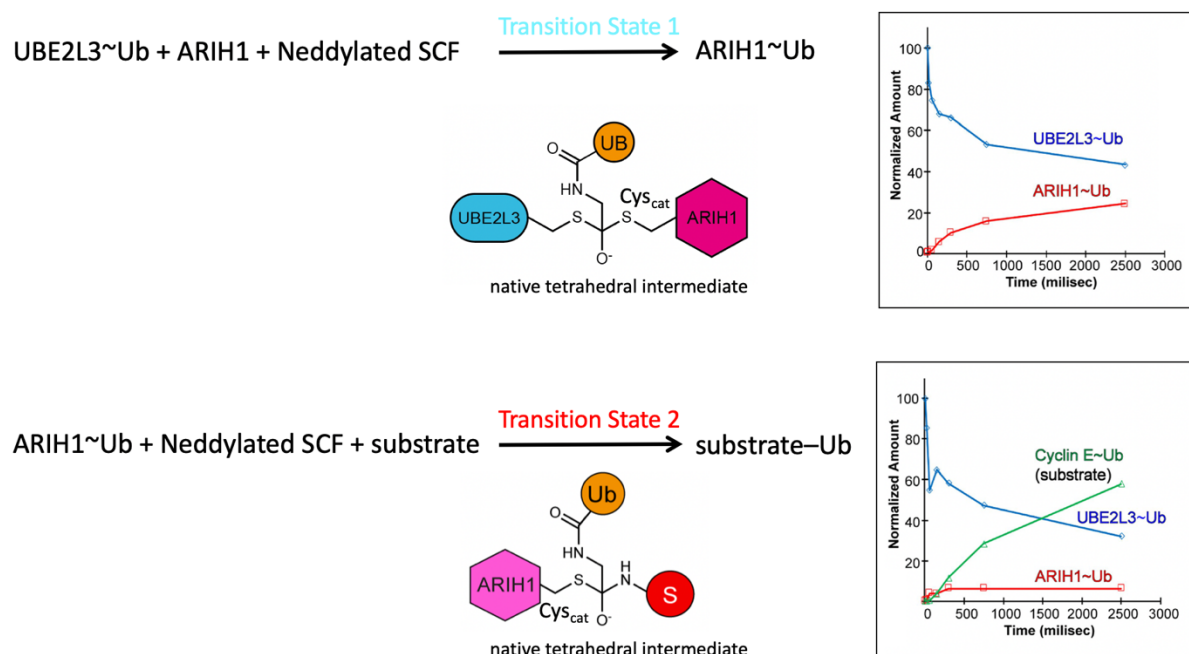


**Figure 9 –E3-E3-mediated ubiquitylation is a two-step reaction.** Top- In the first step of the reaction, ubiquitin is transferred from E2 enzyme to ARIH1 in a neddylated SCF - dependent manner via Transition State 1. Rapid quench flow experiments demonstrate how transfer occurs on a millisecond time scale. Bottom- In the second step of the reaction, ubiquitin is transferred from ARIH1 to the Fbox protein-bound substrate via Transition State 2. Rapid quench flow experiments showing how the substrate~Ub fraction starts to build up in less than 500 ms. Figure adapted from [2].

For this reason, we are aiming to generate a suite of activity-based chemical probes to overcome the short half-life of the native, tetrahedral transition states and stabilize them in order to obtain quality data. Since we are dealing with two transition states, two distinct probes have to be developed: One for the transfer of ubiquitin from UBE2L3 to ARIH1 and one for the ubiquitylation of the substrate by ARIH1. Activity-based probes target catalytic residues on enzymes and hereby depend on the active conformation of them. Consequently, we set out to develop activity-based probes that are able to chemically trap ARIH1's catalytic cysteine, once ARIH1's autoinhibitory Ariadne domain is sequestered by neddylated cullin. Installing an electrophilic chemical handle has been proven to effectively cross-link with the Sulphur group of cysteines[119]. Since ARIH1's cognate E2 UBE2L3 is necessary to transfer ubiquitin to ARIH1, UBE2L3 as well as ubiquitin have to be utilized to generate the first activity-based probe[6]. Likewise, the second step of the transfer cascade involves ubiquitin, ARIH1 as well as the F-box protein-bound substrate. For this purpose, substrate phosphodegron peptides and ubiquitin will be components for the second set of activity-based probes. After generation of aforementioned probes, the successful validation of their reactivity and nativity will be a prerequisite for their utilization in cryo-EM experiments. Ultimately, the goal is to picture the complete cascade of E3-E3-catalyzed ubiquitin transfer to F-box protein-bound substrates.

## Chapter 2 –

A suite of activity-based probes to conquer the structures and concerted mechanism of the RBR E3 ligase ARIH1 and the RING E3 CUL1-RBX1.

In this chapter, parts of the following publication were integrated:

**Horn-Ghetko, D.**, Krist, D.T., Prabu, J.R., Baek, K., Mulder, M.P.C., Kluegel, M., Scott, D.C., Ovaa, H., Kleiger, G., Schulman, B.A. Ubiquitin ligation to F-box protein targets by SCF–RBR E3–E3 super-assembly. *Nature* **590**, 671–676 (2021).

Display items and text were reprinted with permission from Springer Nature.

## 2.1 Generation of a TS1 activity-based probe to stably mimic ubiquitin transfer from E2 to E3

We hypothesized that the E3-E3-dependent ubiquitylation depends on fleeting stabilization of defined catalytic architectures from infinite interconverting protein conformations. Transient, regulated protein-protein interactions choreograph the two chemical intermediates. Thus, based on the principle of microscopic reversibility, chemically stable mimics for the transition states should stabilize typically mobile catalytic domains in rare conformations that drive each reaction. We anticipated this would involve many E3-E3 protein domains, based on dynamic properties of the individual E3s. A prior cryo EM structure suggested that neddylated SCF catalytic elements are relatively mobile: RBX1's RING and CUL1's C-terminal WHB domain are flexibly attached to the intermolecular Cullin/RING domain (C/R), in which CUL1 and RBX1 form a stable complex[110]. NEDD8 is apparently mobile together with CUL1's WHB domain as the helix connecting them to the C/R domain is able to dissolve into a flexible tether. Meanwhile, prior mutational studies suggested that ARIH1 would likewise be dynamic in its conformation upon release from the known, structurally-characterized, stable autoinhibited arrangement[9]. In the first step of the E3-E3 reaction, ubiquitin is transferred from the E2 UBE2L3 to ARIH1's catalytic Cys (Figure 9). Previous studies showed this requires ARIH1-binding to neddylated CUL1-RBX1, which triggers exposure of the ARIH1 catalytic Cys and its subsequent receipt of UBE2L3's bound ubiquitin[9,99]. This reaction involves the formation of a tetrahedral transition state, which we consequently defined as Transition State 1 (TS1). To enable visualizing this reaction intermediate, we developed an activity-based probe (TS1 ABP) with an electrophilic warhead between the UBE2L3 catalytic Cys86 and ubiquitin's terminal Gly75. In contrast to a previously-described triazole-linked ABP of RBR activity, TS1 ABP maintains ubiquitin's Arg74, previously shown to contribute to neddylated CUL1-dependent activation of ARIH1[119]. This was important as the goal was to generate an ABP that would engage ARIH1's Cys<sup>Cat</sup> only when previously activated by a neddylated CRL. The strategy to obtain such ABP was derived from previous studies, in which dii-ubiquitin ABPs were assembled by coupling Ub-MES and a single cysteine-bearing ubiquitin with the help of (E)-3-[2-(bromomethyl)-1,3-dioxolan-2-yl]prop-2-en-1-amine (BmDPA). With this approach, any di-ubiquitin linkage type could be assembled and their reactivity towards Deubiquitinases tested[124].

Instead of creating di-ubiquitin ABPs, we conjugated the Ub-MES-derived reactive ubiquitin species to UBE2L3 to obtain a TS1 ABP (Figure 10a). In order to eliminate unspecific crosslinks when coupling the reactive ubiquitin species to UBE2L3, its extra two cysteines were mutated to alanine (Figure 10b). Ubiquitylation assays with the single cysteine UBE2L3 mutant indicated no deterioration in its activity level compared to wild-type UBE2L3 (data not shown). TS1 ABP synthesis was monitored via LC-MS to check successful conversion and estimate conversion yields (Supplemental Figures 1-5). After two-step purification, pure chromatography fractions of the TS1 ABP were pooled and consequently used in cryo-EM studies or ABP assays. The versatility of this ABP generation approach exceeds the coupling with one E2 enzyme but can be expanded to all other E2 enzymes as long as all cysteines, except for the catalytic one, are mutated to other residues. Additionally, solid phase peptide synthesis-derived peptides with N-terminal cysteine residues can be united with the deprotected Ub-BmDPA species to obtain a full suite of ABPs to profile enzymatic activities.

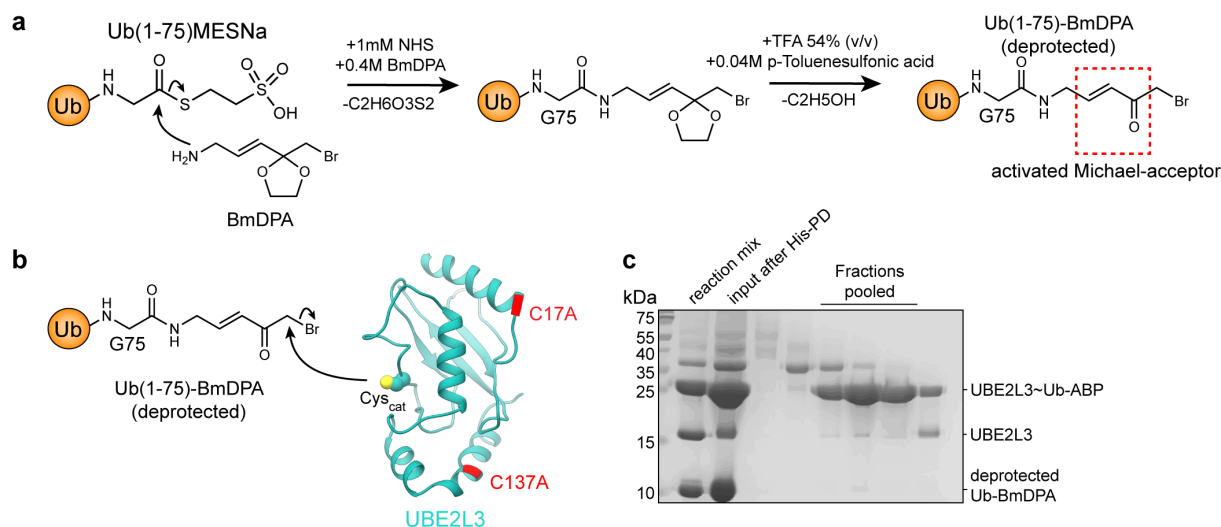


**Figure 10 – Activity-based probe (ABP) to capture E3-E3 ubiquitylation transition state 1.**

**a**, Strategy to generate an ABP to capture transition state 1. A chemical synthesis route was employed to conjugate the intein-derived Ub(1-75)MESNa and (E)-3-[2-(bromomethyl)-1,3-dioxolan-2-yl]prop-2-en-1-amine (BmDPA) to obtain a reactive ubiquitin intermediate. Acidic deprotection of the cyclic acetal yields ubiquitin with an activated Michael-acceptor. **b**, Conjugation of the reactive ubiquitin species to UBE2L3 (C17A, C137A) produces an ABP with an activated vinyl group between ubiquitin's C-terminus and UBE2L3's active site. **c**, SDS-PAGE gel analyzing size-exclusion chromatography fractions of deprotected Ub-BmDPA and UBE2L3 reaction mixture producing TS1 ABP. Figure adapted from [2].

### 2.1.1 Verification and comparison of native CRL-RBR E3-E3 reaction requirements with TS1 ABP conjugation

Ubiquitin is transferred from ARIH1s cognate E2 UBE2L3 to ARIH1s catalytic cysteine in a neddylation-dependent manner. The requirements for reaction with the probe - ARIH1's catalytic cysteine and stoichiometric neddylation of CUL1-RBX1 - have to parallel the native reaction in order to suggest the resultant neddylation of SCF-UBE2L3~ubiquitin~ARIH1 complex is a stable mimic of the transition state 1 ("~" here refers to reactive thioester linkage to an E2 or E3 Cys<sup>cat</sup>, or a chemically-stabilized mimic). Therefore, we set out to sequentially test those requirements by incubating the TS1 ABP with the two E3 ligases.

Indeed, reaction with the TS1 ABP was dependent on the same requirements as the native ubiquitylation reaction. In the absence of neddylation of CUL-RBX1, no reaction could be detected (Figure 11a). Similarly, no reaction was observed when neddylation of CUL-RBX1 was present but ARIH1s catalytic cysteine was mutated to serine (Figure 11a). CUL1-RBX1 could not promote reaction of ARIH1 with the TS1 ABP if it was not previously modified with NEDD8 on its WHB domain (Figure 11b). However, the need for neddylation of CUL can be bypassed by introducing three mutations in ARIH1's autoinhibitory Ariadne domain. By mutating Phe430, Glu431 and Glu503 to alanine, the intramolecular latch tethering ARIH1's Rcat domain to Ariadne domain, thereby occluding ARIH1s catalytic cysteine, is severed and autoinhibition released. The

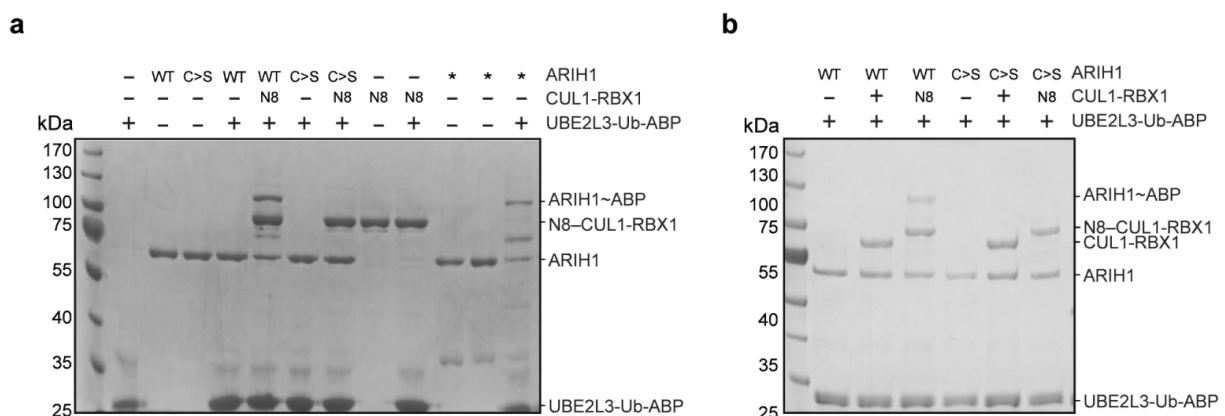


**Figure 11 – Paralleling the native reaction requirements with the TS1 ABP** **a**, SDS-PAGE gel testing UBE2L3~UB-ABP reaction with ARIH1 dependent on its catalytic Cys and requires all components to react. ARIH1\* (F430A, E431A, E503A) circumvents the need for NEDD8 as it was previously shown to relieve autoinhibition. **b**, SDS-PAGE gel displays dependence of Transition State 1 ABP reaction with ARIH1 on neddylation of CUL1-RBX1. Figure adapted from [2].

resultant, hyperactive mutant of ARIH1 is consequently termed ARIH1 open and readily reacts with the TS1 ABP (Figure 11a).

With the TS1 ABP matching the native requirements of the ubiquitylation reaction, we next set out to explore whether mutations on ARIH1- previously identified to impede with ubiquitylation of cyclin- also hinder reaction with the TS1 ABP. Two mutations of ARIH1 (Phe150A and Val123D) are located in ARIH1's UBAL domain in order to disrupt binding to NEDD8 and consequently prevent release of autoinhibition. Indeed, both mutants show reduced activity in comparison to wild-type ARIH1 with Val123D showing less reactivity towards the TS1 ABP. The other three mutations are located in ARIH1's autoinhibitory Ariadne domain. Tyr531A and Arg535A are least reactive with the probe, while W452A shows weak formation of the crosslinked species UBE2L3~Ub~ARIH1.

Taken together, our TS1 ABP not only parallels native reaction requirements for E3-E3-catalyzed ubiquitylation but can also be utilized to screen mutational effects on E3-E3 components.

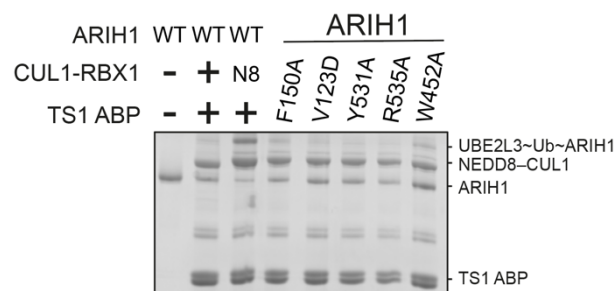


**Figure 12 – ARIH1 mutant reaction profile with TS1 ABP.** SDS-PAGE gel testing UBE2L3~UB-ABP reaction with ARIH1 mutants recently described as defective in CRL-dependent ubiquitylation assays. Figure adapted from [2].

## 2.2 Generation of an activity-based probe to stably mimic ubiquitin transfer from E3-E3 to F-box protein-bound substrate

After ARIH1 captures ubiquitin from UBE2L3, its Cys<sup>cat</sup>-linked ubiquitin is transferred to an SCF-bound substrate (Figure 9). Once again, this reaction undergoes another short-lived, tetrahedral transition state, in which ARIH1, ubiquitin and the acceptor lysine of the substrate are connected. This transition state is referred to as transition state 2. Due to ARIH1's ability to ubiquitylate many distinct substrates recruited by various SCFs, we examined ABP technologies and identified a readily portable "TS2

ABP” strategy: dehydroalanine chemistry linking ubiquitin’s C-terminus to N-terminal acceptor sites on peptide substrates (Figure 13a). With the dehydroalanine strategically placed to serve as target for a nucleophilic attack by ARIH1’s Cys<sup>cat</sup>, a chemically stable mimic of the native transition state 2 could be obtained (Figure 13b). Keeping in mind Cullin-RING ligases can ubiquitylate hundreds of substrates through their intricate mix-and-match system[86,127], we focused on studying CUL1-RBX1 and its cognate substrate receptor family- the F-box proteins. Many F-box proteins bind their target substrates after they have been phosphorylated within a specific sequence. This phosphodegron then typically exhibits high affinity towards its cognate F-box protein and is ubiquitylated shortly after- either through E2-mediated or E3-E3 mediated ubiquitylation[128,129]. Our TS2 ABP synthesis strategy allows for switching between substrate receptor systems as phosphodegron-peptides are obtained by solid phase peptide synthesis. The coupling to Ub-MES follows the same principles for every peptide as well as their consequent purification (Figure 13c). TS2 ABP synthesis was observed via LC-MS to check for successful conversion (Supplemental Figures 6-7).

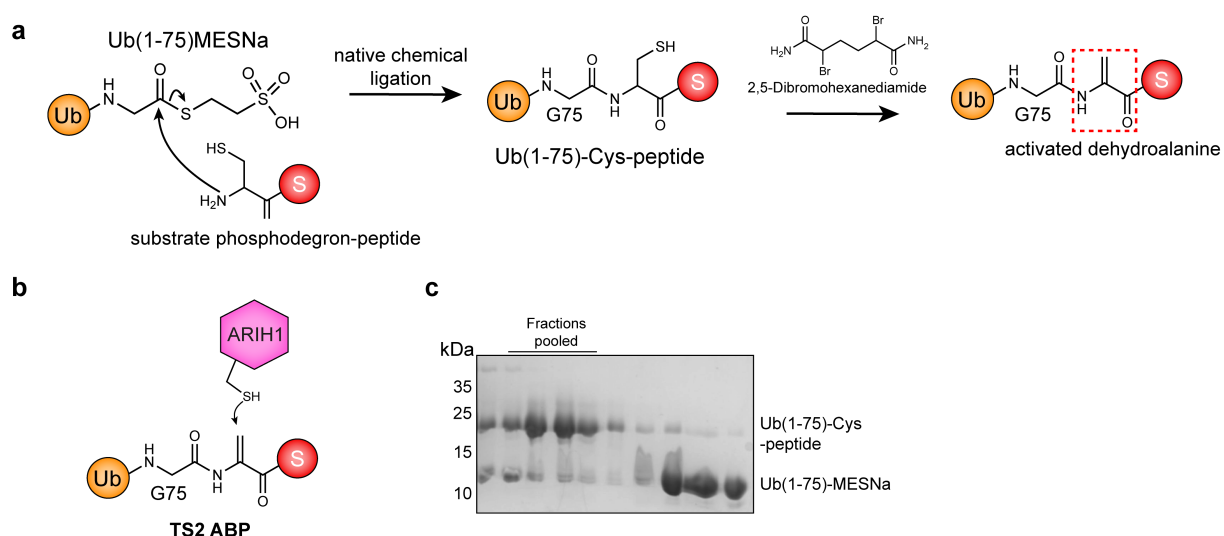


**Figure 13 – Activity-based probes to capture E3-E3 ubiquitylation transition state 2. a,** Semisynthetic strategy to generate TS2 ABPs. A fusion of ubiquitin-MES and a peptidyl SCF substrate with an additional, N-terminal cysteine were combined via native chemical ligation. Consequently, the cysteine was converted to dehydroalanine to obtain a TS2 ABP. **b,** Cross-linking to mimic transition state 2, ubiquitin transfer from ARIH1 to a substrate. The stable mimic contains a thioether bond linking ARIH1’s Cys<sup>cat</sup>, ubiquitin, and the substrate phosphopeptide. This portable strategy was used to generate TS2 ABPs of p27, Cyclin E and I $\kappa$ b $\alpha$ . **c,** SDS-PAGE visualizing size-exclusion chromatography fractions of the Ub-MESNa and phosphopeptide reaction mix producing an TS2 ABP. Figure adapted from [2].

## 2.2.1 Verification and comparison of native CRL-RBR E3-E3 reaction requirements with TS2 ABP conjugation

Going forward with the suite of TS2 ABPs, native determinants of E3-E3 ubiquitylation needed to be paralleled for the probes. Transition State 2 and the Transition State 2 ABPs rely on an additional determinant in comparison to those being necessary for Transition State 1- the cognate substrate-F-box protein pairing. Reaction of TS2 p27 ABP with ARIH1 could be readily detected via SDS-PAGE assay in dependence of ARIH1's Cys<sup>cat</sup> and activation either through neddylated CUL1-RBX1 or mutational relief of ARIH1 autoinhibition (Figure 14a). In the absence of the F-box protein SKP2 or the adaptor CKSHS1, which is required for binding of the p27 phosphodegron to SKP2, no crosslinked ARIH1~ABP species could be observed (Figure 14a). This strongly indicates that the presence of ubiquitin alone is not sufficient for reaction with ARIH1 but reaction is likely driven by the combined affinities of both, ubiquitin and phosphodegron. Dependence on the cognate substrate-F-box protein pairing was tested by incubating TS2 ABPs with unsuitable substrate receptors. Here, high specificity of TS2 ABPs was demonstrated as none of the probes exhibited cross-reactivity (Figure 14b).

E3-E3-catalyzed ubiquitylation was previously show to be an extremely efficient reaction[9] and rapid quench-flow (RQF) experiments with and without SCF substrate demonstrate how product formation in fluorescently-labeled ubiquitylation assays can be observed in a matter of 150 ms (Figure 15a). We next set out to explore how fast

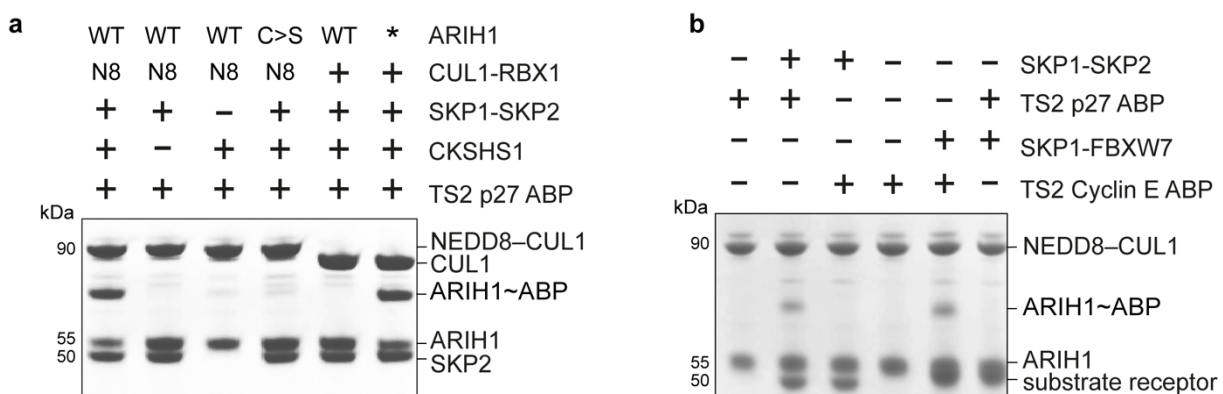


**Figure 14 – Testing native E3-E3 reaction requirements with the TS2 ABP** **a**, SDS-PAGE demonstrating TS2 p27 ABP reaction with ARIH1 requires all elements for native TS2, or use of a mutant version of ARIH1 (ARIH1\*) bypassing the need for NEDD8 for this reaction. **b**, SDS-PAGE testing specificity of TS2 ABPs for cognate F-box proteins. Phosphorylated Cyclin E and p27 are substrates of SCF<sup>FBXW7</sup> and SCF<sup>SKP2</sup>. Figure adapted from [2].

product formation with ABPs occur and how it compares to ubiquitin transfer in the native reactions. Monitoring of stable TS1 mimic formation in an SDS-PAGE assay resulted in faint bands before the five-minute time point but steadily increased until the last one. In contrast to TS1 probing, TS2 mimic formation is only detectable after 15 min incubation while using the same assay conditions. ABP reaction times are much lower compared to the native ubiquitylation reactive and only occurs within minutes while ubiquitylation does so in milli-seconds.

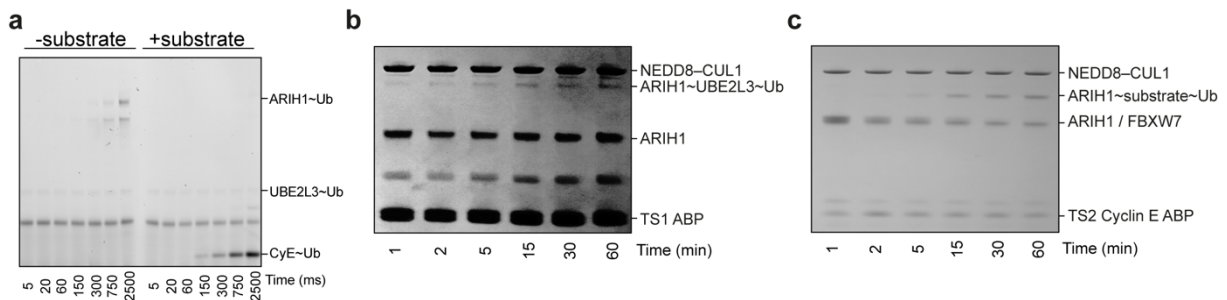


**Figure 15 – Comparing native ubiquitylation versus ABP reaction time scales. a,** SDS-PAGE demonstrating rapid quench-flow assays monitoring ubiquitin transfer from UBE2L3 to ARIH1 (Transition State 1) and ubiquitin transfer from UBE2L3 to Cyclin E via ARIH1/CRL1 (Transition State 1 and 2). **b,** SDS-PAGE monitoring TS1 ABP reaction with ARIH1 to form the stable TS1 mimic ARIH1~UBE2L3~Ub. **c,** SDS-PAGE following TS2 Cyclin E ABP reaction with ARIH1 to form the stable TS2 mimic ARIH1~Cyclin E~Ub. Figure adapted from [2].

## Chapter 3 –

Cryo-EM studies of chemically stabilized Transition State 1 and intermediates enable new insights into transfer from E2 to E3-E3 superassembly

In this chapter, parts of the following publication were integrated:

**Horn-Ghetko, D.**, Krist, D.T., Prabu, J.R., Baek, K., Mulder, M.P.C., Kluegel, M., Scott, D.C., Ovaa, H., Kleiger, G., Schulman, B.A. Ubiquitin ligation to F-box protein targets by SCF–RBR E3–E3 super-assembly. *Nature* **590**, 671–676 (2021).

Display items and text were reprinted with permission from Springer Nature.

### 3.1 Cryo-EM sample preparation & processing

To understand the E3-E3 mechanism, we sought out to determine cryo EM reconstructions of a series of complexes using our proxies and intermediates of the proxies. Because obtaining high quality cryo EM maps is an empirical process, depending on the properties of the multiprotein complexes, we reckoned to make best use of the mix and match principle of SCF ligases and screened several cognate F-box protein/substrate pairs in vitreous ice. Early attempts with un-crosslinked E3-E3 complexes and support films such as carbon or graphene oxide covering the sample grid only yielded low resolution and quality data (data not shown). First structures with sub-nanometer resolution were obtained by performing gradient fixation (GraFix)[130], in which macromolecular complexes undergo mild glutaraldehyde crosslinking during a glycerol gradient. As previously discussed, stable TS1 mimic formation is comparatively slow and complete conversion of ARIH1 to its three-way crosslinked species took several hours to complete. Fortunately, TS1 ABP trapping could occur with all SCF components present without formation of undesired crosslinked

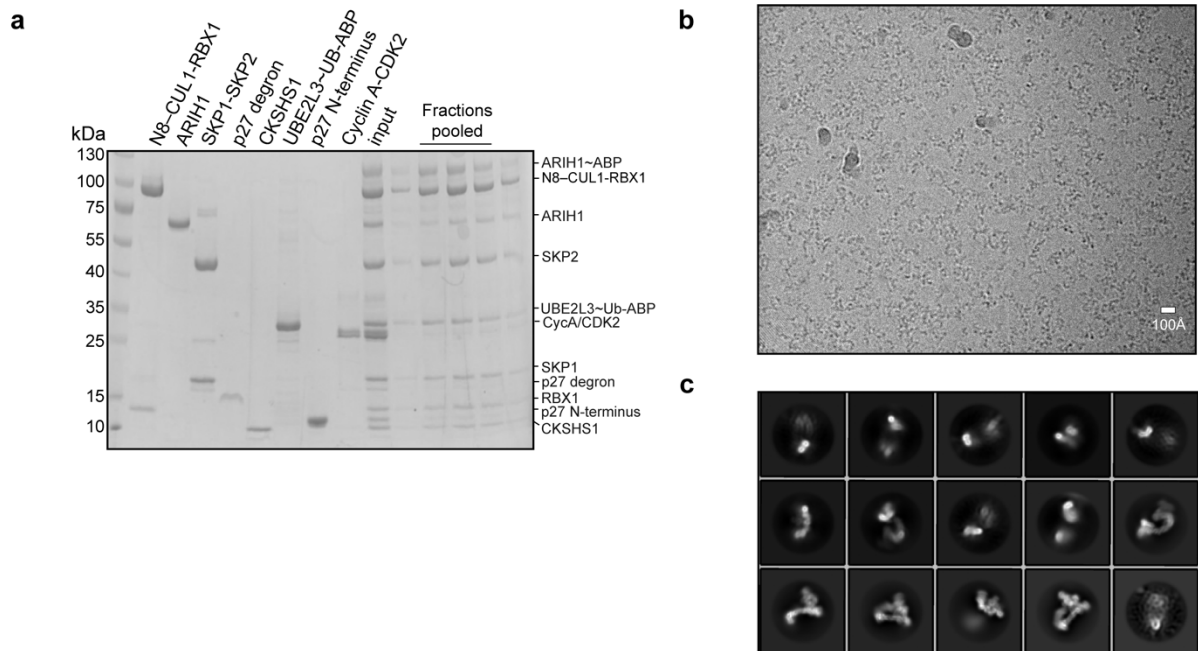


**Figure 16 – Generation of TS1 ABP complex and cryo-EM data.** **a**, SDS-PAGE gel analyzing size-exclusion chromatography fractions of a complex consisting of neddylated SCF<sup>SKP2</sup>, TS1 ABP-coupled ARIH1, p27, CKSHS1, Cyclin A and CDK2. **b**, Representative Cryo-EM micrographs collected on Titan Krios with a pixel size of 1.09Å. Scale bar depicted on bottom right. **c**, 2D class images of Krios dataset starting with five million particles after template-based picking with Gautomatch.

contaminants. We collected data for two neddylated SCF-substrate complexes, including FBXW7 as well as of those containing SKP2/CKSHS1 also bound to a Cyclin A-CDK2-p27 complex. After copurifying our suite of ARIH1-linked ABP reaction products with their cognate SCF complexes, we determined a series of cryo-electron microscopy (cryo-EM) structures at near atomic resolution representing the first step of the E3-E3 ubiquitylation cascade (Figure 16 a-c). In order to determine the full cycle of the E3-E3 cascade, the same Cryo-EM sample preparation pipeline was followed to achieve consistent results. After collection of several thousand micrographs on the Titan Krios microscope, data processing was performed in Relion and followed the same scheme throughout complexes as depicted in Supplementary Figure 8 for the TS1 ABP complex. Here, intensive particle sorting yielded in several classes with some parts of the E3-E3 assembly more prominent than others. With the help of focused, local refinements subcomplexes could be resolved to higher resolution and composite maps of the complete structure stitched together.

### 3.2 Cryo-EM structure of Transition State 1- transfer of ubiquitin from E2 to E3-E3

Cryo EM data for the UBE2L3~ubiquitin~ARIH1 complex with a neddylated SCF<sup>SKP2</sup> assembly were globally refined at 3.8 Å resolution (Supplementary Figure 8, Supplementary data Table 1). Focused reconstructions over the active site at 3.6 Å and over the substrate binding region including the cyclin-dependent kinase complex at 3.5 Å resolution enabled refining the entire UBE2L3~ubiquitin~ARIH1-NEDD8~CUL1-RBX1-SKP1-SKP2-CKSHS1-phosphorylated p27-CDK2-Cyclin A structure. Ubiquitin is readily visualized with its C-terminus poised between the active sites of UBE2L3 and ARIH1's catalytic Rcat domain (Figure 17a-d). Cryo EM data for was also collected for a UBE2L3~ubiquitin~ARIH1 complex with a neddylated SCF<sup>FBXW7</sup> with the Cyclin E phosphodegron bound but only refined to 9.6 Å as collection was performed on a screening microscope (Supplementary table 1).

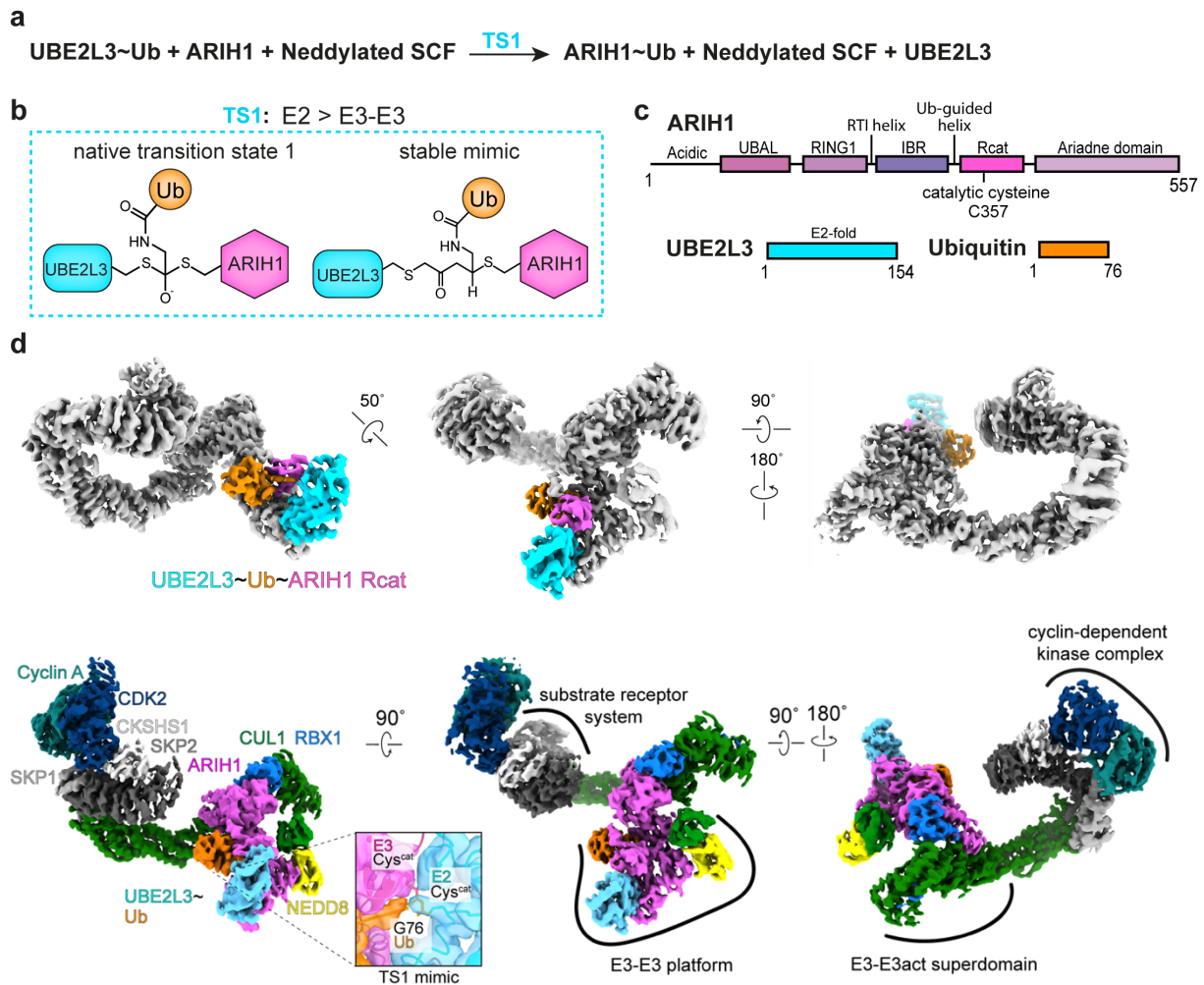


**Figure 17 – Visualizing fleeting transition state 1 in neddylated SCF-ARIH1 RBR E3-E3-catalyzed ubiquitylation** **a**, Neddylated SCF-ARIH1 RBR E3-E3 catalyzes ubiquitylation F-box protein-bound substrates through two transition states whereby ubiquitin’s C-terminus is sequentially handed-over from the catalytic cysteine ( $\text{Cys}^{\text{cat}}$ ) of the E2 UBE2L3 to that of ARIH1 (transition state 1), and then to a substrate’s lysine (transition state 2). **b**, Left, chemical entities in fleeting transition state 1. Right, stable mimic produced by neddylated SCF-dependent ARIH1 reaction with activity-based probe (UBE2L3~Ub-ABP). **c**, ARIH1, UBE2L3 and ubiquitin domain schematic **d**, Top- composite cryo-EM maps representing neddylated  $\text{SCF}^{\text{SKP2}}$ -UBE2L3~ubiquitin~ARIH1 (transition state 1), highlighting the chemically adjoined E2 UBE2L3 (cyan), ubiquitin (orange), and ARIH1 Rcat domain (magenta). Although phospho-p27 and Cyclin A-cdk2 are also in this complex, the corresponding region of the map is not shown for simplification. Bottom- composite cryo-EM maps representing neddylated  $\text{SCF}^{\text{SKP2}}$  UBE2L3~ubiquitin~ARIH1 (transition state 1), highlighting individual subdomain architectures including the substrate receptor system, E3-E3 platform, E3-E3act superdomain and cyclin-dependent kinase complex.

### 3.2.1 Formation of an E3-E3act superdomain is the basis for Ubiquitin transfer by the E3 duo

As previously mentioned, a distinguishing feature of E3-E3 ligases is that interactions between the two individual E3s stimulate ubiquitin ligase activity. This is explained by a central CUL1-RBX1-ARIH1 tri-protein superdomain that amalgamates the two E3s across the evolving catalytic configurations in the E3-E3 ubiquitylation cycle (Figure 17d, Figure 18a, Figure 19a). We consequently term this superdomain “E3-E3act”, reflecting its underlying role in activating ubiquitylation by reversing ARIH1 autoinhibition upon assembly with a neddylation SCF. To form the E3-E3act superdomain, RBX1’s RING reorients and aligns with CUL1’s “CR3” and “4HB” elements. The resultant RBX1-CUL1 surface wraps around roughly half of ARIH1’s Ariadne domain (a 4-helix bundle unique to ARIH-family RBR E3s) (Figure 18b-d). On one side, both RBX1’s canonical E2-binding site and an RBX-specific appendage bind one end of ARIH1’s Ariadne domain and contribute to a 3-way RBX1-CUL1-ARIH1 junction (Figure 18d). The E3-E3act domain is further stabilized by the opposite end of ARIH1’s Ariadne domain binding to CUL1’s CR3 and 4HB subdomains. Notably,

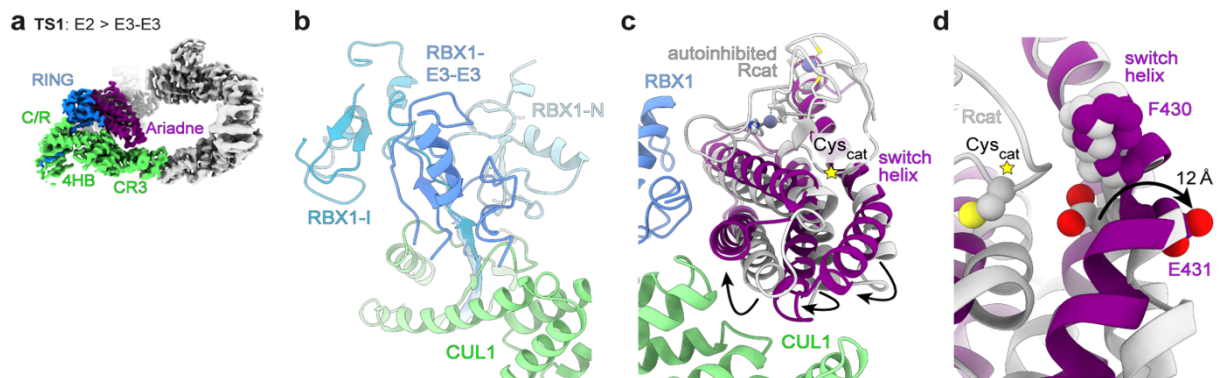


**Figure 18 – A central tri-protein CUL1-RBX1-Ariadne E3-Eact superdomain amalgamates, activates, and directs stepwise neddylation SCF-ARIH1 ubiquitylation a, E3-E3act superdomain with components coloured as in a within composite cryo-EM maps representing transition state 1 (neddylation SCF<sup>SKP2</sup>-dependent ubiquitin transfer from UBE2L3 to ARIH1, top) b, Unique RBX1 RING (blue) and CUL1 (green) arrangement in E3-E3act domain. For reference, the relative RBX1 RING orientations are shown for neddylation in sky (RBX1-N, PDB ID: 4P5O), and in an inhibited complex in teal (RBX1-I, PDB ID: 4F52). c, Superposition of ARIH1’s Ariadne domain bound to CUL1-RBX1 in E3-E3act domain (purple) and without SCF mediating ARIH1 autoinhibition (grey, PDB ID:5UDH). Arrows highlight remodeling upon ARIH1 amalgamation with CUL1-RBX1 causing bend-to-kink activating transition in the “switch helix”. d, Close-up of superposition in c highlighting relocation of switch helix side-chains eliminating the intramolecular latch for ARIH1’s Rcat domain, activating this RBR E3 ligase when bound to the SCF E3 ligase. Figure adapted from [2].**

forming the E3-E3act domain precludes an ARIH1-bound SCF's RING domain from simultaneously activating an E2-type ubiquitin carrying enzyme, in agreement with prior biochemical studies[9] (Supplemental data figure 11b). Comparing Ariadne domain conformations in the E3-E3act superdomain and in autoinhibited ARIH1 reveals twisting accompanying clasping by CUL1-RBX1 (Figure 18c-d). The RBX1-bound region is relatively similar in autoinhibited ARIH1. However, the opposite end of the Ariadne domain is bent when bound to CUL1. This effectively switches ubiquitylation "on", through a 165°-to-125° bend-to-kink transition of a helix, located in ARIH1s Ariadne domain between residues Phe430 and Glu431 (Figure 18c-d). In the absence of a neddylated SCF, these residues face into the Ariadne domain and secure intramolecular interactions with ARIH1's Rcat domain and the following loop. However, in the context of the E3-E3act superdomain, the Glu431 side chain has made an about-face 12Å translation from the center of the Ariadne helical bundle, accompanied by 4 Å outward shifting of Phe430 and relocation of neighboring residues. The occurring kink, in what is now termed as "switch helix", eliminates the intramolecular latch for ARIH1's Rcat domain, thereby relieving autoinhibition and triggering E3-E3 ligase activity (Figure 18c-d). The E3-E3act superdomain also positions the two E3s relative to each other. With ARIH1's Ariadne domain binds the distal end of CUL1-RBX1, each ARIH1-catalyzed ubiquitin transfer reaction connects to hallmark SCF attributes, which include neddylation and substrate recruitment.

### 3.2.2 Transfer of Ubiquitin from E2 to E3-E3 depends on release of autoinhibition by NEDD8 and RBX1

The E3-E3 mechanism depends on neddylation: previous studies showed that ARIH1 binding to endogenous cellular CRLs requires their neddylation and in vitro biochemical studies revealed that cullin neddylation specifically stimulates the first transition state[9,99,111,131]. The EM structure representing this shows ARIH1's Cys<sup>cat</sup> is positioned to receive ubiquitin in an intricate multiprotein assembly that includes NEDD8. This assembly is anchored to and extends 70 Å vertically from the E3-E3act superdomain (Figure 19a-b), and is configured from: (1) the UBE2L3~ubiquitin conjugate, which carries ubiquitin to ARIH1's Cys<sup>cat</sup>; (2) an E3-E3 platform consisting of ARIH1 elements (UBAL, RING1, RTI (RING1-To-IBR) helix, and IBR) and NEDD8 isopeptide-linked to CUL1's WHB domain; and (3) ARIH1's catalytic Rcat domain and a preceding "Ub-guided helix" (Figure 19b).

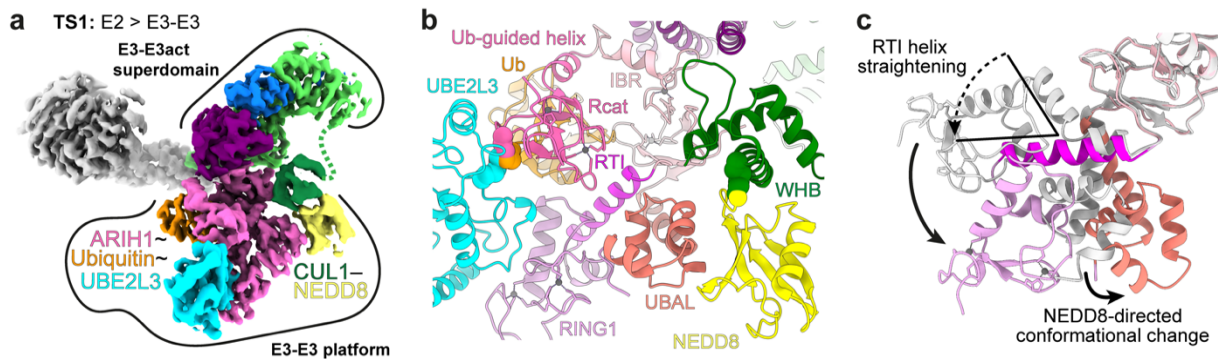


**Figure 19 – E3-E3 transition state 1 catalytic configuration** **a**, Composite cryo-EM map representing transition state 1 (neddylated SCF-dependent ubiquitin transfer from the E2 UBE2L3 to ARIH1) with key catalytic elements coloured. **b**, Close-up of intricate catalytic assembly for transition state 1. UBE2L3~ubiquitin is displayed by a multidomain, multiprotein platform. ARIH1's Ub-guided helix and ensuing Rcat domain bound to ubiquitin form a “ubiquitin transferase module”. **c**, Superposition of ARIH1's UBE2L3~ubiquitin binding elements, in the active E3-E3 (coloured as in **b**) or autoinhibited conformation (grey, PDB ID; 5UDH). Arrows highlight relative remodeling. Figure adapted from [2].

On one side of the E3-E3 platform, UBE2L3~ubiquitin is recruited and bound by ARIH1 RING1, RTI helix and IBR domains (Figure 19a-b). ARIH1's unique UBAL domain is located opposite of where Ubiquitin contacts ARIH1's Ub-guided helix. The UBAL also binds NEDD8 conformationally activated by noncovalent packing with its covalently-linked CUL1 WHB domain. Notably, this NEDD8–CUL1 configuration also activates UBE2D-catalyzed ubiquitylation of neddylation SCF<sup>β-TRCP</sup> substrates (Supplementary figure 11d-e). However, the NEDD8–CUL1 WHB unit faces the opposite direction and is relatively repositioned by  $\approx 70$  Å to bind ARIH1. The catalytic E2~ubiquitin~ARIH1 arrangement, which was not observed in the absence of a neddylation SCF, depends on ARIH1-specific and neddylation SCF elements and rationalizes critical domains and side-chains identified by comprehensive mutagenesis (Figure 19b, Supplementary figure 12a-c) [9]. NEDD8 and its linked CUL1 WHB domain restrict relative positions of ARIH1's UBAL, RTI-helix and IBR elements. Meanwhile, large-scale restraints are imposed by intramolecular interactions involving the E3-E3act superdomain: CUL1's WHB domain is connected to the rest of CUL1; and ARIH1's IBR and Ariadne domains pack against each other. Comparing activated and autoinhibited ARIH1 configurations with their Ariadne domains aligned, shows that binding the active conformation of the UBE2L3~ubiquitin conjugate involves ARIH1 RING1 and IBR subdomain rotations, which includes  $\approx 35^\circ$  adjustment of the RTI-helix and consequent  $\approx 35^\circ$  rotation of ARIH1's UBAL domain toward CUL1's WHB domain (Figure 19c). Lastly, in the structure representing transition state 1, two additional ARIH1 elements capture the

UBE2L3-linked ubiquitin in a canonical RBR catalytic configuration (Figure 19b, Supplementary figure 11f). A “Ub (ubiquitin)-guided helix” – previously an autoinhibitory loop– binds ubiquitin’s Ile44 hydrophobic patch. The Rcat domain embraces ubiquitin’s C-terminal tail, the UBE2L3~ubiquitin active site, and E2 catalytic loops (Supplementary figure 11f). Additionally, Rcat residues at the start of the domain bind ubiquitin’s C-terminal tail in a  $\beta$ -sheet, which ends with ARIH1s catalytic cysteine.

### 3.3 Cryo-EM structures of Transition State 1 intermediates

The TS1 mimic demonstrated how the Rcat domain receives ubiquitin from UBE2L3 and how positioning and remodeling of other domains lead to proper configuration of the Rcat from its autoinhibited conformation. Prior studies have been utilizing UBE2L3 (Cys86Lys) with an isopeptide-linked ubiquitin to study its interaction with ARIH1 in crystallization trials[105,106]. While much was learned about the binding mode of UBE2L3 and ubiquitin to ARIH1, the position of ubiquitin was not fixed and multiple conformations were observed. We set out to study UBE2L3~Ub binding- without reactive moiety in-between- in the context of the E3-E3 superassembly. In the pre-TS1 intermediate, structures of the isopeptide-linked UBE2L3~ubiquitin was utilized to obtain cryo-EM structures (Figure 20a-b). In this intermediate ARIH1’s Rcat domain

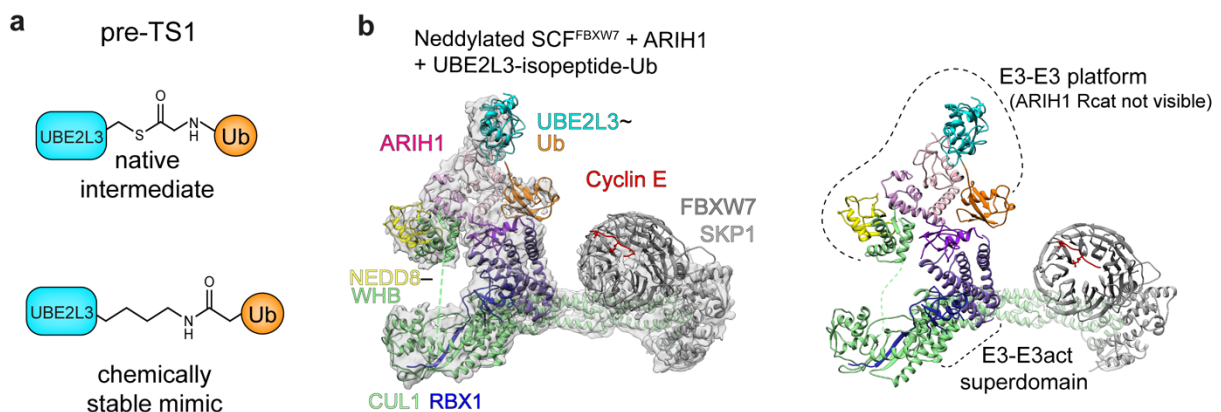


**Figure 20 – Strategy to stabilize the pre-TS1 intermediate and Cryo-EM structures-** **a**, In the pre-TS1 intermediate ubiquitin is linked to the E2 UBE2L3 via a thioester bond and ready to be transferred to ARIH1’s Cys<sup>cat</sup>. The native intermediate is mimicked by replacing the Cys<sup>cat</sup> of ARIH1 with a Lysine and coupling it to ubiquitin C-terminus via isopeptide bonding. **b**, Cryo-EM model with docked ribbon diagram (left) and ribbon diagram (right) of the Neddylated SCF<sup>FBXW7</sup>-ARIH1-UBE2L3~Ub complex. ARIH1’s Rcat is not visible in the pre-TS1 intermediate as it is presumably flexible. Figured adapted from [2].

is not visible, and presumably mobilized through liberation from autoinhibition by the Ariadne domain (Figure 20b). However, ubiquitin was in the same relative position as in the TS1 structures suggesting ubiquitin is locally stabilized through molecular interactions even in the absence of the Ub-guided helix formed by linked between Rcat and IBR domains.

Another way of generating the pre-TS1 intermediate is to skip the acidic deprotection step during the formation of the TS1 ABP (Figure 21a). In principle, this would yield an  $\alpha,\beta$ -unsaturated ketone, however, the synthesis product was not pure. Although this greatly compromised the reactivity of the ABP towards ARIH1's catalytic cysteine, cryo-EM grids were fortuitously prepared after mixing with neddylated SCF<sup>FBXW7</sup>-Cyclin E substrate peptide and ARIH1, data were collected and maps were interpretable for two 3D classes.

Docking structures into one of the classes indicate that this configuration represents the conformational intermediate pre-TS1 (left) and another configuration with ubiquitin loaded onto ARIH1, but with ARIH1 also bound to another UBE2L3~ubiquitin intermediate ready to reload ARIH1's active site after its bound ubiquitin would be transferred to the F-box protein-bound substrate (Figure 21b). Notably, this UBE2L3~ubiquitin-E3-E3 configuration may represent an intermediate along the

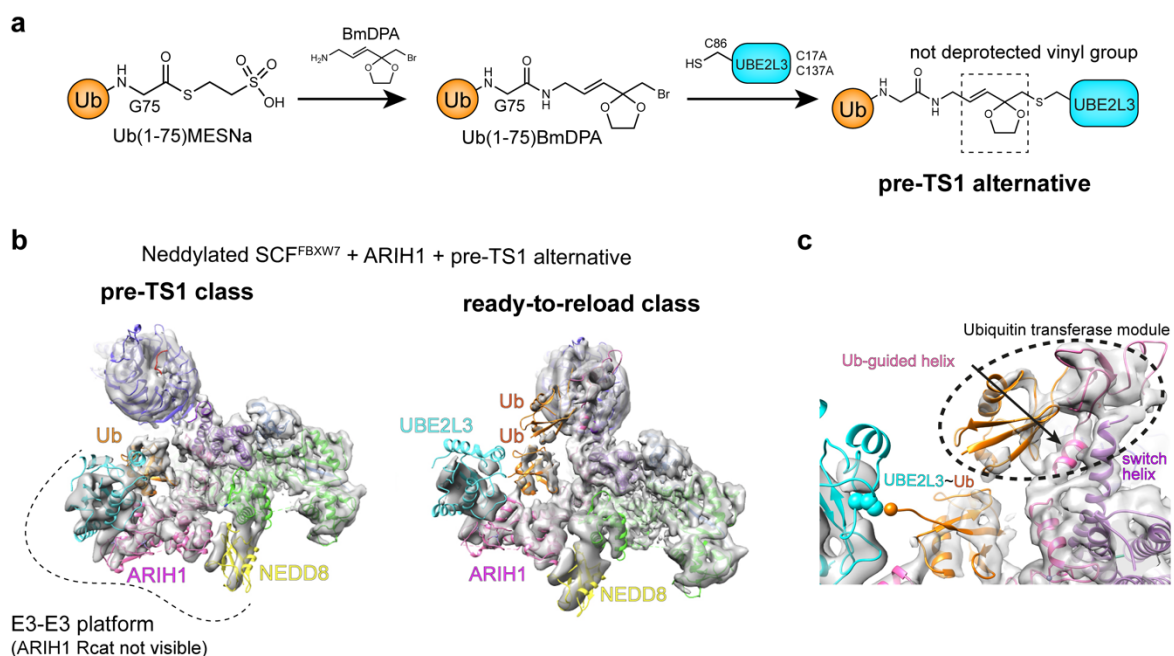


**Figure 21 – Cryo-EM maps of complex between neddylated SCF<sup>FBXW7</sup>-Cyclin E substrate peptide, ARIH1, and a non-activated TS1 ABP reveal two additional intermediate E3-E3 configurations. a**, Synthesis of the non-deprotected TS1 ABP (pre-TS1 alternative). Ub-(1-75)-MESNa was coupled to BmDPA. **b**, Cryo-EM map of the two classes with ribbon diagrams of docked structures. **c**, Close-up of the ready-to-reload intermediate.

conformational trajectory toward the transition state. In this EM map, the ubiquitin transferase module is even further rotated in this EM map than in the reconstructions representing transition state 2 (Figure 21c).

# Chapter 4 –

Cryo-EM of chemically stabilized Transition State 2 and biochemical assays reveal mechanism for E3-E3-catalyzed ubiquitylation of SCF substrates

In this chapter, parts of the following publication were integrated:

**Horn-Ghetko, D.**, Krist, D.T., Prabu, J.R., Baek, K., Mulder, M.P.C., Kluegel, M., Scott, D.C., Ovaa, H., Kleiger, G., Schulman, B.A. Ubiquitin ligation to F-box protein targets by SCF–RBR E3–E3 super-assembly. *Nature* **590**, 671–676 (2021).

**Horn-Ghetko, D.**, Schulman, B.A. New classes of E3 ligases illuminated by chemical probes. *Current Opinion in Structural Biology* **73**, (2022)

Display items and text were reprinted with permission from Springer Nature and Elsevier.

## 4.1 Cryo-EM structures of Transition State 2

The second step of the E3-E3 transfer cascade includes ubiquitin transfer from ARIH1 to SCF substrate (Figure 22a-b). We made best use of the versatile TS2 ABP strategy and screened several F-box proteins in the context of the E3-E3 superassembly TS2 mimic. The TS2 ABP synthesized with a p27 phosphopeptide substrate of SCF<sup>SKP2</sup> enabled a cryo EM structure visualizing E3-E3 ubiquitin targeting at 3.9 Å resolution (Supplementary data Table 1). The map quality allowed docking of many E3-E3 components, including the ubiquitin transferase domain adjacent to SCF<sup>SKP2</sup>-bound p27, and revealed side-chains for some regions (Figure 22d). Structures of other SCFs included SCF<sup>FXBW7</sup> at 3.6 Å with Cyclin E as substrate and SCF<sup>β-TRCP2</sup> with Iκbα at 7.8 Å resolution with the processing scheme being similar for all TS2 complexes (supplementary figure 9). Comparing the cryo EM maps for the two E3-E3 transition states reveals some common features and but different configurations for the catalytic elements (Figure 22d). The active sites for neddylated SCF<sup>SKP2</sup>-dependent ubiquitin transfer from UBE2L3 to ARIH1 and from ARIH1 to SKP2-bound p27 are widely separated, by ≈60 Å. The transition state 2 structure, demonstrating the exact moment in which ubiquitin is transferred from ARIH1 to substrate, displays distinct catalytic configuration, but also share common multiprotein domains with those mediating E3-E3 ubiquitin transfer to ARIH1.

### 4.1.1 Ubiquitin transfer from E3-E3 to substrate involves relocation of the ubiquitin transferase module

Both transition states revolve around the E3-E3<sup>act</sup> superdomain, consistent with prior mutational results[9] (Figure 23a, Supplementary figure 12a). and display a catalytic “ubiquitin transferase module”, with structurally similar ubiquitin binding by ARIH1’s Ub-guided helix and Rcat domain (Figure 22d, Figure 23c). However, for the active site to face the SKP2-bound substrate, the ubiquitin transferase module is rotated ≈90° about the E3-E3<sup>act</sup> superdomain (Figure 23b). On the other side of the E3-E3<sup>act</sup> superdomain, ARIH1’s UBAL, RING1, RTI-helix, and IBR elements are poorly resolved and presumably dynamic in the absence of UBE2L3~ubiquitin, ready to load ARIH1. Ubiquitin is projected toward SKP2 by ARIH1’s Ub-guided helix, which is blocked in its ability to extend further extend by a straight extension of ARIH1’s switch helix beyond

the E3-E3act superdomain (Figure 23c). Several EM map properties suggest this arrangement restricts the F-box protein-bound substrate and ARIH1~ubiquitin active

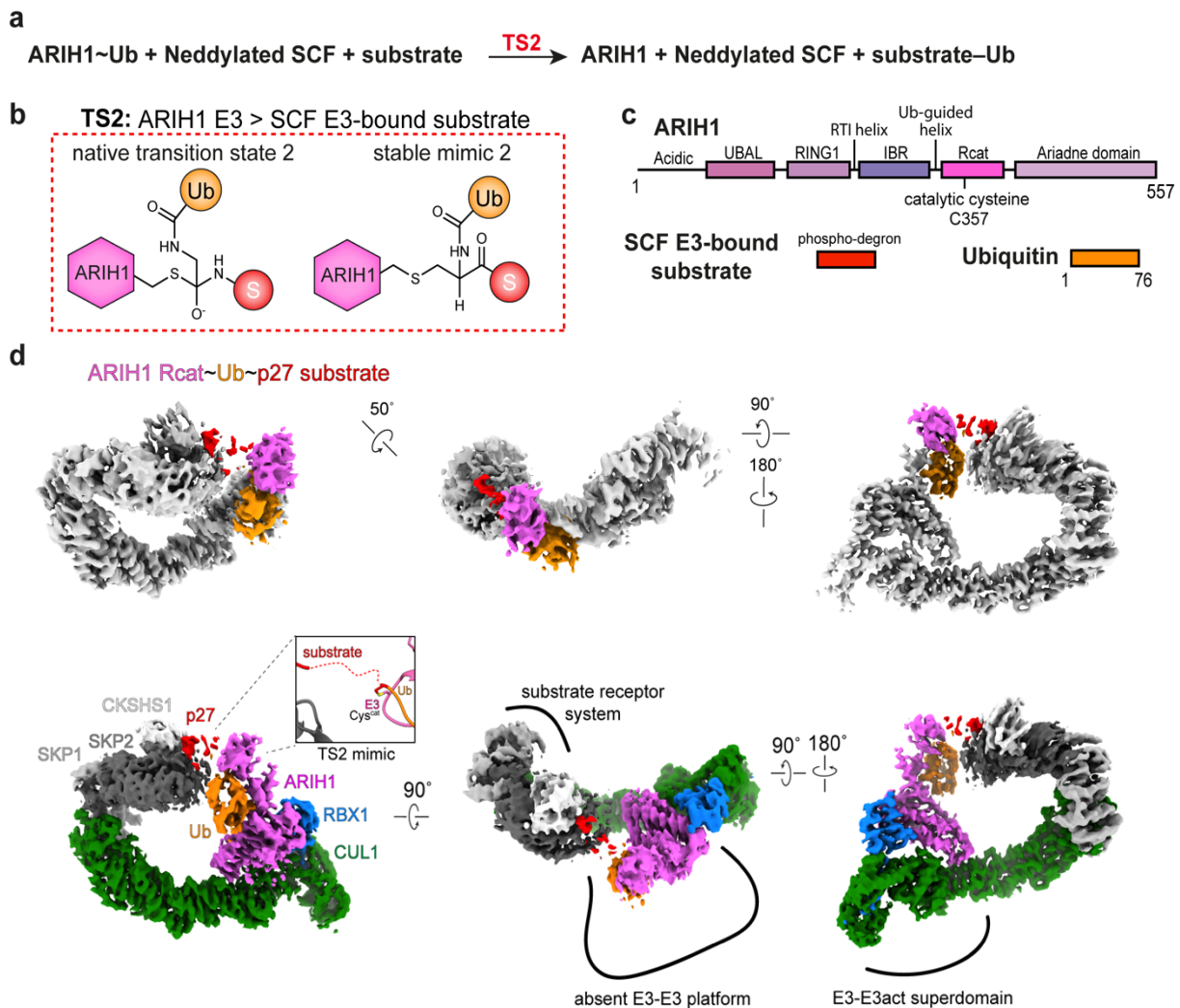


**Figure 22 – Visualizing fleeting transition state 2 in neddylated SCF-ARIH1 RBR E3-E3-catalyzed ubiquitylation** **a**, Neddylated SCF-ARIH1 RBR E3-E3 catalyzes ubiquitylation of an F-box protein-bound substrate through two transition states whereby ubiquitin’s C-terminus is transferred from the catalytic cysteine ( $\text{Cys}^{\text{cat}}$ ) of the E2 UBE2L3 to that of ARIH1 (transition state 1), and then to a substrate’s lysine (transition state 2). **b**, Left, chemical entities in native, fleeting transition state 2. Right, stable mimic produced by neddylated SCF-dependent ARIH1 reaction with activity-based probe (TS2 p27 ABP). **c**, ARIH1, substrate and Ubiquitin domain schematic. **d**, Top- Cryo-EM map representing E3-E3 substrate ubiquitylation (transition state 2), highlighting the adjoined ARIH1’s catalytic Rcat domain (magenta), ubiquitin (orange), p27 substrate (red). Bottom- cryo-EM maps representing neddylated SCF<sup>SKP2</sup> UBE2L3~ubiquitin~ARIH1 (transition state 2), highlighting individual subdomain architectures including the substrate receptor system and E3-E3act superdomain. Note: ARIH1\* and unneddylated SCF was used to improve the EM map quality, as the E3-E3 platform could not be resolved to high resolution even in neddylated complexes.

site within a confined zone, allowing it to move marginally. Comparing the two major classes shows the F-box protein and its recruited substrate in similar positions, varying by  $\approx 10^\circ$  relative to the ubiquitin transferase module and E3-E3act superdomain (Figure 24b). Importantly, both classes direct the peptide p27 substrate toward the ubiquitin transferase active site. Another indication for the flexibility of the ubiquitin transferase module is the relatively poorer resolution than the neighboring E3-E3act superdomain. This could reflect variability in their relative position. This mobility is consistent and much needed with the major relocation of the ubiquitin transferase module occurring after the transition state switch (Figure 23b). The ubiquitin transferase module can rotate even further as mentioned previously. ARIH1's Ub-guided helix is rigidly connected to the Rcat domain's N-terminus, while the Rcat's C-terminus extends into the switch helix extension. This extension bends by  $\approx 90^\circ$  for the Ub-guided helix and

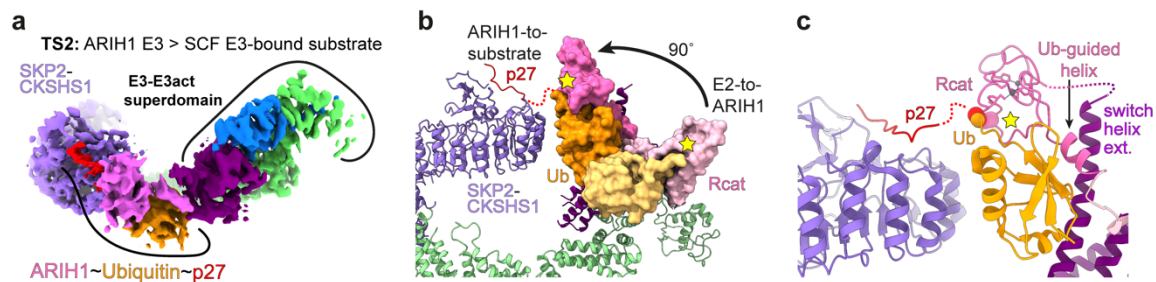


**Figure 23 – E3-E3 transition state 2 catalytic configuration** **a**, Composite cryo-EM map representing transition state 2 (ubiquitin transfer from ARIH1 to SKP2-bound phospho-p27) with key elements coloured. **b**,  $\approx 90^\circ$  reorientation of the ubiquitin transferase module comprising ARIH1's Rcat and Ub-guided helix bound to ubiquitin between transition state 1 (light pink/orange) and 2 (dark pink/orange), after superimposing the two structures over CUL1 and the E3-E3act domain. Active site is denoted with yellow star. **c**, Close-up of transition state 2. Figure adapted from [2].

Rcat domain to capture UBE2L3-linked ubiquitin. However, the straight helix conformation, which may be energetically favored, barricades the ubiquitin transferase module with the active site adjacent to and facing the F-box protein bound substrate.

#### 4.1.2 Other SCF systems

Refinement of the data for the well-studied Fbox protein FBXW7 showed E3-E3 targeting its Cyclin E phosphopeptide substrate engaged via FBXW7's  $\beta$ -propeller domain. This differs from SCF<sup>SKP2</sup>, whose concave leucine-rich repeat domain enwraps its partner CKSHS1 to co-recruit phosphorylated p27, either with or without

additional association with a Cyclin-CDK complex. The cryo-EM maps representing SCF<sup>FBXW7</sup>, SCF<sup>β-TRCP2</sup> and SCF<sup>SKP2</sup> TS2 intermediates demonstrate how ARIH1s active site and the ubiquitin transferase module is still next to the diverse SCF substrate, bound to several F-box proteins (Figure 24a).

We used the catalytic configurations of Transition State 2 to model E3-E3 ubiquitylation of the folded substrate cryptochrome (Supplementary Figure 14d-e). By doing so, we could see how the E3-E3 mechanism could accommodate the folded substrate while being in range for ubiquitylation. The E2-E3 mechanism, however, is not suitable to target Cryptochrome for ubiquitylation as the gap between active site of the E2 and substrate's lysine is too big to allow ubiquitylation (Supplementary Figure 14e).

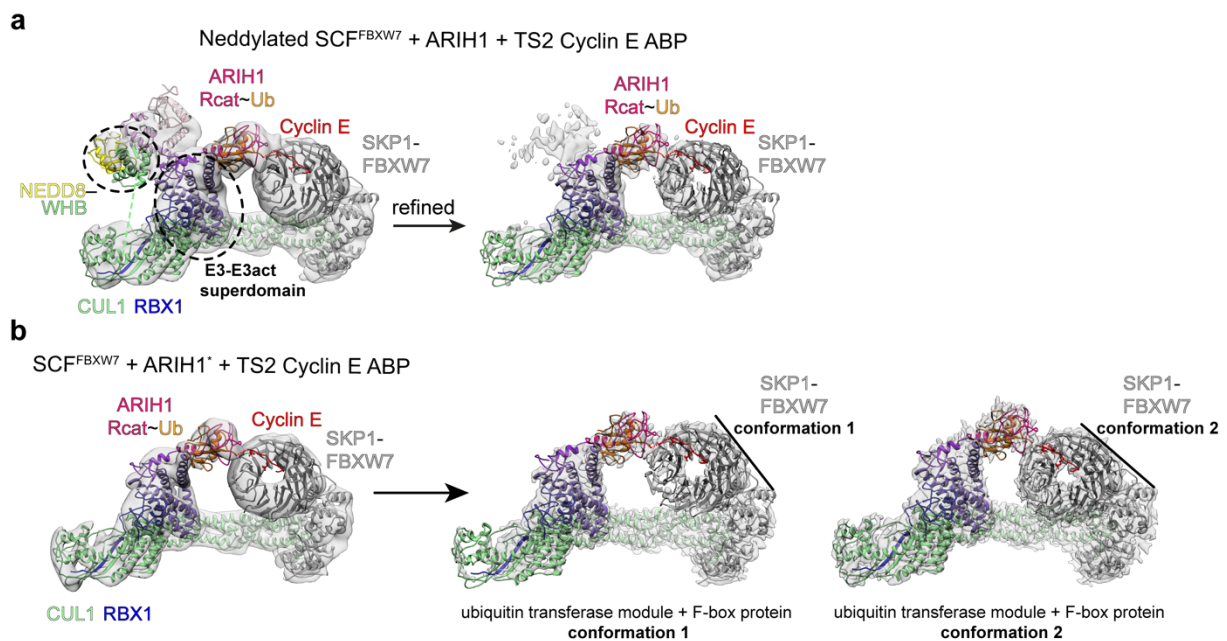


**Figure 24 – Cryo-EM maps of neddylated TS2 assembly and structural heterogeneity.**

**a**, 3D class from the complex representing neddylated SCF<sup>FBXW7</sup>-dependent ubiquitin transfer from ARIH1 to Cyclin E phosphopeptide substrate (captured with TS2 Cyclin E ABP). The ribbon diagram corresponds to SKP1-FBXW7-Cyclin E from a prior crystal structure (PDB ID: 2OVQ), CUL1-RBX1 and the ubiquitin transferase module (ubiquitin linked to ARIH1, bound to the Rcat domain and Ub-guided helix) from the refined structure with SKP2. Upon refinement of the 3D structure to higher resolution, the E3-E3 platform (ARIH1's UBAL, RING1, RTI helix, and IBR and NEDD8 isopeptide-linked to CUL1's WHB domain) disappears and superimposes with the structures for unneddylated SCF<sup>FBXW7</sup> and ARIH1\* captured with the same ABP. **b**, two conformations of TS2 obtained by major classification of the Cryo-EM data are shown in middle and right. Although the conformations differ in their relative positions of the substrate-bound Fbp FBXW7 and ubiquitin transferase module, in both, ARIH1's Ub-guided helix and Rcat domain direct ubiquitin's C-terminus toward the Fbp-bound substrate. Figure adapted from [2].

### 4.1.3 Cryo-EM structures of a Transition State 2 intermediate

Another intermediate of the E3-E3-catalyzed ubiquitylation is visualized with a simpler version of activity-based probes- ubiquitin-vinylmethylester. It mimics the intermediate occurring after ARIH1 has received ubiquitin from UBE2L3 and is on its way to pass it onto the substrate. Cryo-EM data of the SCF<sup>FBXW7</sup> ARIH1~UbVME complex could be classified into three classes (Figure 25a-c). In the most abundant class, the superdomain class, catalytic domains are not visible. However robust signal for the E3-E3 ubiquitylation defining E3-E3act superdomain was obtained. In the pre-TS1 class, a similar conformation could be observed as in the pre-TS1 intermediate. Here, UBE2L3 is bound to ARIH1s RING domain and NEDD8 contacts the UBAL domain. In comparison to the pre-TS1 intermediate, ubiquitin is not present.

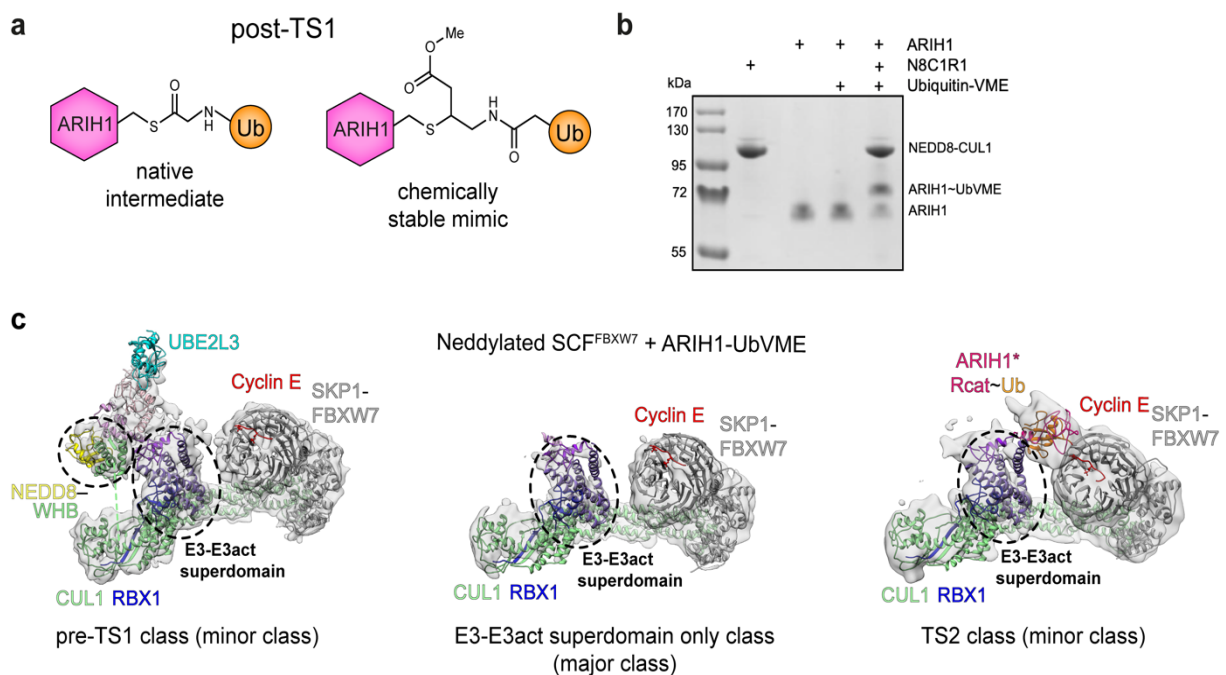


**Figure 25 – Strategy to stabilize the post-TS1 intermediate and Cryo-EM structures-** **a**, In the post-TS1 intermediate, ubiquitin is linked to ARIH1's Cys<sup>cat</sup> via thioester bond. The chemically stable mimic utilized ubiquitin-vinylmethylester (UbVME) to pair ubiquitin to ARIH1's Cys<sup>cat</sup>. **b**, SDS-PAGE demonstrating reaction of UbVME with ARIH1 in dependence of neddylated Cullin. **c**, Cryo-EM structures for the post-TS1 intermediate. Figure adapted from [2].

The scarcest class mimics the conformation of Transition State 2, only displays low resolution density for what might possibly be the ubiquitin transferase module hovering over same location as in Transition State 2. We also set out to prove that how ARIH1 blocks other ubiquitin carrying enzymes once it is bound to ubiquitin on a cullin. For this purpose, we used the stable ARIH1~UbVME proxy in ubiquitylation assays

together with UBE2R or UBE2D demonstrating the proxy inhibiting ubiquitylation (Supplementary data Figure 14f-g). When using an inactive version of ARIH1 (Cys357Ala), however, no ARIH1-mediated inhibition was visible, suggesting only ubiquitin-free ARIH1 could disassemble from the cullin.

## 4.2 Determination of kinetic ubiquitylation parameters and comparison to the E2-E3 mechanism

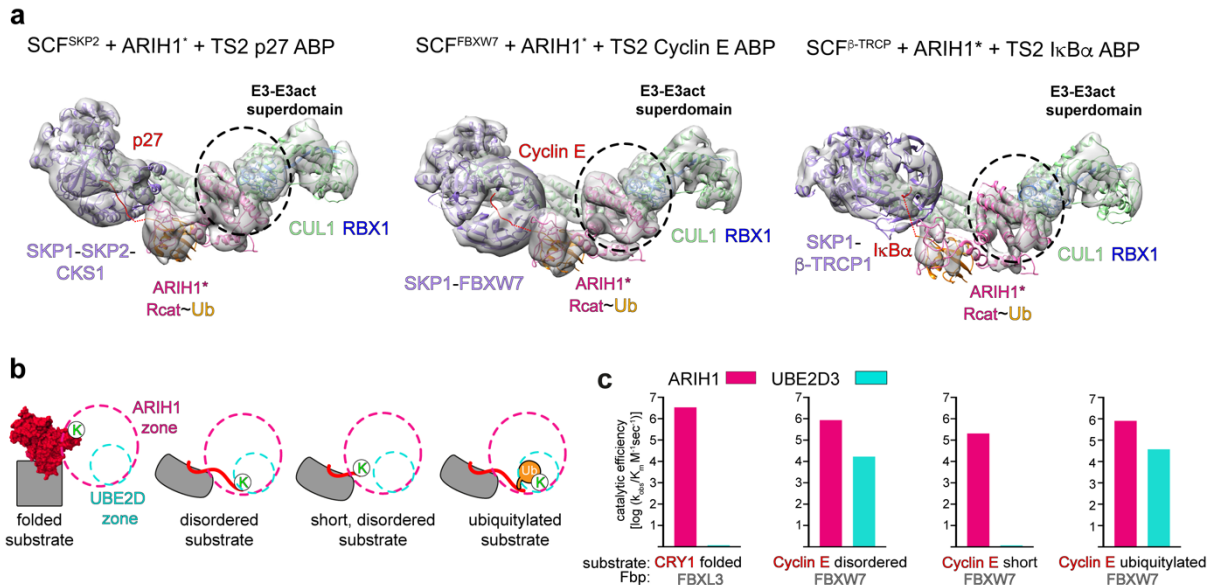


**Figure 26 – ARIH1 ubiquitylation of various substrates recruited to F-box proteins via transition state 2 - a**, The catalytic architecture for transition state 2 - ubiquitin transfer from ARIH1 to an SCF-bound substrate - is conserved for three structurally-divergent F-box protein-substrate assemblies, and for complexes with a neddylated SCF and WT ARIH1 or an SCF lacking NEDD8 and with ARIH1\* (F430A, E431A, E503A) previously shown to relieve autoinhibition and bypass the need for neddylation for transition state 1. (left) Ribbon diagram for the final refined model docked a low-pass filtered cryo-EM map for one of these, SCF<sup>SKP2</sup>. This structure comprises ARIH1\*~ubiquitin~phospho-p27-bound CKSHS1-SKP2-SKP1-CUL1-RBX1, captured with our TS2 p27 ABP. The middle structure shows the cryo-EM map for a complex SCF<sup>FBXW7</sup>, whose substrate-binding domain is a 7-bladed WD40 β-propeller, captured with the TS2 Cyclin E ABP. The ribbon diagram corresponds to SKP1-FBXW7-Cyclin E from a prior crystal structure CUL1-RBX1 and the ubiquitin transferase module (ubiquitin linked to ARIH1, bound to the Rcat domain and Ub-guided helix) from the refined structure with SKP2 (left). The right map displays the cryo-EM 3D model for a complex with SCF<sup>β-TRCP</sup>, captured with the TS2 IκBα ABP. This explains ARIH1's capacity to collaborate with neddylated SCF<sup>β-TRCP</sup> to ubiquitylate IκBα, albeit with lower efficiency than the conventional mechanism whereby RBX1's RING collaborates with the E2 UBE2D. **b**, Cartoons of different F-box proteins (grey) with substrates (red) relative to zones accessible to ubiquitin-linked active sites of ARIH1 (pink) and UBE2D (cyan) based on structural modeling. **c**, Graphs showing mean value of catalytic efficiencies ( $k_{obs}/K_m$ ) for ARIH1 (pink) and UBE2D3 (cyan) mediated ubiquitylation with indicated substrate-Fbp, as depicted in b, N=3 independent experiments. Figure adapted from [2].

To take the generalizable E3-E3 concept a step further, we determined the kinetic parameters of the E3-E3 and E2-E3 mechanism with a range of substrates. In order to do so, we performed rapid quench-flow experiments to obtain catalytic efficiencies and quantitatively compare them later on (Figure 25b-c). We designed experiments in a way to cover different shapes and sizes of substrates and included the folded substrate Cryptochrome, the disordered substrate Cyclin E, a truncated version of the disordered substrate Cyclin E, and a ubiquitylated version of Cyclin E to mimic chain extension. As expected, the catalytic efficiencies for the E3-E3 mechanism were in the same range across all tested SCF substrates. However, a big difference could be observed for the conventional E2-E3 mechanism with UBE2D3. While UBE2D3 is very efficient for SCF<sup>β-TRCP</sup> with its lengthy substrate Iκba, no ubiquitylation could be detected either for the folded substrate or the truncated version of the disordered substrate. This implies that some substrates cannot adopt the optimal geometry that is required for ubiquitylation by the conventional E2-E3 mechanism and are dependent on ubiquitylation by the E3-E3 mechanism.

### 4.3 Comparison of ARIH1-CRL1 and ARIH2-CRL5 E3-E3s

As with ARIH1 and CRL1, both E3 ligases are inactive on their own. Due to the high homology of ARIH1 and ARIH2, accounting up to 40% sequence identity in the same domains, it was anticipated that autoinhibited ARIH2 would fully superimpose with autoinhibited ARIH1. On top of that, CRL1-RBX1 and CRL5-RBX2 are also highly homologous, undeniably leading to the expectation of the neddylated CRL5-RBX2 ARIH2 super-assembly fully superimposing with the other E3-E3 super-assembly. Surprisingly, CUL5-linked NEDD8 neither contacts nor approaches ARIH2 unlike the close interaction of ARIH1's UBAL domain with NEDD8[132] (Figure 26b-c). Instead, NEDD8 binds two domains from CUL5 thereby remodeling the CUL5 structure to expose cryptic binding sites for ARIH2. ARIH2's N-terminal acidic tail tethers the now accessible groove guided by a basic gate in the Cullin. This explains the absolute necessity of ARIH2's N-terminus for its ubiquitylation activity whereas ARIH1's homologous acidic N-terminus is not obligatory. Additionally, upon closer inspection of the autoinhibited ARIH2 structure, several domains including RING1, RING-to-IBR helix and IBR are already aligned in the active configuration even without neddylated

CRL bound. For ARIH1 and other RBRs such as HOIP and Parkin, the activated configuration is only achieved when activating regulatory factors come into effect[2,133]. The strikingly distinct CRL-ARIH E3-E3 assemblies demonstrate how closely related E3 ligases have evolved different mechanisms to achieve the same output and their way to recognize UBL modifications can vary substantially.

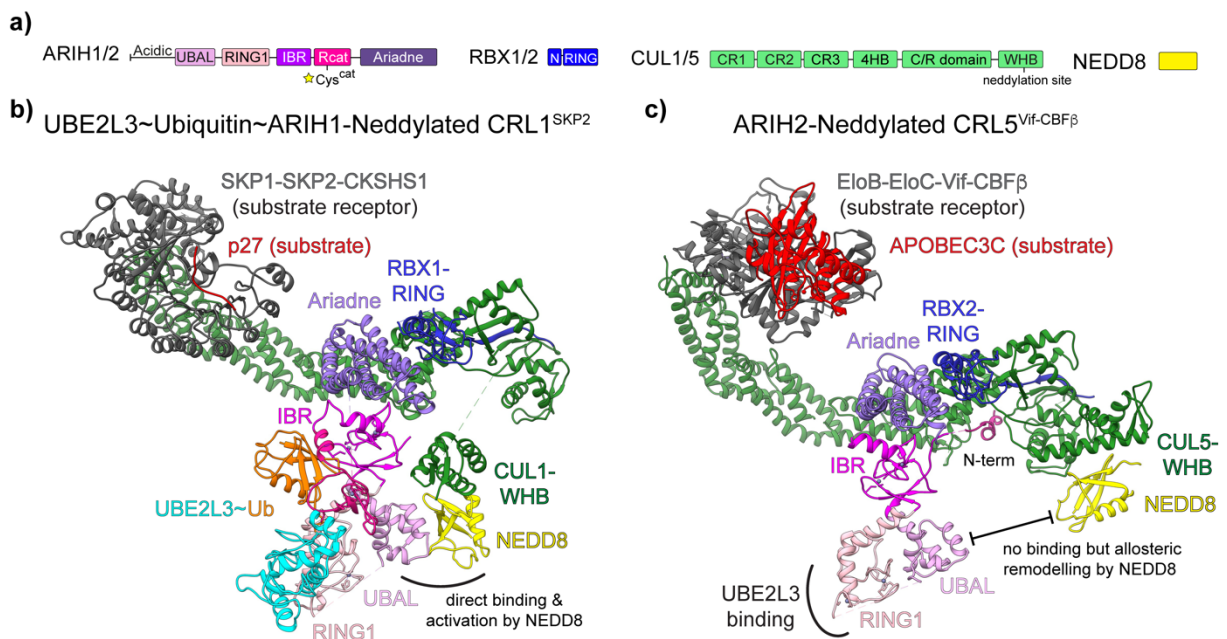


**Figure 27 –Comparison of structural mechanisms of CRL-RBR E3-E3 super-assemblies.**

**a**, E3-E3 assemblies schematically color-coded by proteins and domains. Catalytic cysteines (Cys357 for ARIH1, Cys310 for ARIH2) in Rcat domains are indicated with yellow star. CRL neddylation site is indicated on WHB domain (K720 for CUL1, K724 for CUL5). C/R, cullin–RBX; N, N-terminus. **b**, UBE2L3~UB ABP-guided structure of neddylated CRL1-ARIH1 in presence of SKP2 substrate receptor system. Ubiquitin is transferred to ARIH1’s catalytic cysteine after direct activation and concomitant release of autoinhibitor by neddylated CRL1. **c**, Neddylated CRL5<sup>Vif-CBF $\beta$</sup> -ARIH2 assembly with domains coloured according to **a**). UBE2L3 binding is indicated on ARIH2’s RING1 domain. In contrast to the ARIH1-CRL1 assembly, NEDD8 modification of CRL5 promotes conformational changes in CRL5 to create new binding sites for ARIH2’s N-terminus and thereby allosterically leads to the assembly with ARIH2. Figure adapted from [12].

# Chapter 5 – Discussion

## 5.1 A suite of ABPs to tackle structural endeavors and open up new routes

Our activity-based probes powerfully demonstrate their ability to react with ARIH1 in a neddylated SCF-dependent manner. Their reactivity highly depends on the native determinants of the E3-E3 ubiquitylation cascade and mimics native reaction conditions. This allows their utilization beyond serving as stable transition state mimics and allows to employ them as sensor for mutational effects. This is particularly useful because mutational effects can be mapped to a specific transition state instead of speculating which step of the cascade might be hindered. The formation of a crosslinked ABP~E3 species serves as quite simplistic readout and could be further facilitated by attaching fluorescent tags to the ABP. While readout is facile, heavy temporal optimization needs to be performed in order to spot light differences in reactivity of mutants. Their function as chemically-stable mimics of transition states was essential to obtain high quality cryo EM data and particularly useful to obtain snapshots of catalytic domains in short-lived conformations. Even the earliest structural endeavors of catalytic E3 ligase domains, included high-affinity binding partners such as E2 enzymes to minimize flexibility and motility.

The first structures of a RING E3 ligase (c-cbl) and HECT E3 ligase (E6AP) were both secured with the E2 enzyme UBE2L3 as binding and stabilization partner[3,5]. In recent years, it became more and more apparent, how structures of ABP-bound E3 ligases provide deep mechanistic insights by fixing catalytic domains. MYCBP2 serves as an exceptional example of how activity-based probes can be harnessed to study E3 ligases. Here, they identified MYCPB2 as atypical RING E3 ligase by activity-based proteomic profiling and elucidated its novel RING-Cys-Relay mechanism with biochemical assay and ABP-bound crystal structures[10,11,14].

Our semi-synthetic approach will allow rapid and facile generation of ABPs to match needs. E2 enzymes can readily be exchanged in the TS1 ABP or other types of ABPs created altogether. Conjugation is conceivable for all single-cysteine bearing proteins and peptides. Thus, fully-folded protein substrate ABPs are imaginable as long as mutation of intrinsic cysteine residues do not change folding or binding properties of the substrate. While cysteine replacement mutations might exhibit no deleterious

effects for some ABP components e.g UBE2L3, others suffer from reduced activity as it was demonstrated for UBE2D. Hereby, laborious mutational cysteine substitution screens were necessary in order to regain activity[110]. While it might be worthwhile to do for a few cysteines, larger proteins typically compromise cysteine in the double-digit range- making cysteine substitution screens extremely tedious. It might not be necessary, however, to replace all cysteines in order to couple the target with the reactive ubiquitin species- cysteines that are intrinsically buried in the protein structure or responsible for the coordination of metal atoms are less likely a target of the reactive ubiquitin species.

Even though our suite of ABPs was perfectly fit to work with the E3-E3 system, it could be utilized for other catalytic-cysteine carrying E3 ligases. The UBE2L3 TS1 ABP readily reacted with HECT E3 ligases and other RBR ligases in vitro and in cell lysates (data not shown). Thus, it could be employed for other structural endeavors or activity-based proteomic profiling in the context of cellular systems as colleagues have demonstrated.

## 5.2 Structural insights and principles of the E3-E3 ubiquitylation cascade

Our cryo EM data define structural principles underlying E3-E3-catalyzed ubiquitylation: (1) amalgamation of two individual E3s into a singular E3-E3 assembly activates ubiquitin ligase activity; (2) all catalytic conformations depend on elements from both E3s; and (3) both ubiquitin transfer reactions depend on the key features regulating activity in vivo.

These principles govern a series of structures that depend on SCF regulation, specify targeting of F-box protein-bound substrates, and are generalizable across the mix-and-match F-box protein system. Several previous studies have set the foundation with structures showing the inactive individual E3s and what elements define their inactivity or autoinhibition[74,104,105,131]. Together with our structural data and the intermediates, it is now possible to model a full cycle of E3-E3-catalyzed ubiquitylation (Figure 27a). After a substrate is marked for ubiquitylation, substrate binding to its Fbox protein starts the cycle, by triggering SCF neddylation[85,134,135]. It seems that NEDD8 and RBX1's RING domain would bind autoinhibited ARIH1, with UBE2L3

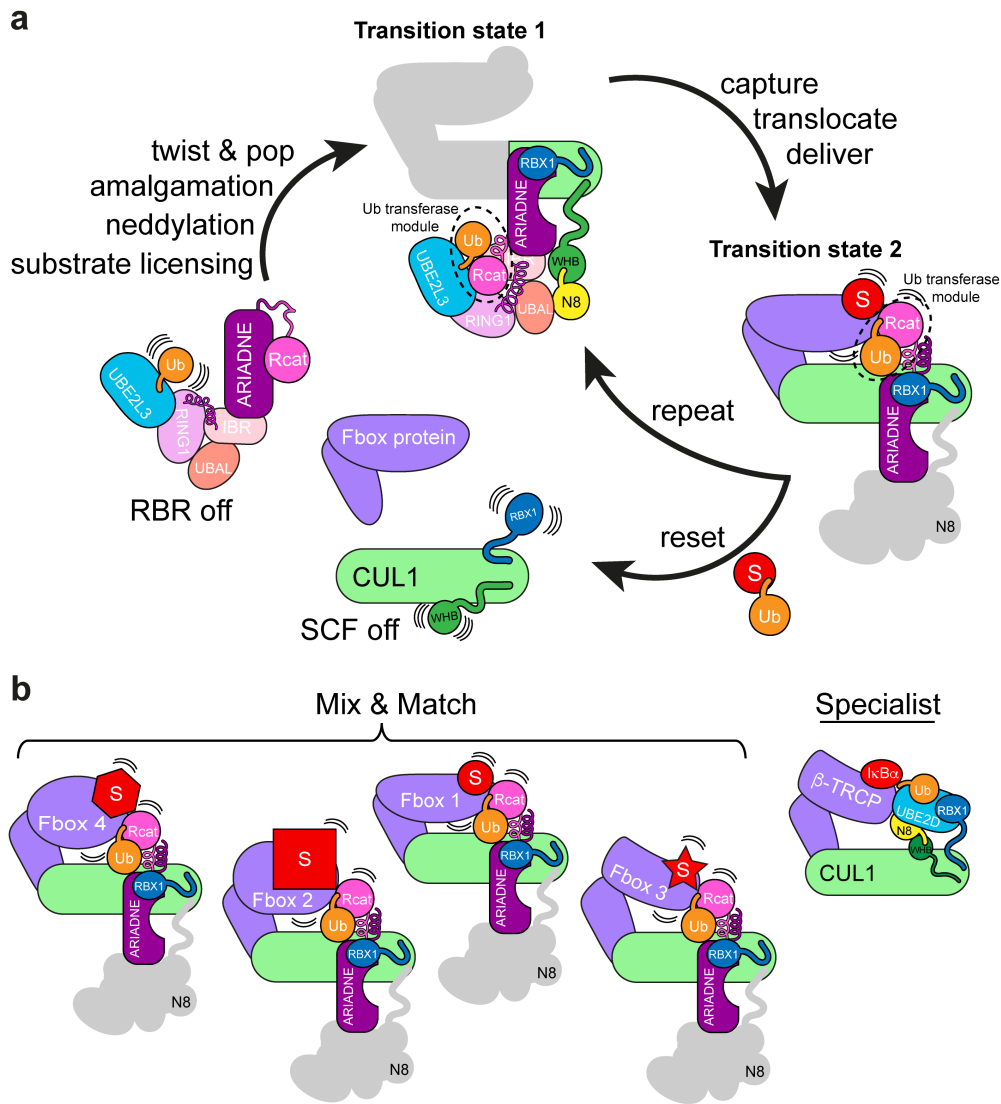


**Figure 28 – Generalizable ubiquitin ligation to F-box protein-bound substrates by transiently amalgamated cullin-RING-RBR E3-E3 ligases. a**, Model for neddylated SCF-ARIH1 cycle: 1) Ubiquitylation is inhibited by lack of stable SCF assembly and ARIH1 autoinhibition. 2) Substrate-binding stabilizes its cognate SCF assembly and elicits neddylation, which enables transient amalgamation with ARIH1. 3) In transition state 1, CUL1-RBX1-bound ARIH1’s Ariadne domain switch helix is twisted, which pops ARIH1’s Rcat domain. Simultaneous ARIH1 remodeling – stabilized by assembly with NEDD8 covalently-linked to and packing with CUL1’s tethered WHB domain - presents UBE2L3’s linked ubiquitin for ARIH1 capture in “ubiquitin transferase module”. 4) After  $\approx 90^\circ$  translocation of the ubiquitin transferase module, in transition state 2, ubiquitin is delivered to F-box protein bound substrate. 5) The cycle either repeats to ubiquitylate another substrate lysine or the E3-E3 disassembles and resets for transient ARIH1 amalgamation with another neddylated SCF. **b**, Ubiquitin carrying enzymes are mix-and-match components of the SCF system. Left, E3-E3 mechanism structurally accommodates substrates recruited to diverse Fbox proteins (left), whereas the conventional E3-E2 configuration with UBE2D is optimal for substrates of select Fbox proteins, exemplified by  $\beta$ -TRCP (right). Figure adapted from [2].

already present, and induce the activating conformational changes. NEDD8, CUL1, and UBE2L3-linked ubiquitin envelop ARIH1 and reposition it so that UBE2L3~ubiquitin

is displayed for catalytic attack. Additionally, ARIH1's former autoinhibitory loop between its IBR and Rcat domain is remodeled to bind ubiquitin's hydrophobic Ile44-centered patch and remains an essential element as ubiquitin-guided helix in the ubiquitin transferase module. Simultaneously, ARIH1's Ariadne domain twists to bind CUL1. The switch helix in the Ariadne domain is kinked and residues responsible for securing the autoinhibitory latch are rotated outwards. Consequently, the Rcat domain is not fixed in its position any longer and able to relocate in order to accept ubiquitin. In the transition state for ubiquitin transfer from E2 to E3-E3, the Rcat engages ubiquitin's C-terminal tail, stabilized by the newly remodeled Ub-guided helix. After ubiquitin capture by ARIH1's Cys<sup>cat</sup>, its linkage with UBE2L3 is severed, and the ubiquitin transferase module can reposition from the other edge of the E3-E3 assembly. With the Rcat domain blocked by the switch helix extension, the highly reactive ARIH1~ubiquitin active site hovers near an F-box protein client substrate. Upon catalytic encounter, ubiquitin is transferred to substrate. Another round of ubiquitylation could occur if the Ub-guided helix and Rcat domain engage another UBE2L3~ubiquitin conjugate bound to the E3-E3 platform. Alternatively, in the absence of an SCF substrate, there may be multiple paths to reset, including ARIH1-catalyzed ubiquitylation of itself or of the F-box protein, or in the absence of ARIH1's covalent linkage to ubiquitin, the ubiquitin-guided helix could reset into the autoinhibitory, unstructured loop and engage an autoinhibited conformation together with the Rcat domain. This could have several effects including remodeling of the switch helix and promoting dissociation of ARIH1 from the neddylated SCF. Consequently, chain-building enzymes would now be able to bind the SCF and use the ubiquitin molecule as a primer for polyubiquitin chains[136,137]. Ultimately, CUL1-RBX1 is also deneddylated via a network sensing substrate degradation[135,138]. Taken together, we have illuminated a full cycle of ubiquitin transfer, catalyzed by two distinct types of E3 ligases. ABPs were essential in stabilizing fleeting transition states and more simple approaches to stabilize conformations were helpful in demonstrating how intermediates of transition states are build the basis for the catalytic events.

### 5.3 Generalizable Cullin-RING ligase substrate specificity

The vast amount of CRLs and their significance in the regulation of a myriad of pathways is justified by its mix and-match principle of substrate receptors

[63,86,139,140]. However, the employment of ARIH1 by CRLs in addition to E2 enzymes might enable the mix-and-match principle in the first place. Neddylated SCF<sup>β-TRCP</sup> and some other CRLs efficiently ubiquitylate substrates employing UBE2D-family E2s, while other E2s are specialized to extend polyubiquitin chains such as the UBE2R- and UBE2G-family E2s[110,137]. The presence of several families of polyubiquitylating E2s could possibly act as a buffer in case one becomes limiting. It remained questionable why CRLs use diverse ubiquitin carrying enzymes – from E2s to RBR E3s – to directly ubiquitylate substrates. Comparing the structures representing E3-E3 ubiquitylation with that showing conventional neddylated SCF<sup>β-TRCP</sup> substrate ubiquitylation by the E2 UBE2D provides a hypothesis (Figure 27b). The catalytic architecture with UBE2D explains its rapid ubiquitylation of neddylated SCF<sup>β-TRCP</sup> substrates- all elements are optimally positioned to deal with the ubiquitylation of the disordered substrate IκBα[110]. However, it is suboptimal for other F-box proteins whose substrates are folded or not within its UBE2Ds relative ubiquitylation zone and consequently, relatively poorly ubiquitylated (Figure 25b-c, Figure 27b). By contrast, the E3-E3 mechanism does not require accurate geometry and can flexibly position its catalytic domain to adjust to the size and shape of distinct SCF substrates, explaining ARIH1's potent ubiquitylation of substrates recruited to numerous diverse neddylated SCFs and other CRLs. We exemplified this by testing both ubiquitylation systems and demonstrated how ARIH1 is capable of ubiquitylating folded substrates such as Cryptochrome or even truncated, disordered substrates. Thus, the E3-E3 structures provide an efficient ubiquitylation mechanism for the defining CRL property: the mix-and-match system of diverse substrate receptors. The structures also redefine the CRL parts-list: mixing-and-matching ubiquitin carrying enzymes are crucial components enabling the ubiquitylation capacity and widespread impact of the neddylated CRL system.

## 5.4 New and old paradigms for E3 ligase mechanism

One surprise was that the E3-E3 mechanism does not simply involve NEDD8 binding to ARIH1, but instead numerous elements from both, neddylated SCF and ARIH1, sculpt each other. Moreover, they do so in a regulated conformational cycle, implying that each individual E3 has evolved to work with the other. It seems likely that that this principle could apply to numerous other E3-E3s. We have demonstrated how

neddylated CUL5-RBX2/ARIH2 E3-E3 employs similar conformations to promote ubiquitylation but is at the same time activated by an allosteric NEDD8-driven mechanism that does not require binding of NEDD8 to ARIH2s UBAL domain[132]. Furthermore, multiple E3s working together is an emerging theme, for example through distinct non-CRL and non-ARIH-based E3-E3s marking their own substrates with specialized linear or branched ubiquitin chains[91,108,109]. Moreover, many E3s – including HOIP and Parkin whose RBR domains adopt similar catalytic conformations as ARIH1 (Supplementary data figure 11f) – mediate stepwise ubiquitylation (or polyubiquitylation) through reactions in series[141,142]. We anticipate that future studies will show how the integration of such catalytic domains in massive assemblies, with regulatory factors determining conformational cycles, direct ubiquitylation of specific substrates.

## 5.5 Future perspectives

The versatility of E3 ligases is seemingly endless with new types of active sites emerging and different types of E3s collaborating. We speculate that parallel structural elements likewise mediate ARIH1 usage by other RBX1-based neddylated CRLs. Together with a multitude of conformations that can be adopted in order to transfer Ub/Ubls to even more exotic acceptor sites, we speculate that new types of ubiquitylation and E3s are yet to be discovered. The rise of activity or avidity-based probes seem tremendously accelerate our understanding of E3 ligases and continue to provide a platform for researchers to jump onto. One system to benefit from this could be one of the most elusive members of the Cullin family- CUL9. CUL9 encompasses both a cullin and an Ariadne-family RBR E3 within a single protein and has been shown to partner up with RBX1 to maintain microtubule integrity[143-146]. Thus, the collaboration of two distinct E3 ligase systems has turned out to be evolutionary worth to unite into one single system. It is unclear if CUL9s presumably autoinhibitory Ariadne domain needs to undergo similar NEDD8-induced activation or in what other shape the ubiquitin system will reveal itself once again.

# Chapter 6- Material & Methods

In this chapter, parts of the following publication were integrated:

**Horn-Ghetko, D.**, Krist, D.T., Prabu, J.R., Baek, K., Mulder, M.P.C., Kluegel, M., Scott, D.C., Ovaa, H., Kleiger, G., Schulman, B.A. Ubiquitin ligation to F-box protein targets by SCF–RBR E3–E3 super-assembly. *Nature* **590**, 671–676 (2021).

Display items and text were reprinted with permission from Springer Nature.

## 6.1 Material

### 6.1.1 DNA- Primers & Plasmids

Primers (Oligonucleotides) were designed according to manufacturer's guidelines for efficient molecular cloning. SnapGene (v5.3) was used to create primer sequences, which were then purchased from Sigma-Aldrich as 100  $\mu$ M solution in water (purification method - desalting). Plasmid DNA was either readily available in the Schulman department or altered by Gibson assembly to generate desired expression vectors. Mutations in target genes were introduced by QuikChange site-directed mutagenesis method. Table 1 lists plasmids used in this study.

**Table 1 – DNA Plasmids**

<b>Plasmid</b>	<b>Resistance</b>	<b>Label</b>
pGEX4T1 GST-TEV-ARIH1	Amp	DHG01
pGEX4T1 GST-TEV-ARIH1 (90-C)	Amp	DHG02
pGEX4T1 GST-TEV-ARIH1 V123D:F150A	Amp	DHG03
pGEX4T1 GST-TEV-ARIH1 V123D	Amp	DHG04
pGEX4T1 GST-TEV-ARIH1 F150A	Amp	DHG05
pGEX4T1 GST-TEV-ARIH1 I188A	Amp	DHG06
pGEX4T1 GST-TEV-ARIH1 K257A:H260A:L261A	Amp	DHG07
pGEX4T1 GST-TEV-ARIH1 W336A:I337A	Amp	DHG08
pGEX4T1 GST-TEV-ARIH1 W336D:I337D	Amp	DHG09
pGEX4T1 GST-TEV-ARIH1 C357A	Amp	DHG10
pGEX4T1 GST-TEV-ARIH1 D402G:A403G:Q404G	Amp	DHG11
pGEX4T1 GST-TEV-ARIH1 A403G:Q404G:E405G	Amp	DHG12
pGEX4T1 GST-TEV-ARIH1 Q404G:E405G:R406G	Amp	DHG13
pGEX4T1 GST-TEV-ARIH1 E405G:R406G:S407G	Amp	DHG14
pGEX4T1 GST-TEV-ARIH1 R406G:S407G:R408G	Amp	DHG15
pGEX4T1 GST-TEV-ARIH1 Q412G:R413G:Y414G	Amp	DHG16
pGEX4T1 GST-TEV-ARIH1 F430A:E431A:E503A	Amp	DHG17
pGEX4T1 GST-TEV-ARIH1 W452A	Amp	DHG18
pGEX4T1 GST-TEV-ARIH1 Y531A	Amp	DHG19
pGEX4T1 GST-TEV-ARIH1 R535A	Amp	DHG20
pGEX4T1 GST-TEV-ARIH1 (90-C) F430A:E431A:E503A	Amp	DHG21
pFastBac CUL1	Amp	DHG22
pFastBac GST-TEV-RBX1	Amp	DHG23
pGEX4T1 GST-TEV-UBE2M	Amp	DHG24
pGEX4T1 GST-TEV-UBE2D2	Amp	DHG25
pGEX4T1 GST-TEV-UBE2L3	Amp	DHG26
pGEX4T1 GST-TEV-UBE2L3 (C17A:C137A)	Amp	DHG27

Plasmid	Resistance	Label
pGEX4T1 GST-TEV-CDC34B	Amp	DHG28
pGEX4T1 GST-Thrombin- APPBP1-UBA3	Amp	DHG29
pGEX4T1 GST-Thrombin-NEDD8	Amp	DHG30
pGEX4T1 GST-Thrombin-NEDD8 I44A	Amp	DHG31
pGEX4T1 GST-Thrombin-NEDD8 Q40E	Amp	DHG32
pGEX4T1 GST-Thrombin-Ubiquitin	Amp	DHG33
pGEX2TK GST-Thrombin-Ubiquitin (S to C)	Amp	DHG34
pTXB1 His-Ubiquitin-intein-Chitin-binding domain	Amp	DHG35
pGEX4T1 GST-TEV-SKP2 <sup>101-C</sup> -SKP1	Amp	DHG36
pGEX4T1 GST-TEV-SKP2-SKP1	Amp	DHG37
pGEX4T1 GST-TEV-CKS1 (5-73)	Amp	DHG38
pGEX4T1 GST-TEV-CYCLIN A	Amp	DHG39
pGEX4T1 GST-TEV-CDK2-CIV1	Amp	DHG40
pGEX4T1 GST-TEV-p27 (22-106)	Amp	DHG41
pGEX4T1 GST-TEV-FBXW7 <sup>ΔD</sup> -SKP1 (FBXW7 263-C)	Amp	DHG42
pFastBac GST-TEV-UBA1	Amp	DHG43
pFastbac SKP1	Amp	DHG44
pFastbac GST-TEV-FBXL3	Amp	DHG45
pFastbac Cryptochrome 1 (1-532)	Amp	DHG46
pRSFduet SKP1 $\Delta\Delta$ (residues 38–43 and 71–82 deleted) $\beta$ -TRCP2	Kan	DHG47

## 6.1.2 Experimental models- Organisms & Strains

**Table 2 – Organisms and Strains**

Organism	Strain	Source
<i>Escherichia coli</i>	DH5- $\alpha$ (K12-derived)	Thermo
<i>Escherichia coli</i>	BL21 Gold (DE3)	Thermo
<i>Escherichia coli</i>	Rosetta 2 (DE3)	Merck Millipore
<i>Spodoptera frugiperda</i>	Sf9	Thermo
<i>Trichopulsia ni</i>	Hi5 BTI-TN-5B1-4	Thermo

### 6.1.3 Buffers

**Table 3 – Buffers**

<b>Name</b>	<b>Composition</b>
His lysis buffer	50 mM Tris base, pH 7.5 200 mM NaCl 20 mM $\beta$ -Mercaptoethanol 2.5 mM PMSF
His wash buffer	50 mM Tris base, pH 7.5 200 mM NaCl 20 mM $\beta$ -Mercaptoethanol
His elution buffer	50 mM Tris base, pH 7.5 200 mM NaCl 300 mM Imidazole 20 mM $\beta$ -Mercaptoethanol
GST lysis buffer ( <i>E.coli</i> )	50 mM Tris base, pH 7.5 200 mM NaCl 4 mM DTT 2.5 mM PMSF
GST lysis buffer (insect cell)	50 mM Tris base, pH 7.5 200 mM NaCl 4 mM DTT 2.5 mM PMSF + cOmplete™ protease inhibitor
GST elution buffer	50 mM Tris base, pH 7.5 200 mM NaCl 10 mM Glutathione 4 mM DTT
IEX buffer A	50 mM Tris base, pH adjusted to protein pI 4 mM DTT
IEX buffer B	50 mM Tris base, pH adjusted to protein pI 1 M NaCl 4 mM DTT
SEC purification buffer	25 mM HEPES pH 7.5 150 mM NaCl 4 mM DTT
Ub-MESNa lysis buffer	20 mM MES, pH 6.5 100 mM NaCl 50 mM Sodium Acetate 2.5 mM PMSF
Ub-MESNa wash buffer	20 mM MES, pH 6.5 100 mM NaCl 50 mM Sodium Acetate
Ub-MESNa elution buffer	20 mM MES, pH 6.5 100 mM NaCl 50 mM Sodium Acetate

<b>Name</b>	<b>Composition</b>
	300 mM Imidazole
Ub-MESNa conversion buffer	20 mM MES, pH 6.5 100 mM NaCl 50 mM Sodium Acetate 100 mM MESNa
Ub-MESNa SEC buffer	20 mM MES, pH 6.5 100 mM NaCl 50 mM Sodium Acetate
Ub-BmDPA buffer 1	50 mM MES, pH 6.5 0.4 M BmDPA 1 mM N-Hydroxysuccinimide
Ub-BmDPA buffer 2	50 mM MES, pH 6.5
Ub-BmDPA buffer 3	40mM Toluensulfonic Acid 54% TFA in H <sub>2</sub> O (v/v)
Ub-BmDPA buffer 4	100 mM Na <sub>2</sub> HPO <sub>4</sub> , pH 6.0 500 mM NaCl 8 M Urea
Ub-BmDPA buffer 5	20 mM Na <sub>2</sub> HPO <sub>4</sub> , pH 6.0 100 mM NaCl
ABP reaction buffer	25 mM HEPES pH 7.5 150 mM NaCl
Cryo-EM SEC buffer	25 mM HEPES pH 7.5 150 mM NaCl 1 mM TCEP
GraFix buffer A	25 mM HEPES pH 7.5 150 mM NaCl 1 mM TCEP 10% Glycerol (w/v)
GraFix buffer B	25 mM HEPES pH 7.5 150 mM NaCl 1 mM TCEP 30% Glycerol (w/v)
desalting buffer	25 mM HEPES pH 7.5 150 mM NaCl 1 mM TCEP

### 6.1.4 Media & Antibiotics

**Table 4 – Media & Antibiotics**

<b>Name</b>	<b>Composition &amp; working concentration</b>
Terrific broth medium (TB)	12 g/l Casein 24 g/l yeast extract 12.54 g/l K <sub>2</sub> HPO <sub>4</sub> 2.31 g/l KH <sub>2</sub> PO <sub>4</sub>
Lysogeny broth medium (LB) Luria Miller formula	10 g/l Tryptone 5 g/l yeast extract 10 g/l NaCl 2.31 g/l KH <sub>2</sub> PO <sub>4</sub>
Super optimal broth with catabolite repression medium (SOC)	20 g/l Tryptone 5 g/l Yeast extract 0.96 g/l MgCl <sub>2</sub> 0.5 g/l NaCl 0.19 g/l KCl 20 mM Glucose
Insect serum-free medium Ex-cell™ 420	6 g/l glucose 0.35 g/l NaHCO <sub>3</sub> 1 g/l L-glutamine
LB agar Luria Miller formula	10 g/l Tryptone 5 g/l yeast extract 10 g/l NaCl 15 g/l Agar-Agar
Ampicillin (Amp)	100 µg/mL
Kanamycin (Kan)	50 µg/mL
Chloramphenicol (Cam)	50 µg/mL

## 6.1.5 Peptides

**Table 5 – Peptides**

<b>Name</b>	<b>Sequence</b>	<b>Use</b>
p27 phosphodegion	KRANRTEENVSDGSPNAGSVEQ(pT)PRRPGLRRR QTDYKDDDDK	Cryo-EM
Cyclin E phosphodegion	KAMLSEQNRASPLPSGLL(pT)PPQ(pS)GKKQSSD YKDDDDK	Cryo-EM
p27 phosphodegion for ABP	CNKRANRTEENVSDGSPNAGSVEQ(pT)PRRPGLR RRQTDYKDDDDK	TS2 ABP
Cyclin E phosphodegion for ABP	CKKAMLSEQNRASPLPSGLL(pT)PPQ(pS)G KKQSSDYKDDDDK	TS2 ABP
IκBα phosphodegion for ABP	CKKERLLDDRHD(pS)GLD(pS)MRDEEDYKDDDDK	TS2 ABP
Cyclin E phosphodegion	KAMLSEQNRASPLPSGLL(pT)PPQ(pS)GRRQSS	ubiquitylation assays
Cyclin E sortasable phosphodegion	GGGGLPSGLL(pT)PPQ(pS)GKKQSSDYKDDDDK	ubiquitylation assays
Cyclin E radiolabeled phosphodegion	KAMLSEQNRASPLPSGLL(pT)PPQ(pS)GRRASY	kinetics
Cyclin E short radiolabeled phosphodegion	KAGLL(pT)PPQ(pS)GRRASY	kinetics
Cyclin E sortasable radiolabeled phosphodegion	GGGGPLPAGLL(pT)PPQ(pS)GRRASY	kinetics
β-catenin radiolabeled phosphodegion	KAAVSHWQQQSYLD(pS)GIH(pS)GATTAPRRASY	kinetics
β-catenin short radiolabeled phosphodegion	KAYLD(pS)GIH(pS)GAGAGAPRRASY-OH	kinetics

All peptides listed in table 5 were obtained from the in-house Biochemistry Core Facility and HPLC purified with TOF-MS determined purity of 95% or more.

## 6.2 Methods

### 6.2.1 Molecular biology

#### 6.2.1.1 DNA isolation & purification

Single colonies were picked from agar plates and inoculated with 5 mL LB medium overnight at 37°C, shaking at 200 rpm. Tubes were spun down the next day and plasmid DNA was isolated with the QIAprep® Spin Miniprep Kit (Qiagen) while following the manufacturer's handbook. 50 µL of EB buffer (Qiagen) was used for elution of DNA. Quality control of plasmids was performed by nanodrop measurement. After sequencing by Eurofins, plasmids were stored at -20°C. dsDNA isolation obtained by PCR was purified after agarose gel electrophoresis. In short, 1 % (w/v) agarose gels were obtained by dissolving according amounts of agarose in 1x TAE buffer while heating in microwave. After cooling SYBR™ Safe DNA Stain (Invitrogen) was added to the 1% agarose solution. PCR samples were mixed with 6x DNA loading dye (NEB). 1 kb plus DNA ladder (Invitrogen) was used to monitor DNA size. Agarose gels were run at constant voltage of 150 V for approximately 30 min. Gel slices were cut and purified after dissolving in EB buffer provided by the QIAquick® Gel Extraction Kit (Qiagen). Elution was performed with 10-20 µl TE buffer, depending on the signal intensity of DNA bands upon blue light transillumination.

#### 6.2.1.2 Cloning

Polymerase Chain Reaction was performed to either generate fragments for Gibson™ Assembly Protocol (in-house) or to introduce mutations via Quikchange Site-directed Mutagenesis. For both reactions Phusion™ High-Fidelity Polymerase (NEB) was used together with its recommended 5x Phusion HF buffer, 200 µM dNTP mix (NEB), 500 nM forward / reverse primer and 1 µL plasmid template in a 50 µL reaction. PCR conditions for Gibson Assembly fragment generation is described in table 6, conditions for Quikchange Mutagenesis in table 7. After PCR and before purification, samples were subjected to Dpn1 digestion at 37°C overnight.

**Table 6 – PCR conditions for Gibson assembly fragments**

Step	Temperature	Time	Cycles
Initial	98°C	120 s	1x
Denaturation			
Denaturation	98°C	15 s	35x
Annealing	60°C	30 s	
Extension	72°C	30 s/kb	
Final extension	72°C	5 min	1x
Hold	4°C	infinite	

**Table 7 – PCR conditions for Quikchange mutagenesis**

Step	Temperature	Time	Cycles
Initial	98°C	120 s	1x
Denaturation			
Denaturation	98°C	15 s	18x
Annealing	60°C	30 s	
Extension	72°C	30 s/kb	
Final	72°C	10 min	1x
extension			
Hold	4°C	infinite	

Gibson™ assembly cloning was carried out according to manufacturer's protocol. In short, backbone and insert were incubated for 2 h at 50°C with 0.2 pmol total DNA and 1:2 ratio of backbone to insert depending on number and size of fragments.

### 6.2.1.3 Transformation of Chemocompetent *E. coli*

In-house generated chemocompetent *E. coli* cells (DH5- $\alpha$  for cloning purposes, other strains for expression- see table 2) were transformed as described as followed: 1  $\mu$ L plasmid DNA (alternatively 10  $\mu$ l for Gibson™ assembly or Quikchange mutagenesis reactions) was added to 50  $\mu$ L chemocompetent cells and incubated on ice for 15 min. After incubation, cells were heat-shocked at 42°C for 45 s and chilled on ice for 2 min before addition of 950  $\mu$ l SOC medium. Cells were then regenerated at 37°C, 800 rpm and 50  $\mu$ l cells (or all cells for cloning purposes) were plated on antibiotic-containing LB agar plates and incubated overnight at 37°C.

For bacmid generation, plasmid DNA was transformed into emBacY cells. Transformations were performed as described for expression but cells were incubated at 37°C at 225 rpm for 6 hours after heat-shock. After incubation ~100  $\mu$ l were plated on LB agar plate containing 200  $\mu$ g/mL ampicillin, 50  $\mu$ g/mL kanamycin, 7  $\mu$ g/mL gentamicin, 10  $\mu$ g/mL tetracycline, 100  $\mu$ g/ml X-gal and 100  $\mu$ M IPTG.

For bacmid isolation, a single, isolated, white bacteria colony was inoculated in 3 ml of LB medium containing 50  $\mu$ g/mL kanamycin, 7  $\mu$ g/mL gentamicin and 10  $\mu$ g/mL tetracycline and grown in a 37°C shaking incubator overnight. The next day, cells were pelleted by centrifugation at 14,000 g for 1 minute.

After removal of the supernatant, 0.3 ml of P1 (Qiagen) was added and resuspended. Then, P2 buffer (Qiagen) was added and mixed gently. After addition of 0.3 ml of 3 M potassium acetate pH 5.5, a thick white precipitate is formed. The tubes were centrifuged for 10 min at 14,000 g and the supernatant transferred to a tube containing 0.8 ml of isopropanol. Sample was chilled at -20°C for 3 h and centrifuged for 20 min at 14,000 g at RT afterwards. The pellet was then washed with 0.5 ml of 70% (v/v) ethanol twice and air dried for 5 to 10 min at RT. 40  $\mu$ L EB buffer (Qiagen) was added

to the pellet without resuspending. Obtained bacmids were stored at 4°C.

## 6.2.2 Protein expression & purification

### 6.2.2.1 Protein expression in *E. coli*

Starter cultures for protein expression were obtained by inoculating single colonies from agar plates in LB medium with appropriate antibiotics overnight at 37°C (~10 ml culture per liter of expression volume). The following day, growth was started by addition of 10 ml starter culture to one liter of TB medium with appropriate antibiotics. Cells were grown until they reached an OD of 0.6-0.8, upon which temperature was reduced to 18°C. When 22°C were reached, expression was induced by addition of IPTG. IPTG concentrations are indicated in table 8. The following day, cultures were harvested at 4500 rpm for 15 min at 4°C and resuspended in suited resuspension buffers.

**Table 8 – Expression conditions**

Protein	Temperature	Time	IPTG conc.	additive
ARIH1 & mutants	16°C	o/n	0.1 mM	0.1 mM ZnCl <sub>2</sub>
E2 enzymes	20 °C	o/n	0.6 mM	
Ubiquitin & variants	20 °C	o/n	0.6 mM	
NEDD8 & mutants	16 °C	o/n	0.6 mM	
SKP1-SKP2	16°C	o/n	0.1 mM	
SKP1-FBXW7	16°C	o/n	0.1 mM	
SKP1-b-TRCP2	16°C	o/n	0.1 mM	
Cyclin A –CDK2	18°C	o/n	0.6 mM	
P27 N-term	18°C	o/n	0.6 mM	
CKSHS1	18°C	o/n	0.6 mM	

### 6.2.2.2 Protein expression in insect cells

Plated insect cells (Hi5 or Sf9) with 50% confluency in Ex Cell 420 medium + 5% fetal calf serum are transfected with pure Bacmid DNA via FuGENE® HD transfection reagent (promega) as described by the manufacturer. After lysis of minimally 60% of insect cells, P1 virus is harvested after centrifugation of cells. P1 virus, used in a dilution range of 1:1000 to 1:5000, is then used to infect 10 ml of Sf9 or Hi5 cells ( $0,5 \times 10^6$  cells/ml) in suspension culture and once again collected after enough cells have been lysed by the virus. This is repeated once. Ultimately, ~10 ml of P3 virus is added to 500 ml cells at  $4 \times 10^6$  cells/ ml in a total and incubated at 27°C for 24 h (155 rpm). After 24 h temperature is decreased to 20°C and incubation continued for additional 40 h. Cells are harvested at 450xg for 15 min.

### 6.2.2.3 Protein purification

After resuspension, cells were subjected to cell lysis via ultrasonication. Ultrasonication was performed on ice for approximately 10 min at 35 % intensity (1s/1s pulse on/off) with a VS T/70 tip mounted on a Sonoplus HD3200 ultrasonication device (Bandelin electronic GmbH). Cell debris and nuclei were removed by centrifugation at 20,000 rpm at 4°C for 30 min (Sorvall Lynx 6000). Appropriate amounts of buffer-equilibrated affinity beads were added to the supernatant (typically 2 mL of bead slurry to one liter of culture). For higher expressing proteins (e.g Ubiquitin) slurry volume was adjusted. Protein supernatant and beads were incubated on a roller for 1 h at 4 °C. After incubation, the solution was transferred to gravity flow columns and beads were washed five times with the bead volume. Elution was performed step-wise (5x bead volume). Elution fractions were checked by SDS-PAGE. If the pI values of GST and target protein was close, on-bead digest was performed by addition of appropriate amounts of His-tagged TEV protease to the beads on column and incubated overnight. Otherwise TEV-site cut was performed in dialysis tubes overnight. After dialysis ion exchange chromatography was executed according to calculated pI values of proteins with prepacked 5 ml Q- or S-sepharose columns (GE Healthcare). After several washes (10x column volume), elution salt gradients were typically set from 5% to 50% buffer B. Elution peaks were checked by SDS-PAGE. Peak fractions were then pooled and concentrated before size exclusion chromatography. Total protein amount was measured via Bradford assay to determine the SEC column size. Typically, SD200 10/300 GL increase columns (GE Healthcare) were used for SEC runs. Peak fractions were once again checked via SDS-PAGE, appropriate fractions pooled, concentrated with Amicon centrifugal filters, aliquots flash-frozen in liquid nitrogen and stored at -80°C.

### 6.2.2.4 Ubiquitin MESNa purification

Starting point for the generation of the activity-based probes was the preparation of His-Ub(1-75)-MESNa. Here, ubiquitin is lacking its terminal glycine 76 in order to mimic appropriate atomic distances and geometry when conjugated to either one of the options described below. N-terminal His-tagging was necessary not only for Ub-MESNa but also for consequent conjugated ABP product purifications. Ub-MESNa was expressed in *E. coli* Rosetta 2 (DE3) and cells were resuspended and lysed in 20 mM HEPES pH 6.8, 50 mM NaOAc, 100 mM NaCl, 2.5 mM PMSF. After lysis Ni-NTA affinity chromatography, protein was concentrated as much as possible in order to have a minimum volume of cleavage buffer added to the CBD-Ubiquitin fusion. The fusion was then cleaved from the chitin-binding domain by diluting it 5:1 (v/v) with 20 mM HEPES pH 6.8, 50 mM NaOAc, 100 mM NaCl, 100 mM MESNa. After overnight incubation at room temperature on a roller, precipitate was spun down for 10 min at 3700xg and supernatant was concentrated to purify it via size-exclusion chromatography (High-Load SD75 10/300). This purification needs to be performed in

a pH range from 6 to 7 as higher pH promotes the hydrolysis of Ub-MESNa and ultimately compromises its reactivity towards coupling it with other ABP components. His-Ub(1-75)-MESNa was analyzed for its hydrolysis percentage via LC-MS in order to make accurate starting material calculation before ABP generation.

## 6.2.3 Generation of activity-based probes

### 6.2.3.1 Generation of a Transition State 1 ABP

His-Ub(1-75)-MESNa was conjugated to (E)-3-[2-(bromomethyl)-1,3-dioxolan-2-yl]prop-2-en-1-amine (BmDPA) (>95% purity, ChiroBlock GmbH) to generate Ub-BmDPA. His-Ub(1-75)-MESNa (up to 10 mg/ml, final concentration after deducting hydrolyzed Ub-MESNa percentage) was mixed with 0.04 M BmDPA and 1 mM N-Hydroxysuccinimide in 50 mM MES pH 6.5, 100 mM NaCl. The reaction was incubated at 90 rpm at room temperature over-night in vertically tilted position of the falcon tube. The next day, the reaction mix was dialyzed into 50mM MES pH 6.5 with Slide-a-Lyzer™ dialysis cassettes (Thermo Fisher) while an aliquot was checked for conversion of Ub-MESNa to Ub-BmDPA via LC-MS (ESI-TOF). The typical conversion rate of this reaction is 100%. After dialysis, deprotection of cyclic ketal was carried out by addition of 0.04 M p-TsOH (dissolved in 54% TFA (v/v)) to Ub-BmDPA and incubated for 1 h at room temperature. The reaction was washed several times with cold ether (20x fold reaction volume) to wash away residual TFA and precipitate out the protein. Three layers were formed during this step: 1. The top ether layer, 2. the middle protein layer and 3. the bottom TFA/H<sub>2</sub>O layer. After removal of the top ether layer, the other two layers were transferred to Eppendorf tubes and centrifuges for 15 min at 16,000xg. Protein flakes were then air dried and resuspended in Ub-BmDPA buffer 4. Ubiquitin was then refolded via dialysis in Ub-BmDPA buffer 5 over-night at 4°C. One milligram of the refolded, deprotected ubiquitin species was ultimately mixed with single-cysteine UBE2L3 (C17A, C137A, 5x fold excess), incubated for 2 h at 30°C and purified via Nickel-affinity as well as size exclusion chromatography, yielding a TS1 UBE2L3-ABP. All cysteines except the catalytic cysteine of UBE2L3 were mutated to alanine as they could possibly interfere with coupling to the deprotected ubiquitin species by acting as unwanted acceptor sites. The last conjugation step can be carried out with any desired, single-cysteine bearing E2 enzyme to utilize the TS1 ABP for other RBR or HECT E3 ligases.

### 6.2.3.2 Formation of an unreacted UBE2L3-ABP

In order to serve as negative control for the TS1 UBE2L3-ABP, an unactivated UBE2L3-ABP was synthesized. Here, His-Ub(1-75)-MESNa was coupled with BmDPA as before but no deprotection of the cyclic ketal was carried out. Addition of single-

cysteine UBE2L3 to this protected ubiquitin-BmDPA species resulted in an unactivated TS1 UBE2L3-ABP.

### 6.2.3.3 Conjugation of ubiquitin to UBE2L3 via an isopeptide-link

UBE2L3's catalytic cysteine Cys86 was mutated to Lysine to enable the conjugation of ubiquitin via an isopeptide link. Therefore, 1  $\mu$ M Uba1, 10  $\mu$ M UBE2L3 (C86K), and 50  $\mu$ M His-ubiquitin were incubated in 50 mM Tris pH 9.5, 50 mM NaCl, 2 mM ATP, 10 mM MgCl<sub>2</sub>, and 1 mM  $\beta$ -Mercaptoethanol. The reaction mix was incubated at 37°C for 18 h. Consequently, the UBE2L3~Ub conjugate was purified by Nickel-affinity pull-down and buffer-exchange on a HiLoad 10/300 Superdex 75 pg size-exclusion chromatography column equilibrated in 25 mM HEPES pH 7.5, 150 mM NaCl and 4 mM DTT.

### 6.2.3.4 Generation of UbVME

UbVME was kindly provided by collaborators of the University of Leiden. The following protocol describes their synthesis approach as published in [2]. The Ub(1–75) peptide, bearing a free N terminus and its side chains protected, was synthesized on a trityl resin by Fmoc solid-phase peptide synthesis procedures (25  $\mu$ mol scale) and removed from the resin using 1,1,1,3,3,3-hexafluoropropan-2-ol (HFIP) as described[147]. Gly-Vinylmethyl ester (VME) (10 equiv.) was coupled to the C-terminus of Ub by using PyBOP (5 equiv.), triethylamine (Et<sub>3</sub>N) (20 equiv.) in DCM (5 mL) and stirred for 16h at ambient temperature. Excess Gly-VME was removed by washing the DCM solution with 1 M KHSO<sub>4</sub>. The organic layer was dried with Na<sub>2</sub>SO<sub>4</sub> and concentrated to dryness in vacuo. To remove the side-chain protecting groups, the residue was taken up in trifluoroacetic acid/ triisopropylsilane/ water (5 mL; 95:2.5:2.5) and stirred for 3h at ambient temperature. The reaction mixture was added to a falcon tube containing ice-cold pentane/diethyl ether (1:3; 40 mL), upon which the product precipitated. The precipitate was isolated by centrifugation (1500xg, 6 min, 4 °C) and washed by three cycles of resuspension in ice-cold diethyl ether and centrifugation. Finally, the pellet was taken up in water/acetonitrile/acetic acid (65:25:10), frozen, and lyophilized. Product was purified by prep-HPLC.

### 6.2.3.5 Generation of TS2 ABPs

Native chemical ligation was used to couple His-Ub(1-75)-MESNa with substrate phosphopeptides (p27, Cyclin E, I $\kappa$ B $\alpha$ ) bearing a N-terminal cysteine as listed in table 5. His-Ub(1-75)-MESNa (200  $\mu$ M final concentration after deducting hydrolyzed Ub-MESNa percentage) and substrate peptide (1000  $\mu$ M final concentration) were mixed after desalting into 50 mM NaPO<sub>4</sub> pH 6.5, 50 mM NaCl and incubated for 1 h at RT

with slight rocking (300 rpm). After 1 h, 2 mM TCEP were added to the reaction mix and further incubated for 1 h. At the end of the reaction, 10x buffer (500 mM NaPO<sub>4</sub> pH 8.0, 500 mM NaCl) was added to 1x final concentration to improve the Ni-NTA purification yield. The Ubiquitin-peptide fusion was then purified via Ni-NTA affinity beads and consequently buffer exchanged via size-exclusion chromatography or desalted into 50 mM NaPO<sub>4</sub> pH 8.0, 50 mM NaCl before the dehydroalanine conversion step. The cysteine bearing Ubiquitin-peptide fusion was converted with 2,5-dibromohexanediamide to dehydroalanine.

Hereby, Tris(2-carboxyethyl)phosphine (1 mM final concentration) was added to the Ub(1–75)-Cys-peptide (700 µl at 300 µM) and incubated for 20 min at room temperature. After desalting (Zeba spin column, 2 ml, 7,000 molecular weight cut-off filter, Thermo Fisher) 2,5-dibromohexanediamide (14 mM final concentration, stock solution dissolved in DMSO) and Ub(1–75)-Cys-peptide were combined in a 2-ml tube in 50 mM NaPO<sub>4</sub> pH 8.0. The reaction mix was first incubated for 30 min at 23°C with rocking at 90 rpm and then at 37°C for 2 h. Finally, the reaction mix was desalted into 50 mM NaPO<sub>4</sub> pH 8.0 (Zeba spin column, 5 ml, 7,000 molecular weight cut-off filter, Thermo Fisher).

## 6.2.4 Biochemical assay

### 6.2.4.1 Pulse-chase assays

Pulse-chase assays were used to monitor Ub transfer from UBE2L3 to either Cyclin E (substrate priming) or ARIH1 (autoubiquitylation). A thioester-linked UBE2L3~Ub intermediate is generated in the pulse-reaction- This was carried out by incubating 10 µM UBE2L3, 0.3 µM UBA1 and 15 µM fluorescent ubiquitin in 25 mM HEPES pH 7.5, 100 mM NaCl, 2.5 mM MgCl<sub>2</sub>, 1 mM ATP at room temperature for 15 min. This reaction was quenched by incubation with 50 mM EDTA on ice for at least 5min and subsequently diluted to 0.67 µM UBE2L3 in 25 mM MES pH 6.5, 100 mM NaCl. For substrate priming assays, the chase reaction mix contained 1 µM NEDD8–CUL1-RBX1, 1 µM substrate receptor (SKP1-FBXW7<sup>ΔD</sup>), 1 µM substrate (single Lys Cyclin E peptide) and 0.75 µM ARIH1 (90-C), in 25 mM MES pH 6.5, 100 mM NaCl. The chase reaction mix was equilibrated on ice for at least 20 min. The reaction was started by mixing chase reaction mix and quenched pulse to yield final concentrations of 0.4 µM UBE2L3, 0.4 µM N8–CUL1-RBX1, 0.4 µM SKP1-FBXW7<sup>ΔD</sup>, 0.4 µM Cyclin E substrate and 0.3 µM ARIH1. Reactions were quenched with 2X SDS-PAGE sample buffer at each dedicated time point. For autoubiquitylation assays, the chase initiation mix consisted of 1 µM NEDD8–CUL1-RBX1 and 0.75 µM ARIH1 (90-C) in the same buffer but the quenched pulse reaction was further diluted to yield a final E2~UB concentration of 80 nM. All reactions were carried out on ice. SDS-PAGE was performed under non-reducing conditions and the gel scanned on an Amersham Typhoon imager (GE Healthcare).

#### 6.2.4.2 TS1 UBE2L3-ABP assays

In the first transition state, ubiquitin is transferred from UBE2L3 to ARIH1. The requirements for the reaction with the probe are monitored in this assay to compare it to the native reaction. Reaction components (ARIH1- either FL WT or FL C357S, N8-CUL1-RBX1) were stoichiometrically mixed (1  $\mu$ M per component) in 25 mM HEPES pH 7.8, 150 mM NaCl and preincubated on ice for at least 10 min. After incubation, 10-fold excess of TS1 ABP was added to the reaction mix to start the reaction. Quenching was performed by the addition of 2X SDS-PAGE sample buffer after 2 h incubation on ice.

#### 6.2.4.3 TS2 ABP assays

In the second transition state ubiquitin is transferred to an SCF-bound substrate. Several TS2 ABPs have been synthesized and tested for their requirements to react with ARIH1 and their specificity to react only in presence of the substrate's cognate substrate receptor. Additionally, the effect of ARIH1 mutations, identified via the transition state 2 structures, were tested for their ability to react with the TS2 ABPs. The reaction components (ARIH1 90-C, either NEDD8-CUL1-RBX1 or CUL1-RBX1 and the substrate receptor systems) were stoichiometrically mixed (2  $\mu$ M per component) in 25 mM HEPES pH 7.8, 150 mM NaCl, 1 mM TCEP and preincubated on ice for at least 10 min. After incubation, 2-fold excess of TS2. Reaction was quenched by the addition of 2X SDS-PAGE sample buffer at dedicated time points. All reactions were carried out at room temperature.

The following methods for the next section have been performed by collaborators from the University of Las Vegas.

### 6.2.5 Enzyme kinetics

#### 6.2.5.1 Rapid-quench flow kinetics to dissect the E3-E3 ubiquitin transfer mechanism

Fluorescent Ubiquitin was thioester-linked to UBE2L3 in a "pulse" reaction incubating 10  $\mu$ M UBE2L3, 15  $\mu$ M fluorescent Ub, and 400 nM UBA1 in 25 mM HEPES, 150 mM NaCl, 2.5 mM MgCl<sub>2</sub>, 1 mM ATP, pH 7.5 for 13 minutes at room temperature. The pulse reaction was quenched with 25 mM HEPES, 150mM NaCl, 50 mM EDTA, pH 7.5 such that the final concentration of UBCH7~\*UB was 800 nM and incubated on ice for 5 min. Rapid quench flow experiments were performed at RT by placing 800 nM UBE2L3~\*UB in syringe one and 600 nM ARIH1, 800 nM NEDD8-CUL1-RBX, 800 nM SKP1-FBXW7<sup>AD</sup>, with or without 4  $\mu$ M Cyclin E in 25mM HEPES, 150 mM NaCl, 0.5

mg/ml BSA, pH 7.5 in syringe two. Syringes were mixed and quenched with 2X SDS-Sample buffer at the indicated times. Reaction products were separated on 4-12% Bis-Tris gels, scanned on a Typhoon imager, and quantified using ImageQuant software.

#### 6.2.5.2 Estimating the $K_m$ of ARIH1 and UBE2D for various SCF-substrate complexes.

Single-encounter reactions between  $^{32}\text{P}$ -labeled substrate and SCF were assembled in a reaction buffer containing 30 mM Tris, pH 7.5, 100 mM NaCl, 5 mM  $\text{MgCl}_2$ , 2 mM ATP and 1 mM DTT. For Cyclin E, ubiquitylated Cyclin E, and Cyclin E short peptide substrates and ARIH1, stock solutions of E1, ubiquitin and UBE2L3 were prepared (tube 2) and incubated for 5 minutes at room temperature prior to the addition of cold competitor substrate (for ubiquitylated Cyclin E, competitor substrate was free peptide without sortased UB). In a separate tube, neddylated CUL1-RBX1, SKP1- FBXW7 $\Delta^D$ , and  $^{32}\text{P}$ -labeled substrate were incubated for 5 minutes (tube 1) and then equally distributed to Eppendorf tubes. A 2-fold dilution series of ARIH1 was prepared, followed by the addition of an equal volume from the dilution series to each Eppendorf tube containing the SCF-labeled substrate complex. Reactions were initiated by adding an equal volume from tube 2 to each Eppendorf tube. After 10 seconds, reactions were quenched with 2x SDS-PAGE loading buffer containing 100 mM Tris-HCl, pH 6.8, 20% glycerol, 30 mM EDTA, 4% SDS, and 0.02% bromophenol blue. For Cyclin E, ubiquitylated Cyclin E, and Cyclin E short peptide substrates and UBE2D, stock solutions of E1 and ubiquitin were prepared and then distributed to Eppendorf tubes. UBE2D3 aliquots from a 2-fold dilution series were then added to each tube followed by the addition of cold competitor substrate. Ubiquitylation reactions were initiated by adding equal volumes of SCF-labeled substrate from tube 1 that had been prepared as described above. For  $\beta$ -catenin and  $\beta$ -catenin short peptide substrates and ARIH1, stock solutions of E1, ubiquitin and UBE2L3 were prepared (tube 2) and incubated for 5 minutes at room temperature prior to distributing equal volumes to Eppendorf tubes. The ARIH1 dilution series was then added to each tube followed by the addition of cold competitor substrate. The reactions were initiated by the addition of equal volumes of SCF-labeled substrate mixture (now containing SKP1- $\beta$ -TRCP2) from tube 1, incubated for 10 seconds, and quenched as described above. For  $\beta$ -catenin and  $\beta$ -catenin short peptide substrates and UBE2D3, the procedure was identical to that for Cyclin E except that the SCF complex contained SKP1- $\beta$ -TRCP2. For ARIH1 or UBE2D3 and CRY1 substrate (bound to SKP1-FBXL3),  $^{32}\text{P}$ -labeled human ubiquitin was used to detect product formation. As CRY1 dissociation from SCF does not occur over the time course, these reactions are also single-encounter regarding substrate and SCF. For all reactions, substrates and products were separated on 18% SDS-PAGE gels followed by autoradiography and the quantification of unmodified substrate or products containing at least one or more Ubiquitins (Image Quant TL software; GE). The fraction of product formed was plotted as a function of

the UBE2D or ARIH1 concentration and fit to the Michaelis-Menten Model (Graphpad Prism software). For the ARIH1 titration and CRY1 substrate, the fraction of  $^{32}\text{P}$ -labeled ubiquitin that had been converted to ubiquitylated CRY1 was quantified and then normalized to the value corresponding to the highest concentration of ARIH1. For all reactions, the final SCF and  $^{32}\text{P}$ -labeled substrate (or CRY1) concentrations were 0.25  $\mu\text{M}$ , E1 was 0.5  $\mu\text{M}$ , unlabeled ubiquitin was 30  $\mu\text{M}$ , UBE2L3 was 5  $\mu\text{M}$ , and cold competitor peptide was 100  $\mu\text{M}$ . All experiments were performed in triplicate.

### 6.2.5.3 Estimating the rate of ubiquitin transfer ( $k_{\text{obs}}$ ) from ARIH1 and UBE2D to substrate.

Reactions that were single-encounter between  $^{32}\text{P}$ -labeled substrate and SCF were assembled in reaction buffer as described in the previous section. For Cyclin E, ubiquitylated Cyclin E, and Cyclin E short peptide substrates and ARIH1, E1 (1  $\mu\text{M}$ ), ubiquitin (60  $\mu\text{M}$ ) and UBE2L3 (10  $\mu\text{M}$ ) were incubated for 5 minutes (tube 2) at room temperature prior to the addition of cold competitor substrate (200  $\mu\text{M}$ ). In a separate tube (tube 1), neddylated CUL1-RBX1, SKP1- FBXW7 $^{\Delta\text{D}}$ , and  $^{32}\text{P}$ -labeled substrate (0.5  $\mu\text{M}$ ) were incubated for 5 minutes followed by the addition of ARIH1 (5  $\mu\text{M}$ ). Each mixture was loaded into separate channels of a Kintek rapid quench flow instrument (RQF-3) followed by the collection of time points that were quenched in 2X SDS-PAGE loading buffer. Substrate and products were resolved on 18% SDS-PAGE gels and quantified (Image Quant TL software; GE). The fraction of labeled peptide substrate that had been converted to product were then plotted as a function of time (Mathematica) and fit to a previously described closed form solution to estimate the rate of substrate priming ( $k_{\text{obs}}$ )[148]. The same procedure was employed for Cyclin E, ubiquitylated Cyclin E, and Cyclin E short peptide substrates and UBE2D3, except that UBE2D3 (20  $\mu\text{M}$ ) was used instead of UBE2L3 and ARIH1 was not added to tube 1. The procedure used for Cyclin E was also employed for  $\beta$ -catenin and  $\beta$ -catenin short peptide substrates and ARIH1 except that SKP1- $\beta$ -TRCP2 was used and ARIH1 was added to tube 2 following the addition of cold competitor peptide. An identical procedure was used for  $\beta$ -catenin and  $\beta$ -catenin short peptide substrates and UBE2D3 as for Cyclin E except that SKP1- $\beta$ -TRCP2 was used and the final SCF and labeled substrate concentrations were 0.5  $\mu\text{M}$  and 0.1  $\mu\text{M}$ , respectively. For CRY1, normalized ubiquitylated CRY1 was fit to a single-phase exponential decay function (Graphpad Prism software) owing to the fact that CRY1 does not dissociate from SCF during the time course. All experiments were performed in triplicate.

## 6.2.6 Cryo-EM

### 6.2.6.1 Sample preparation

It was crucial for all ABP complex samples to convert as much ARIH1 to the stable transition state mimic as possible before complex purification. This was done by optimizing reaction time, buffer and temperature. If leftover ARIH1 was present after the probing reaction, it was essential to purify it away from the transition state mimic in order to obtain a homogeneous Cryo-EM sample.

UBE2L3-ABP complex samples were generated by pre-equilibrating subcomplexes on ice in equimolar ratio (10  $\mu$ M final component concentration) in 25 mM HEPES pH 7.8, 150 mM NaCl, followed by addition of 10-fold excess UBE2L3-ABP to initiate three-way cross-linking. To ensure maximal conversion of ARIH1, samples were incubated for 2 h at room temperature. Samples were then purified via size-exclusion chromatography in 25 mM HEPES pH 7.8, 150 mM NaCl, 1 mM TCEP and thereafter concentrated for crosslinking via GraFix [130]. GraFix peak fractions were desalted (Zeba Spin Columns, 0.5 ml, 7 kDa molecular weight cut-off, Thermo) into size-exclusion buffer and concentrated to 0.6 mg/ml. 3  $\mu$ l of sample was applied to R1.2/1.3 holey carbon grids (Quantifoil), blotted for 3 s at  $\sim$ 100% humidity and 4°C, and plunge-frozen in liquid ethane by using a Vitrobot Mark IV. Substrate-ABP complex samples were also prepared by pre-equilibrating subcomplexes on ice in equimolar ratio in 25 mM HEPES pH 7.8, 150 mM NaCl, 1 mM TCEP before adding 5-fold excess substrate-ABP. Maximal conversion of ARIH1 was achieved by incubation for 2.5h on ice. Subsequent treatment of substrate-ABP samples was identical to UBE2L3-ABP samples with the exception of concentrating crosslinked, desalted complexes to only 0.3 mg/ml before plunging.

### 6.2.6.2 Data collection

Screening datasets were collected on a Talos Arctica transmission electron microscope (TEM) at 200 kV equipped with a Falcon II direct detector (linear mode). Approximately 700-800 micrographs were collected per dataset with a pixel size of 1.997 Å, defocus range of -1.5 to -3.5  $\mu$ m and a total exposure of around 60-70  $e^- \text{Å}^{-2}$  split across 40 frames. After screening, bigger datasets were collected on a Titan/Krios TEM at 300 kV equipped with a post-GIF Gatan K3 Summit direct electron detector (counting mode). Between 9.000 to 11.000 movies were collected per sample with either 0.851 Å or 1.09 Å pixel size, a total exposure ranging from 60 to 80  $e^- \text{Å}^{-2}$  and defocus values from -0.8 to -3.2  $\mu$ m.

### 6.2.6.3 Data processing

RELION 3.0 [149] was used to align and dose-weight raw movie frames. Each drift-corrected micrograph was then CTF-corrected via Gctf[150]. Particle picking was performed with Gautomatch (K. Zhang, MRC Laboratory of Molecular Biology). RELION 3.0 was ultimately used to do 2D classification, initial model building, 3D classification, global and local 3D refinement, particle polishing and post-processing.

### 6.2.6.4 Model building

In order to facilitate model building for the TS1 ABP-ARIH1 neddylated SCF<sup>SKP2</sup> complex, a composite map has been generated by merging several focused maps (Supplemental figure 8, supplementary data table 1) via the PHENIX combine focused maps feature [151]. The final refined map of the class, showing prominent density for the catalytic core, was used as base map onto which the focused maps were resampled. This map displayed main and side chain densities for most parts, which enabled modeling and refining the atomic coordinates. A base model was generated by using structures of prior subcomplexes and components (RCSB Protein Data Bank codes: 1LDJ, 5UDH, 2AST, 6TTU, 1H27). Structures were manually placed into the composited map and then fit by rigid-body refinement via UCSF Chimera [152]. Real space refinements and further needed manual model building was performed for accurate geometry and map-to-model correlation. COOT[153] was used for manual modeling and Phenix.refine[154] was used for real space refinement. The obtained model was used for the TS2 p27 ABP SCF<sup>SKP2</sup> complex map. Here, map quality allowed real-space refinement of the E3-E3act superdomain but only docking of the ubiquitin transferase domain (Supplementary data figure 10d-f). The ribbon models in figure 1 have been created as follows: The refined TS1 ABP SCF<sup>SKP2</sup> model was used as template for the pre-TS1 intermediate model. Resolution allowed docking of the model into the pre-TS1 map. Since ARIH's Rcat domain is not visible, it was removed from the model. The substrate receptor was exchanged by fitting a prior crystal structure of SKP1-FBXW7-Cyclin E (PDB: 2OVQ) into the EM-density.

The same crystal structure was used to exchange the Fbox-protein from the TS1 ABP SCF<sup>SKP2</sup> model to FBXW7. The receptor head conformation for FBXW7 in the TS1 ABP structure was obtained by fitting it into a lower resolution structure of TS1 ABP SCF<sup>FBXW7</sup> (supplementary data table 1). The post-TS1 class models were also obtained by using the refined TS1 ABP model and FBXW7 crystal structure as basis (class pre-TS1 and superdomain class) for fitting into cryo-EM density. The refined TS2 p27 ABP SCF<sup>SKP2</sup> structure was docked into TS2 Cyclin E ABP structure and SKP2 was consequently exchanged with the FBXW7 crystal structure via docking into cryo-EM density.

## References

1. Huibregtse JM, Scheffner M, Beaudenon S, Howley PM: **A family of proteins structurally and functionally related to the E6-AP ubiquitin-protein ligase.** *Proc Natl Acad Sci U S A* 1995, **92**:2563-2567.
2. Horn-Ghetko D, Krist DT, Prabu JR, Baek K, Mulder MPC, Klugel M, Scott DC, Ovaa H, Kleiger G, Schulman BA: **Ubiquitin ligation to F-box protein targets by SCF-RBR E3-E3 super-assembly.** *Nature* 2021, **590**:671-676.
3. Zheng N, Wang P, Jeffrey PD, Pavletich NP: **Structure of a c-Cbl-UbcH7 complex: RING domain function in ubiquitin-protein ligases.** *Cell* 2000, **102**:533-539.
4. Brzovic PS, Rajagopal P, Hoyt DW, King MC, Klevit RE: **Structure of a BRCA1-BARD1 heterodimeric RING-RING complex.** *Nat Struct Biol* 2001, **8**:833-837.
5. Huang L, Kinnucan E, Wang G, Beaudenon S, Howley PM, Huibregtse JM, Pavletich NP: **Structure of an E6AP-UbcH7 complex: insights into ubiquitination by the E2-E3 enzyme cascade.** *Science* 1999, **286**:1321-1326.
6. Wenzel DM, Lissounov A, Brzovic PS, Klevit RE: **UBCH7 reactivity profile reveals parkin and HHARI to be RING/HECT hybrids.** *Nature* 2011, **474**:105-108.
7. Riley BE, Loughheed JC, Callaway K, Velasquez M, Brecht E, Nguyen L, Shaler T, Walker D, Yang Y, Regnstrom K, et al.: **Structure and function of Parkin E3 ubiquitin ligase reveals aspects of RING and HECT ligases.** *Nat Commun* 2013, **4**:1982.
8. Stieglitz B, Rana RR, Koliopoulos MG, Morris-Davies AC, Schaeffer V, Christodoulou E, Howell S, Brown NR, Dikic I, Rittinger K: **Structural basis for ligase-specific conjugation of linear ubiquitin chains by HOIP.** *Nature* 2013, **503**:422-426.
9. Scott DC, Rhee DY, Duda DM, Kelsall IR, Olszewski JL, Paulo JA, de Jong A, Ovaa H, Alpi AF, Harper JW, et al.: **Two Distinct Types of E3 Ligases Work in Unison to Regulate Substrate Ubiquitylation.** *Cell* 2016, **166**:1198-1214 e1124.
10. Pao KC, Wood NT, Knebel A, Rafie K, Stanley M, Mabbitt PD, Sundaramoorthy R, Hofmann K, van Aalten DMF, Virdee S: **Activity-based E3 ligase profiling uncovers an E3 ligase with esterification activity.** *Nature* 2018, **556**:381-385.
11. Mabbitt PD, Loreto A, Dery MA, Fletcher AJ, Stanley M, Pao KC, Wood NT, Coleman MP, Virdee S: **Structural basis for RING-Cys-Relay E3 ligase activity and its role in axon integrity.** *Nat Chem Biol* 2020, **16**:1227-1236.
12. Horn-Ghetko D, Schulman, B.A. : **New classes of E3 ligases illuminated by chemical probes.** . *Current Opinion in Structural Biology* 2022, **TBD**.
13. Otten EG, Werner E, Crespillo-Casado A, Boyle KB, Dharamdasani V, Pathe C, Santhanam B, Randow F: **Ubiquitylation of lipopolysaccharide by RNF213 during bacterial infection.** *Nature* 2021, **594**:111-116.
14. Ahel J FA, Grabarczyk DB, Roitinger E, Deszcz L, Lehner A, Virdee S, Clausen T: **E3 ubiquitin ligase RNF213 employs a non-canonical zinc finger active site and is allosterically regulated by ATP.** edn 10.05.2021. Edited by. bioRxiv; 2021. /10.1101/2021.05.10.443411
15. Perteau M, Shumate A, Perteau G, Varabyou A, Breitwieser FP, Chang YC, Madugundu AK, Pandey A, Salzberg SL: **CHESS: a new human gene catalog curated from thousands of large-scale RNA sequencing experiments reveals extensive transcriptional noise.** *Genome Biol* 2018, **19**:208.
16. Walsh CT, Garneau-Tsodikova S, Gatto GJ, Jr.: **Protein posttranslational modifications: the chemistry of proteome diversifications.** *Angew Chem Int Ed Engl* 2005, **44**:7342-7372.
17. Vijay-Kumar S, Bugg CE, Cook WJ: **Structure of ubiquitin refined at 1.8 Å resolution.** *J Mol Biol* 1987, **194**:531-544.

18. Cadwell K, Coscoy L: **Ubiquitination on nonlysine residues by a viral E3 ubiquitin ligase.** *Science* 2005, **309**:127-130.
19. Davies CW, Vidal SE, Phu L, Sudhamsu J, Hinkle TB, Chan Rosenberg S, Schumacher FR, Zeng YJ, Schwerdtfeger C, Peterson AS, et al.: **Antibody toolkit reveals N-terminally ubiquitinated substrates of UBE2W.** *Nat Commun* 2021, **12**:4608.
20. Pruneda JN, Damgaard RB: **Ester-linked ubiquitination by HOIL-1 controls immune signalling by shaping the linear ubiquitin landscape.** *FEBS J* 2021, **288**:5903-5908.
21. Komander D, Rape M: **The ubiquitin code.** *Annu Rev Biochem* 2012, **81**:203-229.
22. Komander D: **The emerging complexity of protein ubiquitination.** *Biochem Soc Trans* 2009, **37**:937-953.
23. Chaugule VK, Walden H: **Specificity and disease in the ubiquitin system.** *Biochem Soc Trans* 2016, **44**:212-227.
24. Bassermann F, Eichner R, Pagano M: **The ubiquitin proteasome system - Implications for cell cycle control and the targeted treatment of cancer.** *Biochim Biophys Acta* 2013, 10.1016/j.bbamcr.2013.02.028.
25. Streich FC, Jr., Haas AL: **Activation of ubiquitin and ubiquitin-like proteins.** *Subcell Biochem* 2010, **54**:1-16.
26. Katzmann DJ, Babst M, Emr SD: **Ubiquitin-dependent sorting into the multivesicular body pathway requires the function of a conserved endosomal protein sorting complex, ESCRT-I.** *Cell* 2001, **106**:145-155.
27. Harper JW, Schulman BA: **Structural complexity in ubiquitin recognition.** *Cell* 2006, **124**:1133-1136.
28. Haas AL, Siepmann TJ: **Pathways of ubiquitin conjugation.** *Faseb J* 1997, **11**:1257-1268.
29. Thrower JS, Hoffman L, Rechsteiner M, Pickart CM: **Recognition of the polyubiquitin proteolytic signal.** *Embo J* 2000, **19**:94-102.
30. Johnson ES, Bartel B, Seufert W, Varshavsky A: **Ubiquitin as a degradation signal.** *Embo J* 1992, **11**:497-505.
31. Bodnar NO, Rapoport TA: **Molecular Mechanism of Substrate Processing by the Cdc48 ATPase Complex.** *Cell* 2017, **169**:722-735 e729.
32. Bodnar N, Rapoport T: **Toward an understanding of the Cdc48/p97 ATPase.** *F1000Res* 2017, **6**:1318.
33. Tenno T, Fujiwara K, Tochio H, Iwai K, Morita EH, Hayashi H, Murata S, Hiroaki H, Sato M, Tanaka K, et al.: **Structural basis for distinct roles of Lys63- and Lys48-linked polyubiquitin chains.** *Genes Cells* 2004, **9**:865-875.
34. Gomez-Diaz C, Jonsson G, Schodl K, Deszcz L, Bestehorn A, Eislmayr K, Almagro J, Kavirayani A, Seida M, Fennell LM, et al.: **The ubiquitin ligase HOIL-1L regulates immune responses by interacting with linear ubiquitin chains.** *iScience* 2021, **24**:103241.
35. Emmerich CH, Ordureau A, Strickson S, Arthur JS, Pedrioli PG, Komander D, Cohen P: **Activation of the canonical IKK complex by K63/M1-linked hybrid ubiquitin chains.** *Proc Natl Acad Sci U S A* 2013, **110**:15247-15252.
36. Nishikawa H, Ooka S, Sato K, Arima K, Okamoto J, Klevit RE, Fukuda M, Ohta T: **Mass spectrometric and mutational analyses reveal Lys-6-linked polyubiquitin chains catalyzed by BRCA1-BARD1 ubiquitin ligase.** *J Biol Chem* 2004, **279**:3916-3924.
37. Brzovic PS, Lissounov A, Christensen DE, Hoyt DW, Klevit RE: **A UbcH5/ubiquitin noncovalent complex is required for processive BRCA1-directed ubiquitination.** *Mol Cell* 2006, **21**:873-880.
38. Brzovic PS, Keeffe JR, Nishikawa H, Miyamoto K, Fox D, 3rd, Fukuda M, Ohta T, Klevit R: **Binding and recognition in the assembly of an active BRCA1/BARD1 ubiquitin-ligase complex.** *Proc Natl Acad Sci U S A* 2003, **100**:5646-5651.

39. Gatti M, Pinato S, Maiolica A, Rocchio F, Prato MG, Aebersold R, Penengo L: **RNF168 promotes noncanonical K27 ubiquitination to signal DNA damage.** *Cell Rep* 2015, **10**:226-238.
40. Mevissen TET, Komander D: **Mechanisms of Deubiquitinase Specificity and Regulation.** *Annu Rev Biochem* 2017, **86**:159-192.
41. Zong Z, Zhang Z, Wu L, Zhang L, Zhou F: **The Functional Deubiquitinating Enzymes in Control of Innate Antiviral Immunity.** *Adv Sci (Weinh)* 2021, **8**:2002484.
42. Shrestha R, Das C: **Crystal structure of the Thr316Ala mutant of a yeast JAMM deubiquitinase: implication of active-site loop dynamics in catalysis.** *Acta Crystallogr F Struct Biol Commun* 2021, **77**:163-170.
43. Maurer T, Wertz IE: **Length Matters: MINDY Is a New Deubiquitinase Family that Preferentially Cleaves Long Polyubiquitin Chains.** *Mol Cell* 2016, **63**:4-6.
44. Fisher RD, Wang B, Alam SL, Higginson DS, Robinson H, Sundquist WI, Hill CP: **Structure and ubiquitin binding of the ubiquitin-interacting motif.** *J Biol Chem* 2003, **278**:28976-28984.
45. Swatek KN, Komander D: **Ubiquitin modifications.** *Cell Res* 2016, **26**:399-422.
46. Kazlauskaitė A, Kondapalli C, Gourlay R, Campbell DG, Ritorto MS, Hofmann K, Alessi DR, Knebel A, Trost M, Muqit MM: **Parkin is activated by PINK1-dependent phosphorylation of ubiquitin at Ser65.** *Biochem J* 2014, **460**:127-139.
47. Gladkova C, Maslen SL, Skehel JM, Komander D: **Mechanism of parkin activation by PINK1.** *Nature* 2018, **559**:410-414.
48. Schubert AF, Gladkova C, Pardon E, Wagstaff JL, Freund SMV, Steyaert J, Maslen SL, Komander D: **Structure of PINK1 in complex with its substrate ubiquitin.** *Nature* 2017, **552**:51-56.
49. Kazlauskaitė A, Muqit MM: **PINK1 and Parkin - mitochondrial interplay between phosphorylation and ubiquitylation in Parkinson's disease.** *FEBS J* 2015, **282**:215-223.
50. Knipscheer P, Sixma TK: **Protein-protein interactions regulate Ubl conjugation.** *Curr Opin Struct Biol* 2007, **17**:665-673.
51. Muller S, Hoege C, Pyrowolakis G, Jentsch S: **SUMO, ubiquitin's mysterious cousin.** *Nat Rev Mol Cell Biol* 2001, **2**:202-210.
52. Macauley MS, Errington WJ, Okon M, Scharpf M, Mackereth CD, Schulman BA, McIntosh LP: **Structural and dynamic independence of isopeptide-linked RanGAP1 and SUMO-1.** *J Biol Chem* 2004, **279**:49131-49137.
53. Girdwood DW, Tatham MH, Hay RT: **SUMO and transcriptional regulation.** *Semin Cell Dev Biol* 2004, **15**:201-210.
54. Zhao C, Denison C, Huibregtse JM, Gygi S, Krug RM: **Human ISG15 conjugation targets both IFN-induced and constitutively expressed proteins functioning in diverse cellular pathways.** *Proc Natl Acad Sci U S A* 2005, **102**:10200-10205.
55. Lorick KL, Jensen JP, Fang S, Ong AM, Hatakeyama S, Weissman AM: **RING fingers mediate ubiquitin-conjugating enzyme (E2)-dependent ubiquitination.** *Proc Natl Acad Sci U S A* 1999, **96**:11364-11369.
56. Lu JY, Lin YY, Qian J, Tao SC, Zhu J, Pickart C, Zhu H: **Functional dissection of a HECT ubiquitin E3 ligase.** *Molecular & cellular proteomics : MCP* 2008, **7**:35-45.
57. Weiss ER, Popova E, Yamanaka H, Kim HC, Huibregtse JM, Gottlinger H: **Rescue of HIV-1 release by targeting widely divergent NEDD4-type ubiquitin ligases and isolated catalytic HECT domains to Gag.** *PLoS Pathog* 2010, **6**:e1001107.
58. Aragon E, Goerner N, Zaromytidou AI, Xi Q, Escobedo A, Massague J, Macias MJ: **A Smad action turnover switch operated by WW domain readers of a phosphoserine code.** *Genes Dev* 2011, **25**:1275-1288.

59. Argenzio E, Bange T, Oldrini B, Bianchi F, Peesari R, Mari S, Di Fiore PP, Mann M, Polo S: **Proteomic snapshot of the EGF-induced ubiquitin network.** *Molecular systems biology* 2011, **7**:462.
60. Wong JJ, Pung YF, Sze NS, Chin KC: **HERC5 is an IFN-induced HECT-type E3 protein ligase that mediates type I IFN-induced ISGylation of protein targets.** *Proc Natl Acad Sci U S A* 2006, **103**:10735-10740.
61. Pandya RK, Partridge JR, Love KR, Schwartz TU, Ploegh HL: **A structural element within the HUWE1 HECT domain modulates self-ubiquitination and substrate ubiquitination activities.** *J Biol Chem* 2010, **285**:5664-5673.
62. Ogunjimi AA, Briant DJ, Pece-Barbara N, Le Roy C, Di Guglielmo GM, Kavsak P, Rasmussen RK, Seet BT, Sicheri F, Wrana JL: **Regulation of Smurf2 ubiquitin ligase activity by anchoring the E2 to the HECT domain.** *Mol Cell* 2005, **19**:297-308.
63. Harper JW, Schulman BA: **Cullin-RING Ubiquitin Ligase Regulatory Circuits: A Quarter Century Beyond the F-Box Hypothesis.** *Annu Rev Biochem* 2021, **90**:403-429.
64. Bosu DR, Kipreos ET: **Cullin-RING ubiquitin ligases: global regulation and activation cycles.** *Cell Div* 2008, **3**:7.
65. Zhao Y, Sun Y: **Cullin-RING Ligases as attractive anti-cancer targets.** *Curr Pharm Des* 2013, **19**:3215-3225.
66. Wang X, Martin DS: **The COP9 signalosome and cullin-RING ligases in the heart.** *Am J Cardiovasc Dis* 2015, **5**:1-18.
67. Pan ZQ: **Cullin-RING E3 Ubiquitin Ligase 7 in Growth Control and Cancer.** *Adv Exp Med Biol* 2020, **1217**:285-296.
68. Fouad S, Wells OS, Hill MA, D'Angiolella V: **Cullin Ring Ubiquitin Ligases (CRLs) in Cancer: Responses to Ionizing Radiation (IR) Treatment.** *Front Physiol* 2019, **10**:1144.
69. Yu C, Mao H, Novitsky EJ, Tang X, Rychnovsky SD, Zheng N, Huang L: **Gln40 deamidation blocks structural reconfiguration and activation of SCF ubiquitin ligase complex by Nedd8.** *Nat Commun* 2015, **6**:10053.
70. Haagenson KK, Tait L, Wang J, Shekhar MP, Polin L, Chen W, Wu GS: **Cullin-3 protein expression levels correlate with breast cancer progression.** *Cancer Biol Ther* 2012, **13**:1042-1046.
71. Jin L, Williamson A, Banerjee S, Philipp I, Rape M: **Mechanism of ubiquitin-chain formation by the human anaphase-promoting complex.** *Cell* 2008, **133**:653-665.
72. Xing W, Busino L, Hinds TR, Marionni ST, Saifee NH, Bush MF, Pagano M, Zheng N: **SCF(FBXL3) ubiquitin ligase targets cryptochromes at their cofactor pocket.** *Nature* 2013, **496**:64-68.
73. Kamura T, Conrad MN, Yan Q, Conaway RC, Conaway JW: **The Rbx1 subunit of SCF and VHL E3 ubiquitin ligase activates Rub1 modification of cullins Cdc53 and Cul2.** *Genes Dev* 1999, **13**:2928-2933.
74. Zheng N, Schulman BA, Song L, Miller JJ, Jeffrey PD, Wang P, Chu C, Koepp DM, Elledge SJ, Pagano M, et al.: **Structure of the Cul1-Rbx1-Skp1-F boxSkp2 SCF ubiquitin ligase complex.** *Nature* 2002, **416**:703-709.
75. Schulman BA, Carrano AC, Jeffrey PD, Bowen Z, Kinnucan ER, Finnin MS, Elledge SJ, Harper JW, Pagano M, Pavletich NP: **Insights into SCF ubiquitin ligases from the structure of the Skp1-Skp2 complex.** *Nature* 2000, **408**:381-386.
76. Podust VN, Brownell JE, Gladysheva TB, Luo RS, Wang C, Coggins MB, Pierce JW, Lightcap ES, Chau V: **A Nedd8 conjugation pathway is essential for proteolytic targeting of p27Kip1 by ubiquitination.** *Proc Natl Acad Sci U S A* 2000, **97**:4579-4584.

77. Read MA, Brownell JE, Gladysheva TB, Hottelet M, Parent LA, Coggins MB, Pierce JW, Podust VN, Luo RS, Chau V, et al.: **Nedd8 modification of cul-1 activates SCF(beta(TrCP))-dependent ubiquitination of I kappa B alpha.** *Mol Cell Biol* 2000, **20**:2326-2333.
78. Wu K, Chen A, Pan ZQ: **Conjugation of Nedd8 to CUL1 enhances the ability of the ROC1-CUL1 complex to promote ubiquitin polymerization.** *J Biol Chem* 2000, **275**:32317-32324.
79. Morimoto M, Nishida T, Honda R, Yasuda H: **Modification of cullin-1 by ubiquitin-like protein Nedd8 enhances the activity of SCF(skp2) toward p27(kip1).** *Biochem Biophys Res Commun* 2000, **270**:1093-1096.
80. Duda DM, Scott DC, Calabrese MF, Zimmerman ES, Zheng N, Schulman BA: **Structural regulation of cullin-RING ubiquitin ligase complexes.** *Curr Opin Struct Biol* 2011, **21**:257-264.
81. Bohnsack RN, Haas AL: **Conservation in the mechanism of Nedd8 activation by the human AppBp1-Uba3 heterodimer.** *J Biol Chem* 2003, **278**:26823-26830.
82. Monda JK, Scott DC, Miller DJ, Lydeard J, King D, Harper JW, Bennett EJ, Schulman BA: **Structural conservation of distinctive N-terminal acetylation-dependent interactions across a family of mammalian NEDD8 ligation enzymes.** *Structure* 2013, **21**:42-53.
83. Cavadini S, Fischer ES, Bunker RD, Potenza A, Lingaraju GM, Goldie KN, Mohamed WI, Faty M, Petzold G, Beckwith RE, et al.: **Cullin-RING ubiquitin E3 ligase regulation by the COP9 signalosome.** *Nature* 2016, **531**:598-603.
84. Lingaraju GM, Bunker RD, Cavadini S, Hess D, Hassiepen U, Renuis M, Fischer ES, Thoma NH: **Crystal structure of the human COP9 signalosome.** *Nature* 2014, **512**:161-165.
85. Enchev RI, Scott DC, da Fonseca PC, Schreiber A, Monda JK, Schulman BA, Peter M, Morris EP: **Structural basis for a reciprocal regulation between SCF and CSN.** *Cell Rep* 2012, **2**:616-627.
86. Wang K, Deshaies RJ, Liu X: **Assembly and Regulation of CRL Ubiquitin Ligases.** *Adv Exp Med Biol* 2020, **1217**:33-46.
87. Goldenberg SJ, Cascio TC, Shumway SD, Garbutt KC, Liu J, Xiong Y, Zheng N: **Structure of the Cand1-Cul1-Roc1 complex reveals regulatory mechanisms for the assembly of the multisubunit cullin-dependent ubiquitin ligases.** *Cell* 2004, **119**:517-528.
88. Zheng J, Yang X, Harrell JM, Ryzhikov S, Shim EH, Lykke-Andersen K, Wei N, Sun H, Kobayashi R, Zhang H: **CAND1 binds to unneddylated CUL1 and regulates the formation of SCF ubiquitin E3 ligase complex.** *Mol Cell* 2002, **10**:1519-1526.
89. Mosadeghi R, Reichermeier KM, Winkler M, Schreiber A, Reitsma JM, Zhang Y, Stengel F, Cao J, Kim M, Sweredoski MJ, et al.: **Structural and kinetic analysis of the COP9-Signalosome activation and the cullin-RING ubiquitin ligase deneddylation cycle.** *Elife* 2016, **5**.
90. Stieglitz B, Morris-Davies AC, Koliopoulos MG, Christodoulou E, Rittinger K: **LUBAC synthesizes linear ubiquitin chains via a thioester intermediate.** *EMBO Rep* 2012, **13**:840-846.
91. Tokunaga F, Iwai K: **LUBAC, a novel ubiquitin ligase for linear ubiquitination, is crucial for inflammation and immune responses.** *Microbes Infect* 2012, **14**:563-572.
92. Ikeda F, Deribe YL, Skanland SS, Stieglitz B, Grabbe C, Franz-Wachtel M, van Wijk SJ, Goswami P, Nagy V, Terzic J, et al.: **SHARPIN forms a linear ubiquitin ligase complex regulating NF-kappaB activity and apoptosis.** *Nature* 2011, **471**:637-641.
93. Wu CJ, Conze DB, Li T, Srinivasula SM, Ashwell JD: **NEMO is a sensor of Lys 63-linked polyubiquitination and functions in NF-kappaB activation.** *Nat Cell Biol* 2006, **8**:398-406.

94. Smit JJ, Monteferrario D, Noordermeer SM, van Dijk WJ, van der Reijden BA, Sixma TK: **The E3 ligase HOIP specifies linear ubiquitin chain assembly through its RING-IBR-RING domain and the unique LDD extension.** *Embo J* 2012, **31**:3833-3844.
95. Spratt DE, Julio Martinez-Torres R, Noh YJ, Mercier P, Manczyk N, Barber KR, Aguirre JD, Burchell L, Purkiss A, Walden H, et al.: **A molecular explanation for the recessive nature of parkin-linked Parkinson's disease.** *Nat Commun* 2013, **4**:1983.
96. Chaugule VK, Burchell L, Barber KR, Sidhu A, Leslie SJ, Shaw GS, Walden H: **Autoregulation of Parkin activity through its ubiquitin-like domain.** *Embo J* 2011, **30**:2853-2867.
97. Kitada T, Asakawa S, Hattori N, Matsumine H, Yamamura Y, Minoshima S, Yokochi M, Mizuno Y, Shimizu N: **Mutations in the parkin gene cause autosomal recessive juvenile parkinsonism.** *Nature* 1998, **392**:605-608.
98. Trempe JF, Sauve V, Grenier K, Seirafi M, Tang MY, Menade M, Al-Abdul-Wahid S, Krett J, Wong K, Kozlov G, et al.: **Structure of Parkin Reveals Mechanisms for Ubiquitin Ligase Activation.** *Science* 2013, **340**:1451-1455.
99. Kellsall IR, Duda DM, Olszewski JL, Hofmann K, Knebel A, Langevin F, Wood N, Wightman M, Schulman BA, Alpi AF: **TRIAD1 and HHARI bind to and are activated by distinct neddylated Cullin-RING ligase complexes.** *EMBO J* 2013, **32**:2848-2860.
100. Wenzel DM, Klevit RE: **Following Ariadne's thread: a new perspective on RBR ubiquitin ligases.** *BMC Biol* 2012, **10**:24.
101. Marin I: **RBR ubiquitin ligases: Diversification and streamlining in animal lineages.** *J Mol Evol* 2009, **69**:54-64.
102. Walden H, Rittinger K: **RBR ligase-mediated ubiquitin transfer: a tale with many twists and turns.** *Nat Struct Mol Biol* 2018, **25**:440-445.
103. Aguilera M, Oliveros M, Martinez-Padron M, Barbas JA, Ferrus A: **Ariadne-1: a vital Drosophila gene is required in development and defines a new conserved family of ring-finger proteins.** *Genetics* 2000, **155**:1231-1244.
104. Duda DM, Olszewski JL, Schuermann JP, Kurinov I, Miller DJ, Nourse A, Alpi AF, Schulman BA: **Structure of HHARI, a RING-IBR-RING Ubiquitin Ligase: Autoinhibition of an Ariadne-Family E3 and Insights into Ligation Mechanism.** *Structure* 2013, **21**:1030-1041.
105. Dove KK, Olszewski JL, Martino L, Duda DM, Wu XS, Miller DJ, Reiter KH, Rittinger K, Schulman BA, Klevit RE: **Structural Studies of HHARI/UbcH7 approximately Ub Reveal Unique E2 approximately Ub Conformational Restriction by RBR RING1.** *Structure* 2017, **25**:890-900 e895.
106. Yuan L, Lv Z, Atkison JH, Olsen SK: **Structural insights into the mechanism and E2 specificity of the RBR E3 ubiquitin ligase HHARI.** *Nat Commun* 2017, **8**:211.
107. Ahel J, Lehner A, Vogel A, Schleiffer A, Meinhart A, Haselbach D, Clausen T: **Moyamoya disease factor RNF213 is a giant E3 ligase with a dynein-like core and a distinct ubiquitin-transfer mechanism.** *Elife* 2020, **9**.
108. Hwang CS, Shemorry A, Auerbach D, Varshavsky A: **The N-end rule pathway is mediated by a complex of the RING-type Ubr1 and HECT-type Ufd4 ubiquitin ligases.** *Nat Cell Biol* 2010, **12**:1177-1185.
109. Pan M, Zheng Q, Wang T, Liang L, Mao J, Zuo C, Ding R, Ai H, Xie Y, Si D, et al.: **Structural insights into Ubr1-mediated N-degron polyubiquitination.** *Nature* 2021, **600**:334-338.
110. Baek K, Krist DT, Prabu JR, Hill S, Klugel M, Neumaier LM, von Gronau S, Kleiger G, Schulman BA: **NEDD8 nucleates a multivalent cullin-RING-UBE2D ubiquitin ligation assembly.** *Nature* 2020, **578**:461-466.

111. Huttenhain R, Xu J, Burton LA, Gordon DE, Hultquist JF, Johnson JR, Satkamp L, Hiatt J, Rhee DY, Baek K, et al.: **ARIH2 Is a Vif-Dependent Regulator of CUL5-Mediated APOBEC3G Degradation in HIV Infection.** *Cell Host Microbe* 2019, **26**:86-99 e87.
112. Lin AE, Ebert G, Ow Y, Preston SP, Toe JG, Cooney JP, Scott HW, Sasaki M, Saibil SD, Dissanayake D, et al.: **ARIH2 is essential for embryogenesis, and its hematopoietic deficiency causes lethal activation of the immune system.** *Nat Immunol* 2013, **14**:27-33.
113. Heinzlmeir S, Muller S: **Selectivity aspects of activity-based (chemical) probes.** *Drug Discov Today* 2021, 10.1016/j.drudis.2021.10.021.
114. Fang H, Peng B, Ong SY, Wu Q, Li L, Yao SQ: **Recent advances in activity-based probes (ABPs) and affinity-based probes (AfBPs) for profiling of enzymes.** *Chem Sci* 2021, **12**:8288-8310.
115. Mathur S, Fletcher AJ, Branigan E, Hay RT, Virdee S: **Photocrosslinking Activity-Based Probes for Ubiquitin RING E3 Ligases.** *Cell Chem Biol* 2020, **27**:74-82 e76.
116. Hemelaar J, Borodovsky A, Kessler BM, Reverter D, Cook J, Kolli N, Gan-Erdene T, Wilkinson KD, Gill G, Lima CD, et al.: **Specific and covalent targeting of conjugating and deconjugating enzymes of ubiquitin-like proteins.** *Mol Cell Biol* 2004, **24**:84-95.
117. Henneberg LT, Schulman BA: **Decoding the messaging of the ubiquitin system using chemical and protein probes.** *Cell Chem Biol* 2021, **28**:889-902.
118. Meledin R, Mali SM, Kleifeld O, Brik A: **Activity-Based Probes Developed by Applying a Sequential Dehydroalanine Formation Strategy to Expressed Proteins Reveal a Potential alpha-Globin-Modulating Deubiquitinase.** *Angew Chem Int Ed Engl* 2018, **57**:5645-5649.
119. Pao KC, Stanley M, Han C, Lai YC, Murphy P, Balk K, Wood NT, Corti O, Corvol JC, Muqit MM, et al.: **Probes of ubiquitin E3 ligases enable systematic dissection of parkin activation.** *Nat Chem Biol* 2016, **12**:324-331.
120. Huang X, Dixit VM: **Drugging the undruggables: exploring the ubiquitin system for drug development.** *Cell Res* 2016, **26**:484-498.
121. Krist DT, Foote PK, Statsyuk AV: **UbFluor: A Fluorescent Thioester to Monitor HECT E3 Ligase Catalysis.** *Curr Protoc Chem Biol* 2017, **9**:11-37.
122. Haj-Yahya N, Hemantha HP, Meledin R, Bondalapati S, Seenaiyah M, Brik A: **Dehydroalanine-based diubiquitin activity probes.** *Org Lett* 2014, **16**:540-543.
123. Weber A, Elliott PR, Pinto-Fernandez A, Bonham S, Kessler BM, Komander D, El Oualid F, Krappmann D: **A Linear Diubiquitin-Based Probe for Efficient and Selective Detection of the Deubiquitinating Enzyme OTULIN.** *Cell Chem Biol* 2017, **24**:1299-1313 e1297.
124. Li G, Liang Q, Gong P, Tencer AH, Zhuang Z: **Activity-based diubiquitin probes for elucidating the linkage specificity of deubiquitinating enzymes.** *Chem Commun (Camb)* 2014, **50**:216-218.
125. Hein JE, Fokin VV: **Copper-catalyzed azide-alkyne cycloaddition (CuAAC) and beyond: new reactivity of copper(I) acetylides.** *Chem Soc Rev* 2010, **39**:1302-1315.
126. Liang LJ, Chu GC, Qu Q, Zuo C, Mao J, Zheng Q, Chen J, Meng X, Jing Y, Deng H, et al.: **Chemical Synthesis of Activity-Based E2-Ubiquitin Probes for the Structural Analysis of E3 Ligase-Catalyzed Transthiolation.** *Angew Chem Int Ed Engl* 2021, **60**:17171-17177.
127. Lydeard JR, Schulman BA, Harper JW: **Building and remodelling Cullin-RING E3 ubiquitin ligases.** *EMBO Rep* 2013, **14**:1050-1061.
128. Orlicky S, Tang X, Willems A, Tyers M, Sicheri F: **Structural basis for phosphodependent substrate selection and orientation by the SCFCdc4 ubiquitin ligase.** *Cell* 2003, **112**:243-256.

129. Tang X, Orlicky S, Liu Q, Willems A, Sicheri F, Tyers M: **Genome-wide surveys for phosphorylation-dependent substrates of SCF ubiquitin ligases.** *Methods Enzymol* 2005, **399**:433-458.
130. Kastner B, Fischer N, Golas MM, Sander B, Dube P, Boehringer D, Hartmuth K, Deckert J, Hauer F, Wolf E, et al.: **GraFix: sample preparation for single-particle electron cryomicroscopy.** *Nat Methods* 2008, **5**:53-55.
131. Dove KK, Kemp HA, Di Bona KR, Reiter KH, Milburn LJ, Camacho D, Fay DS, Miller DL, Klevit RE: **Two functionally distinct E2/E3 pairs coordinate sequential ubiquitination of a common substrate in *Caenorhabditis elegans* development.** *Proc Natl Acad Sci U S A* 2017, **114**:E6576-E6584.
132. Kostrhon S, Prabu JR, Baek K, Horn-Ghetko D, von Gronau S, Klugel M, Basquin J, Alpi AF, Schulman BA: **CUL5-ARIH2 E3-E3 ubiquitin ligase structure reveals cullin-specific NEDD8 activation.** *Nat Chem Biol* 2021, 10.1038/s41589-021-00858-8.
133. Spratt DE, Walden H, Shaw GS: **RBR E3 ubiquitin ligases: new structures, new insights, new questions.** *Biochem J* 2014, **458**:421-437.
134. Emberley ED, Mosadeghi R, Deshaies RJ: **Deconjugation of Nedd8 from Cull1 is directly regulated by Skp1-F-box and substrate, and the COP9 signalosome inhibits deneddylated SCF by a noncatalytic mechanism.** *J Biol Chem* 2012, **287**:29679-29689.
135. Fischer ES, Scrima A, Bohm K, Matsumoto S, Lingaraju GM, Faty M, Yasuda T, Cavadini S, Wakasugi M, Hanaoka F, et al.: **The molecular basis of CRL4DDB2/CSA ubiquitin ligase architecture, targeting, and activation.** *Cell* 2011, **147**:1024-1039.
136. Wu K, Kovacev J, Pan ZQ: **Priming and extending: a UbcH5/Cdc34 E2 handoff mechanism for polyubiquitination on a SCF substrate.** *Mol Cell* 2010, **37**:784-796.
137. Hill S, Reichermeier K, Scott DC, Samentar L, Coulombe-Huntington J, Izzi L, Tang X, Ibarra R, Bertomeu T, Moradian A, et al.: **Robust cullin-RING ligase function is established by a multiplicity of poly-ubiquitylation pathways.** *Elife* 2019, **8**.
138. Bornstein G, Ganoth D, Hershko A: **Regulation of neddylation and deneddylation of cullin1 in SCFSkp2 ubiquitin ligase by F-box protein and substrate.** *Proc Natl Acad Sci U S A* 2006, **103**:11515-11520.
139. Zimmerman ES, Schulman BA, Zheng N: **Structural assembly of cullin-RING ubiquitin ligase complexes.** *Curr Opin Struct Biol* 2010, **20**:714-721.
140. Sarikas A, Hartmann T, Pan ZQ: **The cullin protein family.** *Genome Biol* 2011, **12**:220.
141. Lechtenberg BC, Rajput A, Sanishvili R, Dobaczewska MK, Ware CF, Mace PD, Riedl SJ: **Structure of a HOIP/E2~ubiquitin complex reveals RBR E3 ligase mechanism and regulation.** *Nature* 2016, **529**:546-550.
142. Wauer T, Simicek M, Schubert A, Komander D: **Mechanism of phospho-ubiquitin-induced PARKIN activation.** *Nature* 2015, **524**:370-374.
143. Li Z, Xiong Y: **Cytoplasmic E3 ubiquitin ligase CUL9 controls cell proliferation, senescence, apoptosis and genome integrity through p53.** *Oncogene* 2017, 10.1038/onc.2017.141.
144. Li Z, Pei XH, Yan J, Yan F, Cappell KM, Whitehurst AW, Xiong Y: **CUL9 mediates the functions of the 3M complex and ubiquitylates survivin to maintain genome integrity.** *Mol Cell* 2014, **54**:805-819.
145. Gama V, Swahari V, Schafer J, Kole AJ, Evans A, Huang Y, Cliffe A, Golitz B, Sciaky N, Pei XH, et al.: **The E3 ligase PARC mediates the degradation of cytosolic cytochrome c to promote survival in neurons and cancer cells.** *Sci Signal* 2014, **7**:ra67.
146. Jackson PK: **Regulating microtubules and genome stability via the CUL7/3M syndrome complex and CUL9.** *Mol Cell* 2014, **54**:713-715.

147. de Jong A, Merckx R, Berlin I, Rodenko B, Wijdeven RH, El Atmioui D, Yalcin Z, Robson CN, Neeffjes JJ, Ovaas H: **Ubiquitin-based probes prepared by total synthesis to profile the activity of deubiquitinating enzymes.** *Chembiochem* 2012, **13**:2251-2258.
148. Pierce NW, Kleiger G, Shan SO, Deshaies RJ: **Detection of sequential polyubiquitylation on a millisecond timescale.** *Nature* 2009, **462**:615-619.
149. Zivanov J, Nakane T, Forsberg BO, Kimanius D, Hagen WJ, Lindahl E, Scheres SH: **New tools for automated high-resolution cryo-EM structure determination in RELION-3.** *Elife* 2018, **7**.
150. Zhang K: **Gctf: Real-time CTF determination and correction.** *J Struct Biol* 2016, **193**:1-12.
151. Adams PD, Afonine PV, Bunkoczi G, Chen VB, Davis IW, Echols N, Headd JJ, Hung LW, Kapral GJ, Grosse-Kunstleve RW, et al.: **PHENIX: a comprehensive Python-based system for macromolecular structure solution.** *Acta Crystallogr D Biol Crystallogr* 2010, **66**:213-221.
152. Pettersen EF, Goddard TD, Huang CC, Couch GS, Greenblatt DM, Meng EC, Ferrin TE: **UCSF Chimera--a visualization system for exploratory research and analysis.** *J Comput Chem* 2004, **25**:1605-1612.
153. Emsley P, Lohkamp B, Scott WG, Cowtan K: **Features and development of Coot.** *Acta Crystallogr D Biol Crystallogr* 2010, **66**:486-501.
154. Afonine PV, Klaholz BP, Moriarty NW, Poon BK, Sobolev OV, Terwilliger TC, Adams PD, Urzhumtsev A: **New tools for the analysis and validation of cryo-EM maps and atomic models.** *Acta Crystallogr D Struct Biol* 2018, **74**:814-840.
155. Scott DC, Sviderskiy VO, Monda JK, Lydeard JR, Cho SE, Harper JW, Schulman BA: **Structure of a RING E3 Trapped in Action Reveals Ligation Mechanism for the Ubiquitin-like Protein NEDD8.** *Cell* 2014, **157**:1671-1684.
156. Duda DM, Borg LA, Scott DC, Hunt HW, Hammel M, Schulman BA: **Structural insights into NEDD8 activation of cullin-RING ligases: conformational control of conjugation.** *Cell* 2008, **134**:995-1006.
157. Condos TE, Dunkerley KM, Freeman EA, Barber KR, Aguirre JD, Chaugule VK, Xiao Y, Konermann L, Walden H, Shaw GS: **Synergistic recruitment of UbcH7~Ub and phosphorylated Ubl domain triggers parkin activation.** *EMBO J* 2018, **37**.

# Abbreviations

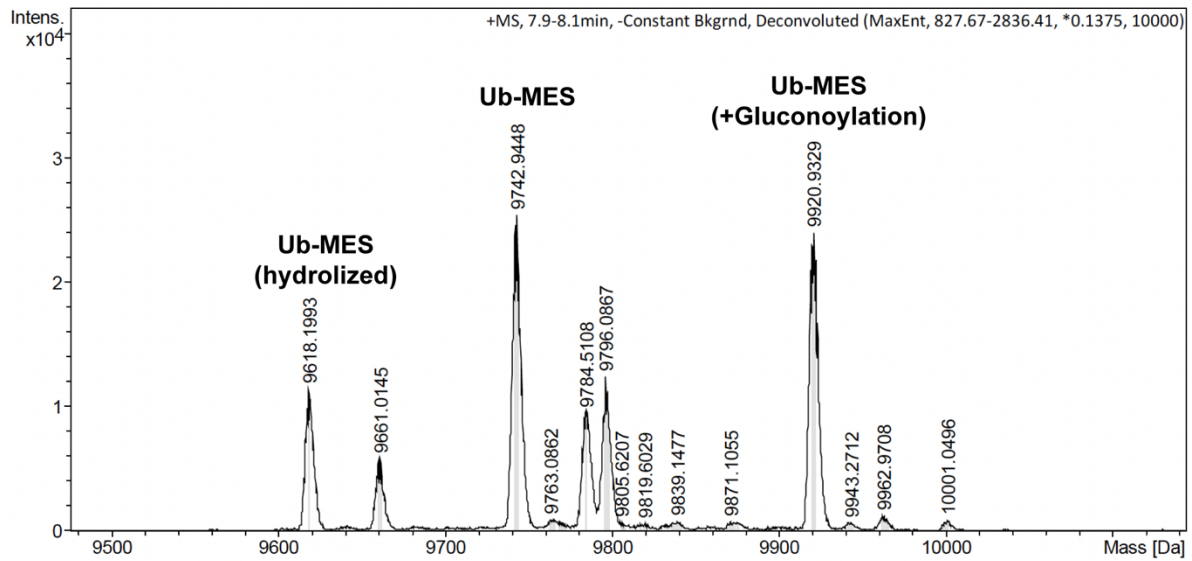
HECT – Homologous to the E6-AP Carboxyl Terminus  
RING – Really Interesting New Gene  
NEDD8 – Neural-precursor-cell-Expressed Developmentally Down-regulated 8  
CRL – Cullin RING Ligase  
ARIH – Ariadne homologue  
RBR – RING-in-between-RING  
SCF – SKP1-CUL1-Fbox  
SKP1 – S-phase kinase-associated protein 1  
SKP2 – S-phase kinase-associated protein 2  
Cryo-EM – Cryo-electron microscopy  
FBXW7 – F-Box and WD Repeat Domain Containing 7  
b-TRCP – beta-transducin repeat containing  
I $\kappa$ B $\alpha$  – nuclear factor of kappa light polypeptide gene enhancer in B-cells inhibitor, alpha  
UBE2L3 – Ubiquitin Conjugating Enzyme E2 L3  
DNA – deoxyribonucleic acid  
RNA – ribonucleic acid  
PTM – post-translational modification  
ATP – adenosine triphosphate  
UBD – ubiquitin-binding domain  
ERAD – Endoplasmatic reticulum-associated degradation  
NF- $\kappa$ B – nuclear factor 'kappa-light-chain-enhancer' of activated B-cells  
LUBAC – linear ubiquitin chain assembly complex  
BRCA1/BARD1 – breast cancer 1/ BRCA1 associated RING Domain 1  
RNF168 – Ring Finger Protein 168  
DUBs – Deubiquitinases  
UCH – Ubiquitin C-terminal hydrolases  
USP – Ubiquitin-specific processing protease  
OUT – Ovarian tumor protease  
MJD – Machado-Josephin domain  
JAB1 – c-Jun activation domain-binding protein-1  
MIU – Motif interacting with ubiquitin

MINDY – MIU-containing novel DUB  
UFM – Ubiquitin-Fold-Modifier 1  
JAMM – JAB1/MPN/Mov34 metalloenzyme  
ZUP – Zinc finger containing ubiquitin peptidase 1  
PTEN – Phosphatase and Tensin homolog  
SUMO – Small Ubiquitin-Related Modifier  
ISG15 – Interferon-stimulated gene 15  
FAT10 – leukocyte antigen-F adjacent transcript 10  
MNSF $\beta$  – Monoclonal nonspecific suppressor factor beta  
GTP – guanosine triphosphate  
RanBP2 – RAN Binding Protein 2  
MYCBP2 – MYC Binding Protein 2  
NEDD4 – Neural precursor cell expressed developmentally down-regulated  
EGFR – Epidermal Growth Factor Receptor  
HIV gag – human immunodeficiency virus group specific antigen  
TGF- $\beta$  – transforming growth factor beta  
JNK – c-jun N-terminal kinases  
HERC – HECT And RLD Domain Containing  
RLD – RCC1-like domain  
HUWE1 – HECT, UBA and WWE domain containing 1  
SMAD7 – SMAD Family Member 7  
SMURF1 – SMAD Specific E3 Ubiquitin Protein Ligase 1  
CUL – Cullin  
RBX1 – Ring-box 1  
CAND1 – Cullin Associated and Neddylation Dissociated 1  
NAE – NEDD8 activating enzyme  
APP-BP1 – amyloid beta precursor protein-binding protein 1  
UBA3 – ubiquitin-activating enzyme 3  
CSN – Casein Beta  
NEMO – NF-kappa-B essential modulator  
HOIP – HOIL interacting protein 1  
HOIL – Heme-oxidized IRP2 ubiquitin ligase 1  
TRIAD – All-Trans Retinoic Acid Inducible RING Finger  
ANKIB – Ankyrin Repeat and IBR Domain Containing 1

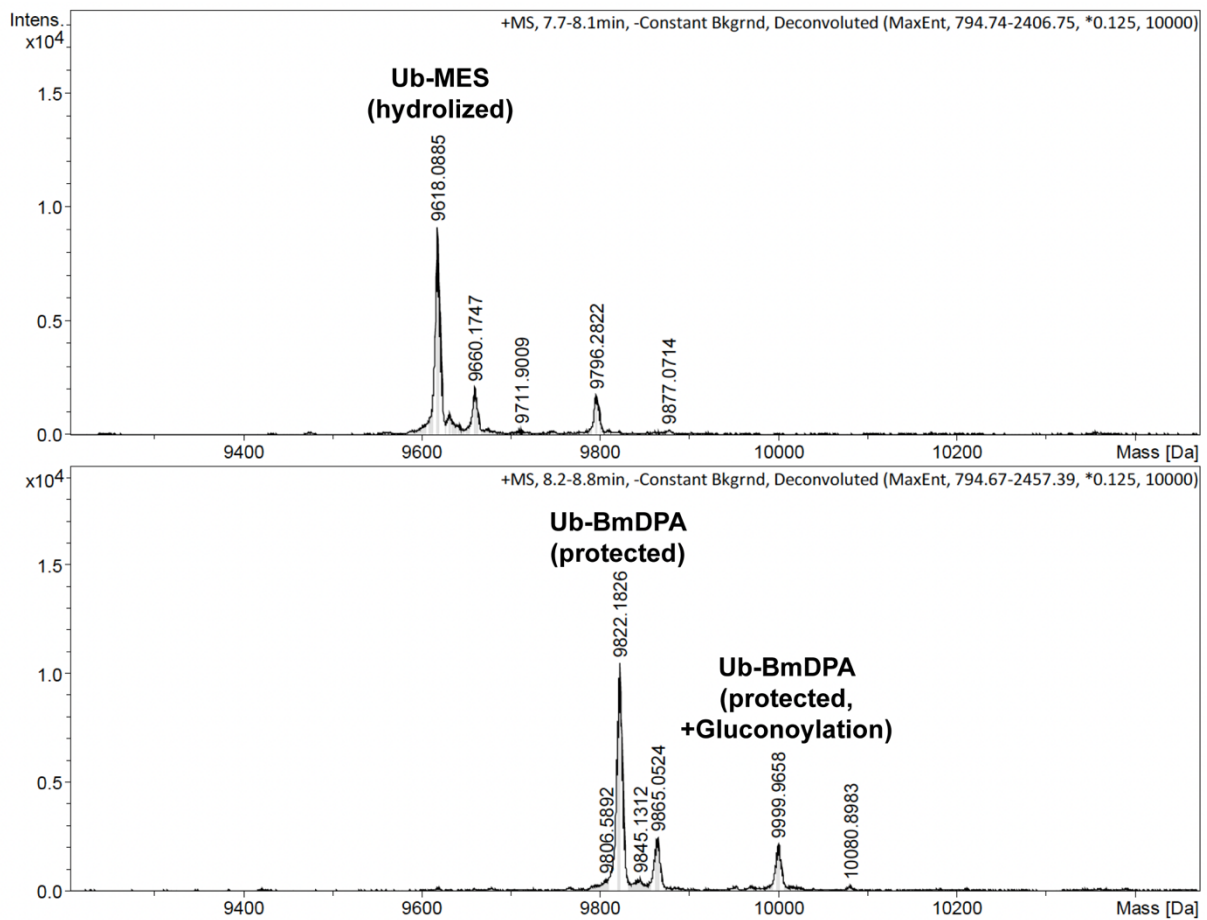
RTI – RING-to-IBR  
IBR – In-between-RING  
RCR – RING-Cys-Relay  
RNF213 – Ring finger protein 213  
LPS – Lipopolysaccharide  
ABP – Activity-based probe  
CTD – C-terminal domain  
Ubr1 – Ubiquitin Protein Ligase E3 Component N-Recognin 1  
Ufd4 – Ubiquitin fusion degradation protein 4  
p27/CDKN1B – Cyclin Dependent Kinase Inhibitor 1B  
MESNa – Sodium-2-Mercaptoethanesulfonic acid  
OTULIN – OTU Deubiquitinase With Linear Linkage Specificity  
Dha – dehydroalanine  
TS1/2 – Transition State 1/2  
SDS-PAGE – sodium dodecylsulfate polyacrylamide gel electrophoresis  
CKSHS1 – HUMAN CYCLIN DEPENDENT KINASE SUBUNIT, TYPE 1  
RQF – rapid quench-flow  
GraFix – gradient fixation  
CDK2 – cyclin dependent kinase 2  
CR1-3 – cullin repeat 1-3  
4HB – four helix bundle  
WHB – winged helix bundle  
UBAL – ubiquitin and ubiquitin-like protein-associated domain  
EM – electron microscopy  
UbVME – ubiquitin-vinylmethylester  
 $K_{obs}$  – observed rate constant  
 $K_M$  – Michaelis Constant  
PMSF – phenylmethanesulphonyl fluoride  
DTT – dithiothreitol  
HEPES – 4-(2-hydroxyethyl)-1-piperazineethanesulfonic acid  
MES – 2-(N-morpholino)ethanesulfonic acid  
BmDPA – (E)-3-[2-(bromomethyl)-1,3-dioxolan-2-yl]prop-2-en-1-amine  
TCEP – Tris(2 carboxyethyl)phosphine  
HPLC – high pressure liquid chromatography

TOF-MS – time-of-flight mass spectrometry  
LB – lysogeny broth  
PCR – polymerase chain reaction  
IPTG – Isopropyl  $\beta$ - d-1-thiogalactopyranoside  
RT – room temperature  
OD – optical density  
TB – terrific broth  
LC-MS – liquid chromatography mass spectrometry  
TFA – trifluoroacetic acid  
ESI-TOF – Electrospray-ionization time-of-flight  
Fmoc – Fluorenylmethoxycarbonyl  
PyBOP – Benzotriazol-1-yl-oxytripyrrolidinophosphonium-hexafluorophosphat  
Ni-NTA – Nickel-nitriloacetic acid  
DMSO – dimethylsulfoxide  
CRY1 – cryptochrome 1  
TEM – transmission electron microscope  
CTF – contrast transfer function

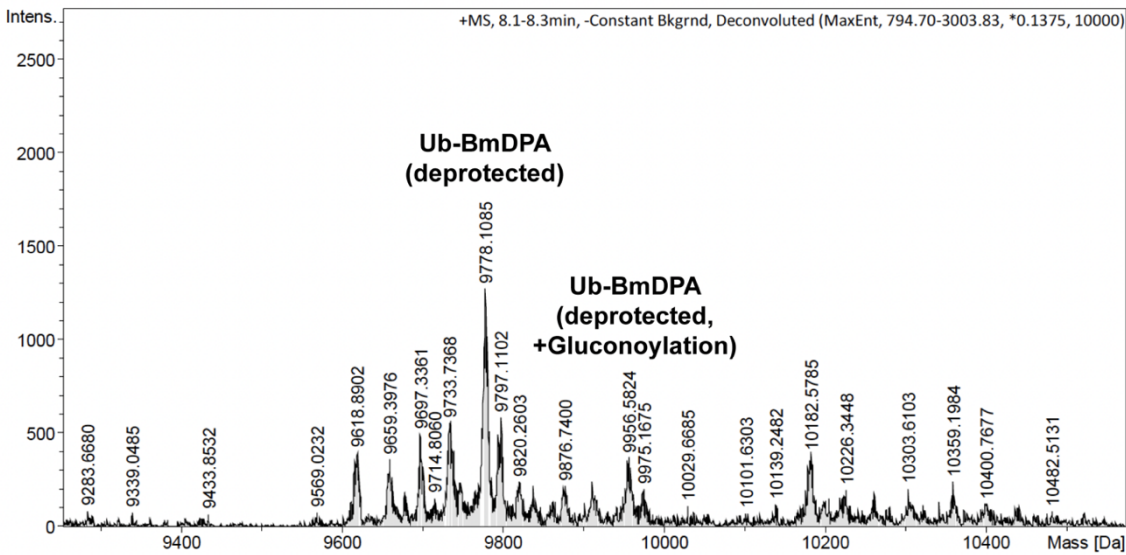
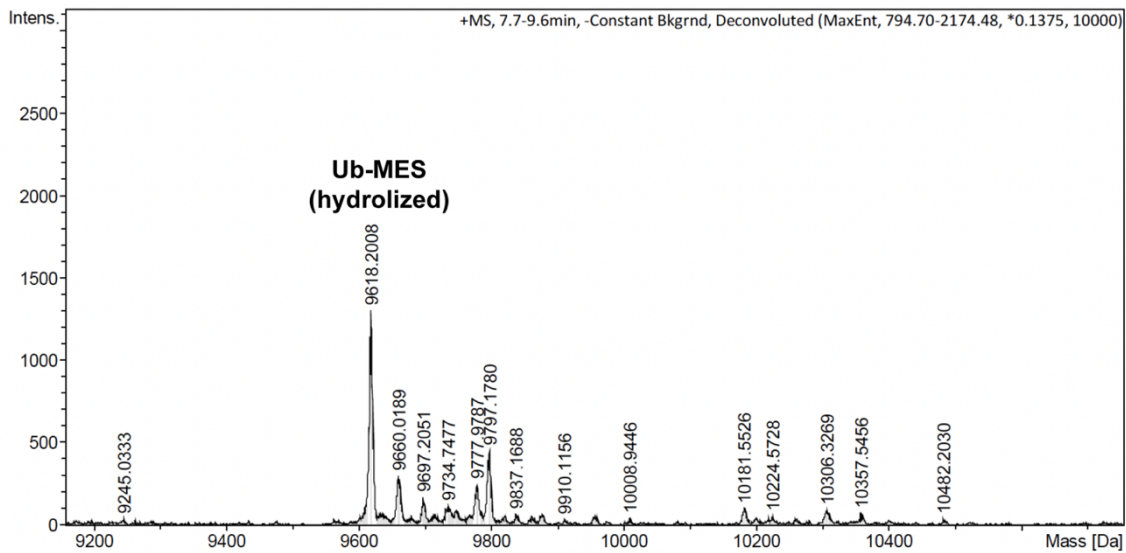
# Appendix



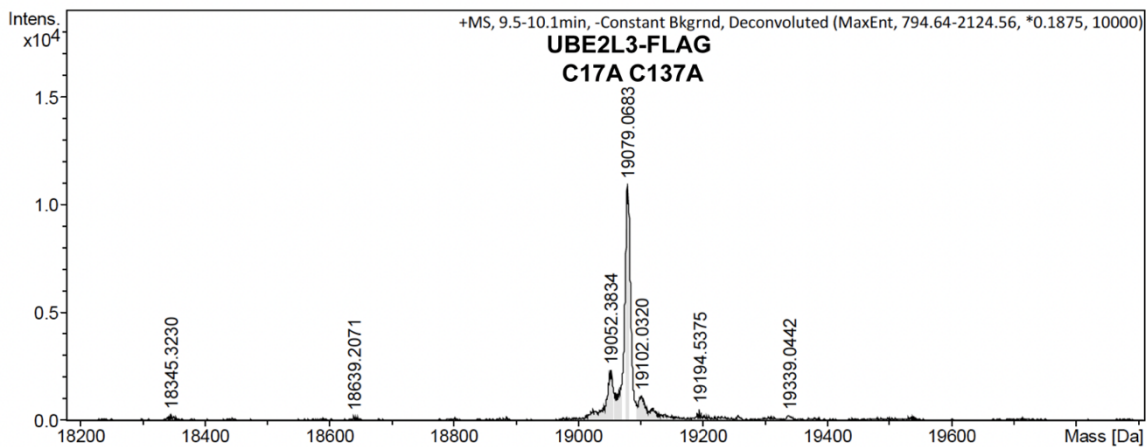
**Supplemental Figure 1- LC-MS analysis of Ubiquitin-MES**



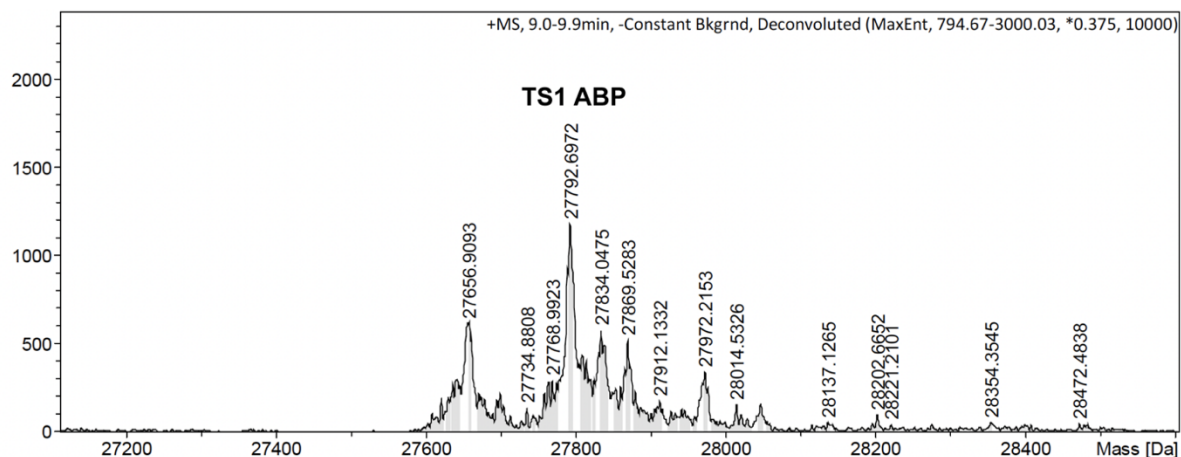
**Supplemental Figure 2- LC-MS analysis of Ubiquitin-BmDPA before deprotection**



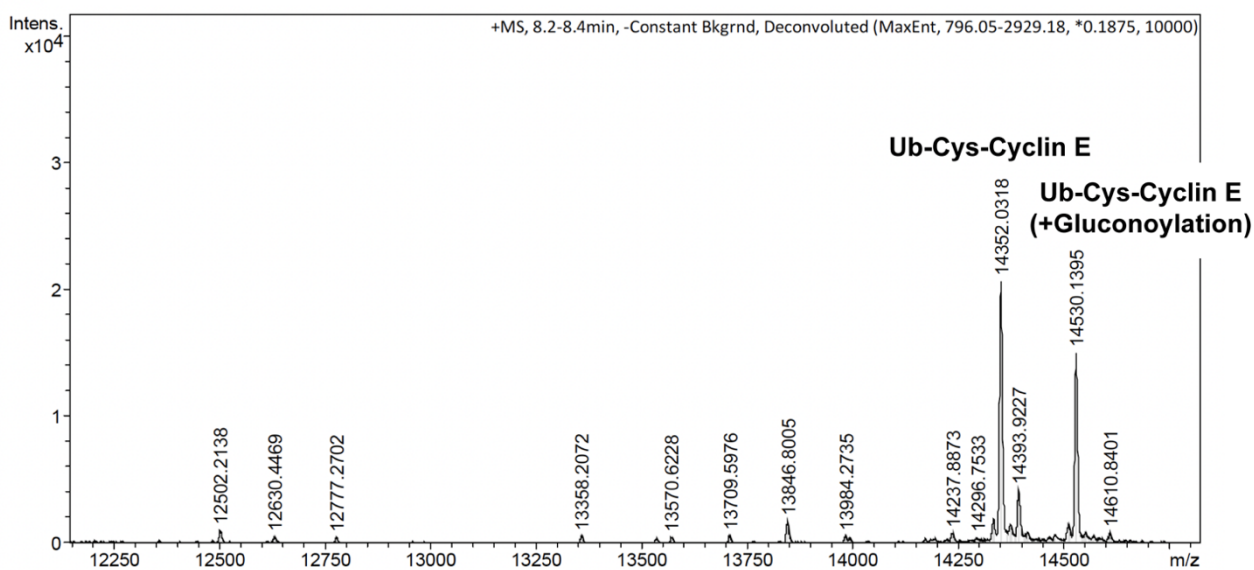
**Supplemental Figure 3- LC-MS analysis of Ubiquitin-BmDPA after deprotection**



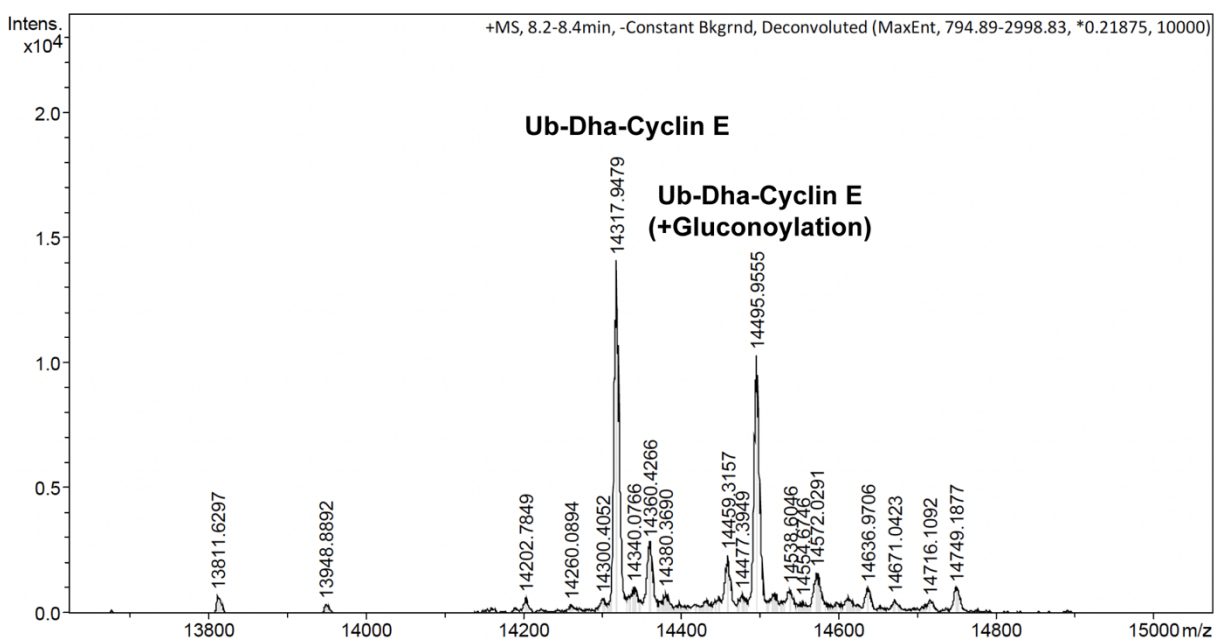
**Supplemental Figure 4- LC-MS analysis of FLAG-tagged, single-cysteine UBE2L3**



**Supplemental Figure 5- LC-MS analysis of Transition State 1 ABP (UBE2L3~Ub)**



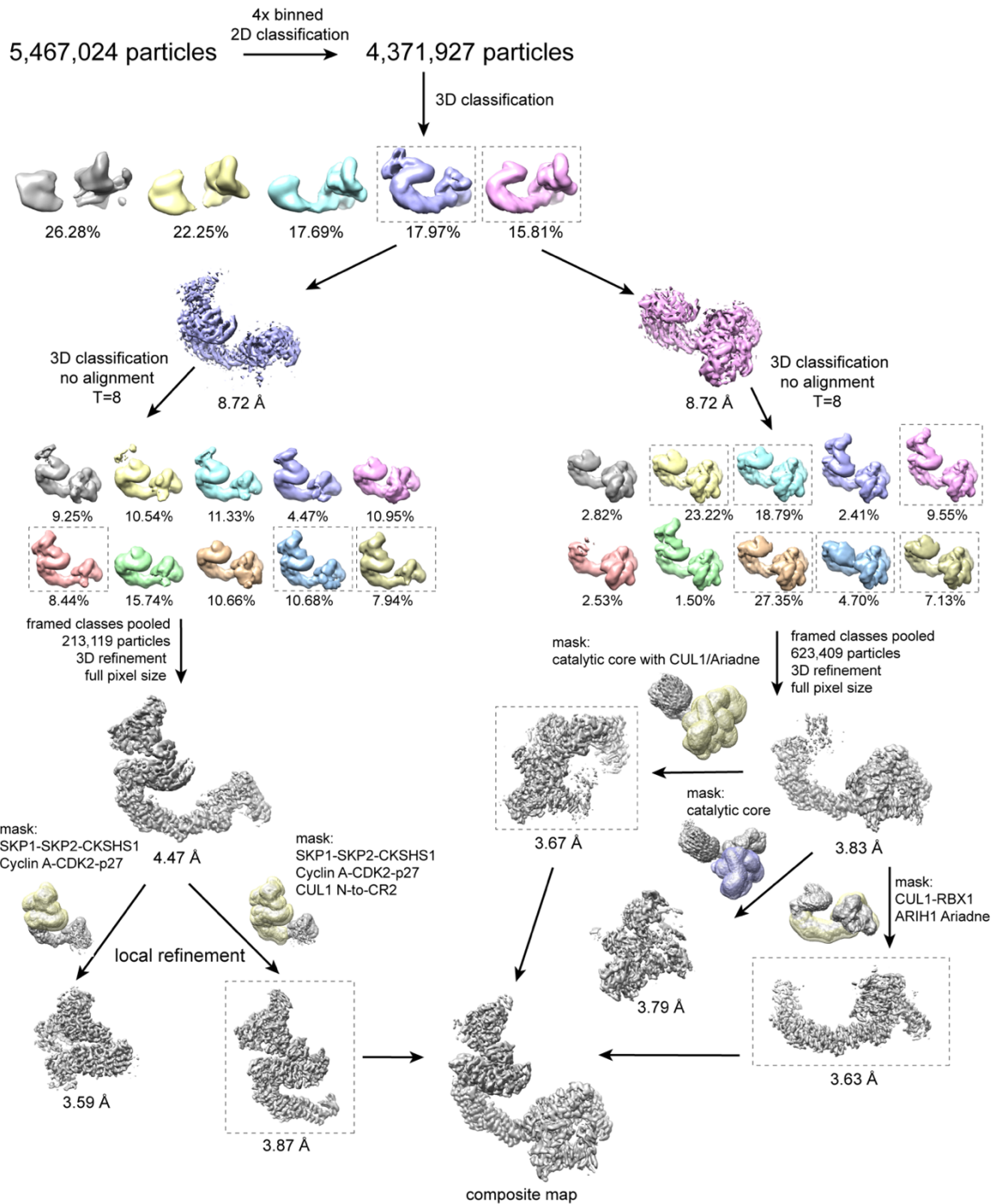
**Supplemental Figure 6- LC-MS analysis of Ubiquitin-Cys-Cyclin E phosphodegrom**



**Supplemental Figure 7- LC-MS analysis of Transition State 2 Cyclin E ABP**

### Transition State 1:

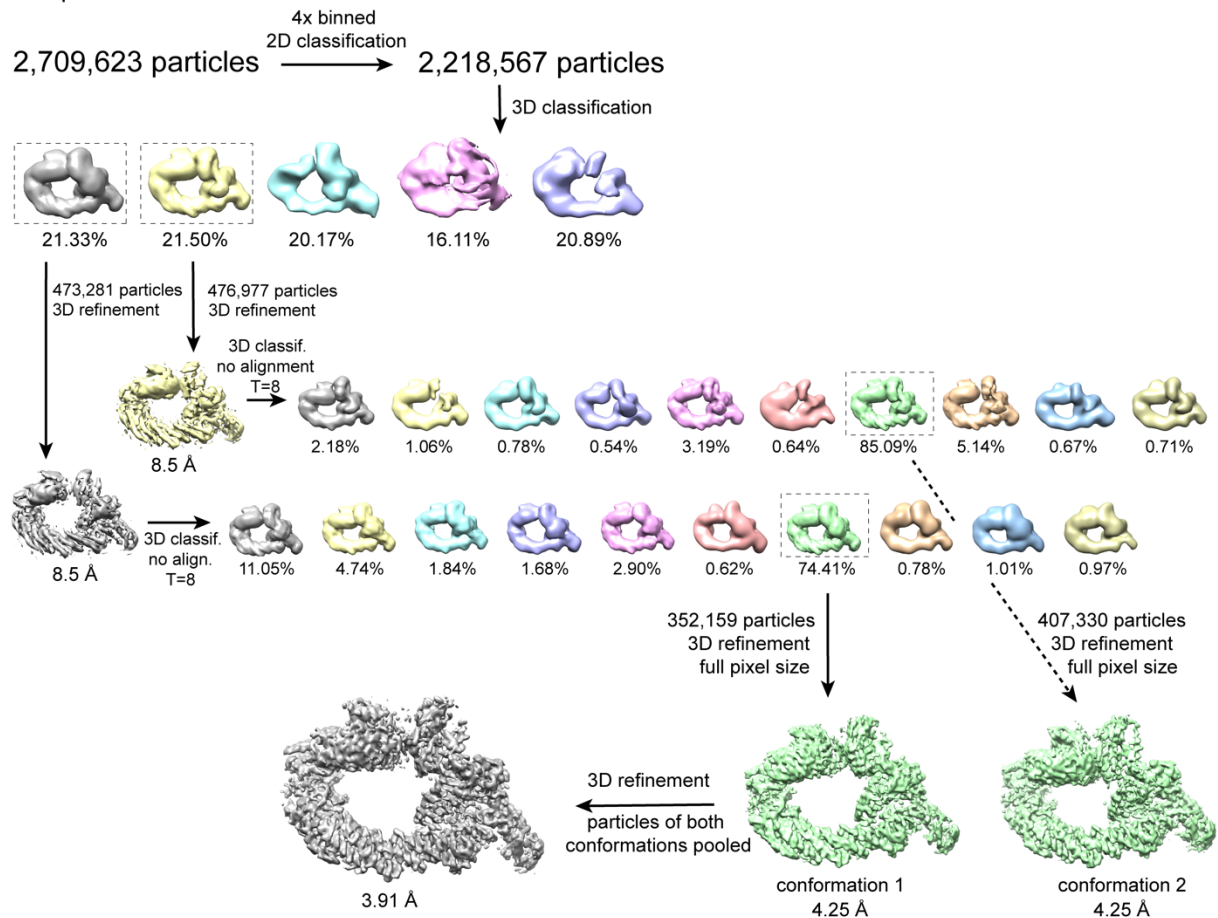
TS1 ABP - SCF<sup>SKP2</sup>, Cyclin A, CDK2



**Supplemental Figure 8- Cryo-EM image processing flowchart of the complex representing Transition State 1, neddylated SCF<sup>SKP2</sup>-dependent ubiquitin transfer from the E2 UBE2L3 to ARIH1.** a, Cryo-EM image processing flowchart for complex representing Transition State 1: UBE2L3~ubiquitin~ARIH1-NEDD8–CUL1-RBX1-SKP1-SKP2-CKSHS1-p27-Cyclin A-CDK2. Two distinct classes, one displaying prominent density for the substrate binding region and one for the E3-E3 catalytic core, were identified during 3D classification. Further classifications without image alignment yielded a more homogenous set of particles after similar classes had been pooled. Overall maps were refined to 4.47 Å and 3.83 Å, respectively. Refinements with local angular searches and masks covering defined. Figure adapted from [2].

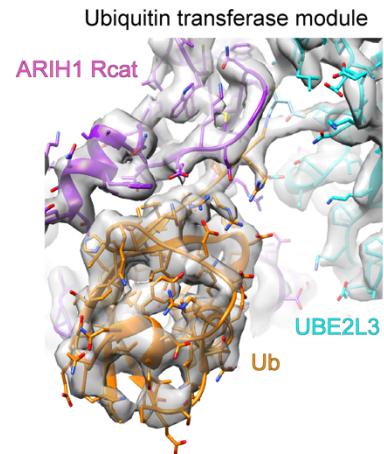
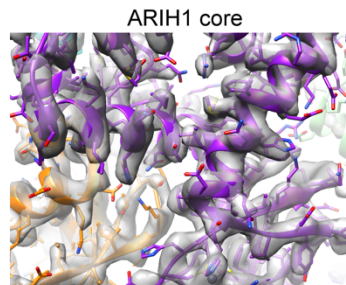
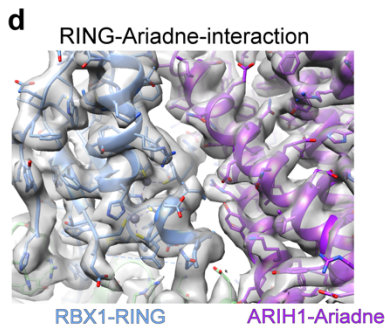
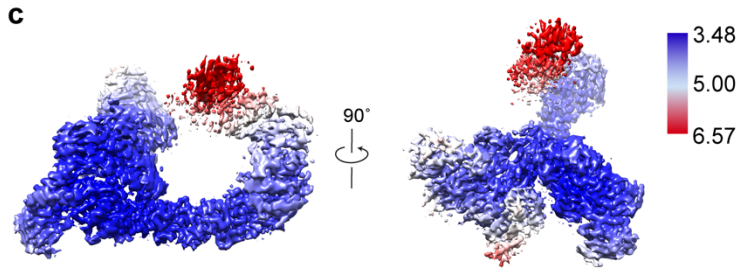
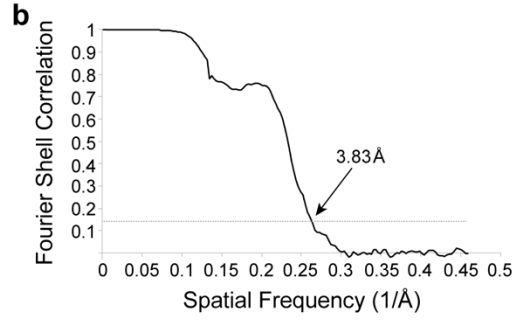
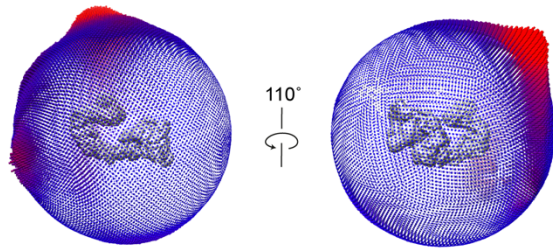
## Transition state 2:

TS2 p27 ABP SCF<sup>SKP2</sup>

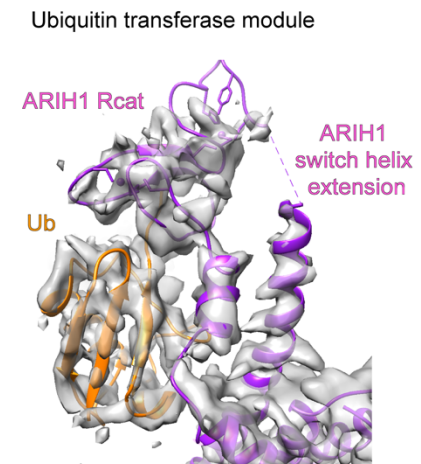
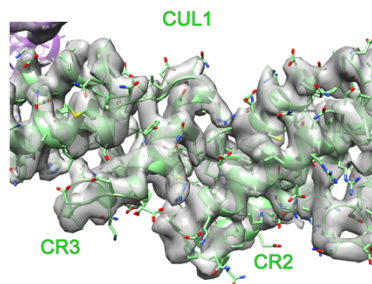
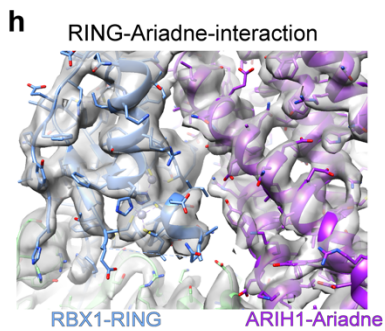
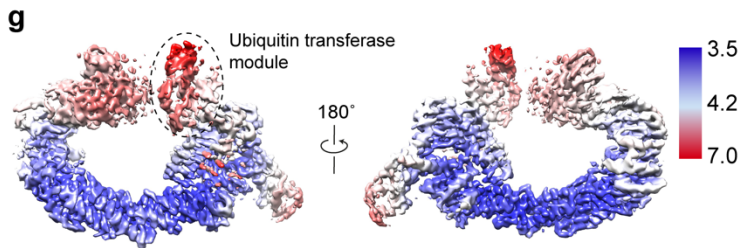
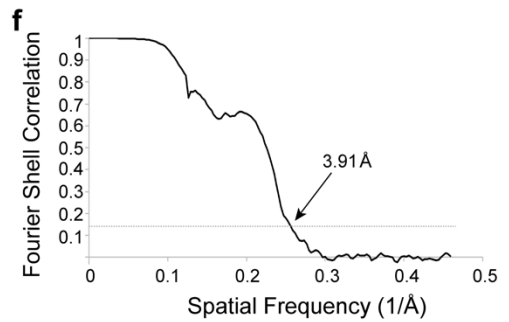
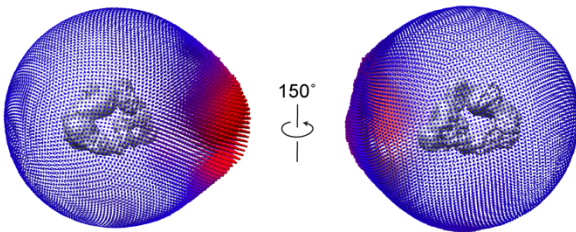


**Supplemental Figure 9- Cryo-EM image processing flowchart of the complex representing Transition State 2, SCF<sup>SKP2</sup>-dependent ubiquitin transfer from ARIH1 to the substrate phospho-p27.** Cryo-EM image processing flowchart. 3D classification yielded two major classes. These classes differed in their orientation of the Fbox-protein SKP2. This orientational flexibility of the Fbox protein was also seen for complexes with other substrate receptors such as FBXW7 and  $\beta$ -TRCP. Further classifications were carried out to obtain homogenous particle sets. Both conformations were refined to an overall resolution of 4.25 Å. Pooling and collectively refining the particles of both conformations resulted in an overall increased map resolution of 3.91 Å and improved map quality of the E3-E3act domain and CUL1 scaffold. Figure adapted from [2]

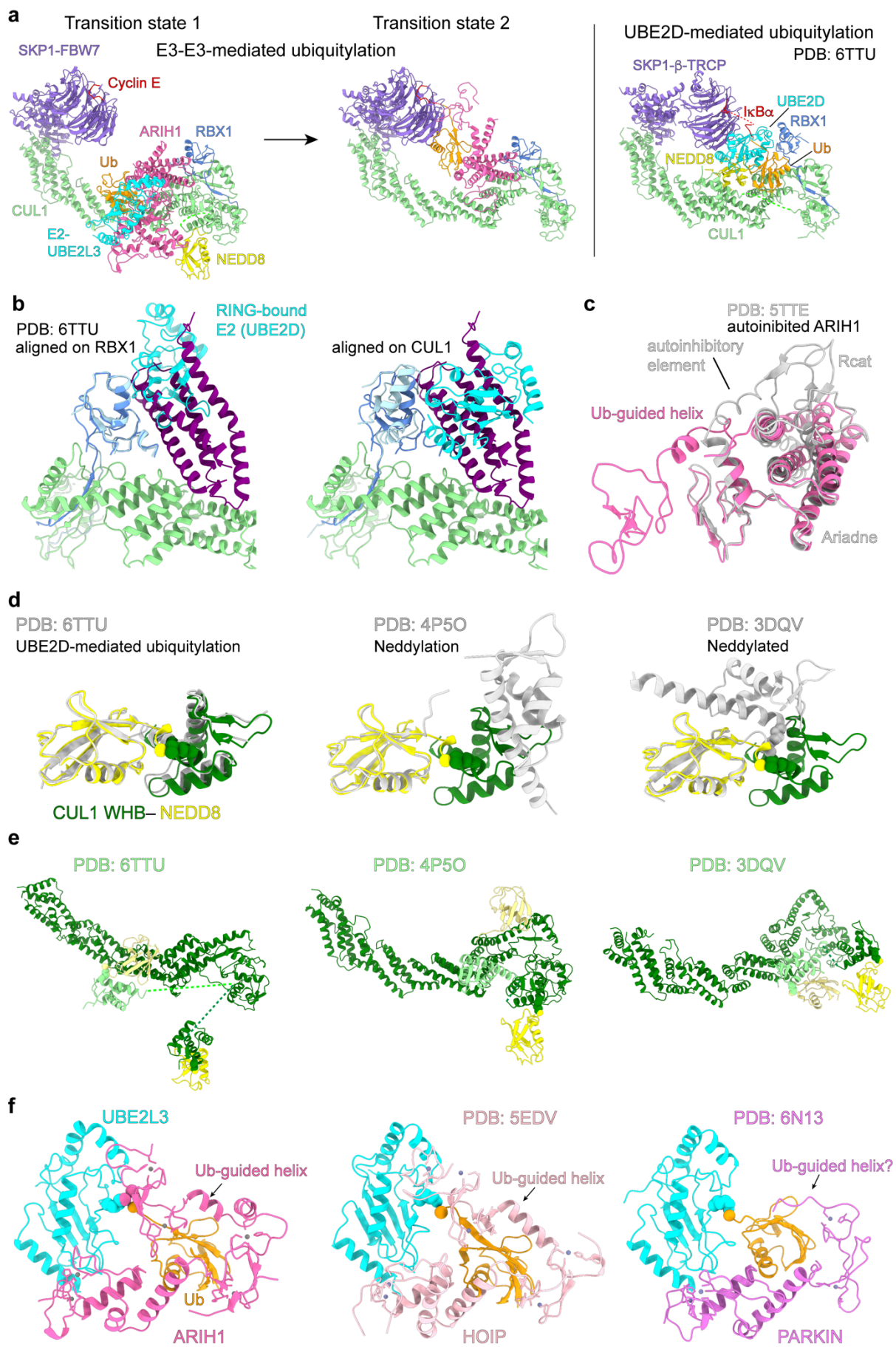
**a Transition state 1: E2 > ARIH1 E3-neddylated SCF<sup>SKP2</sup> E3**



**e Transition state 2: ARIH1 E3 > SCF<sup>SKP2</sup> E3-bound p27 substrate**

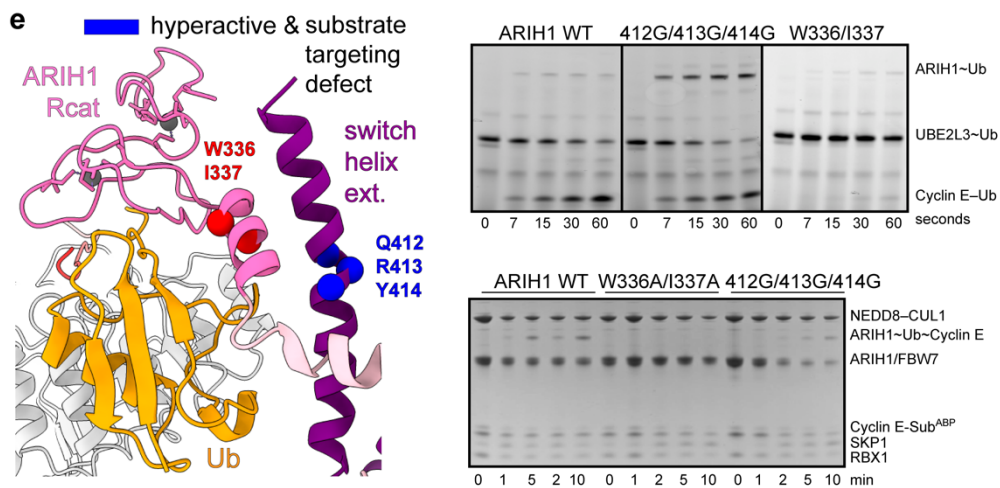
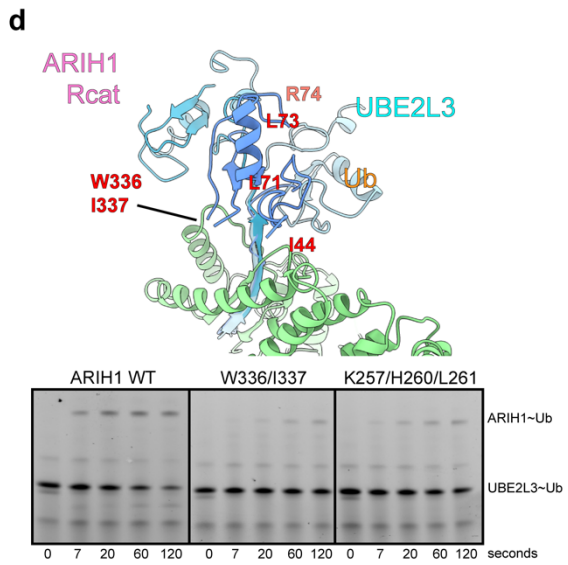
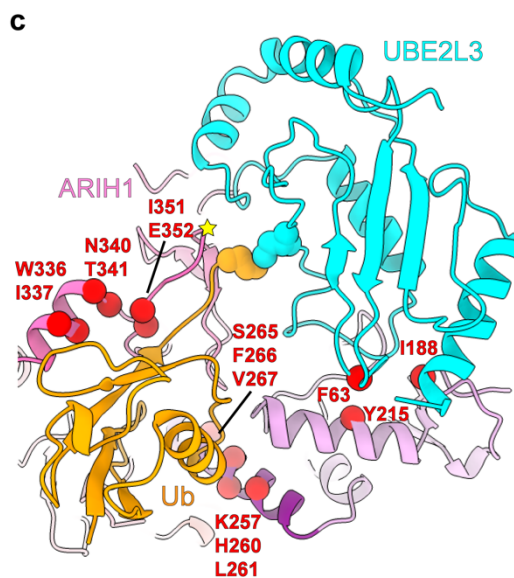
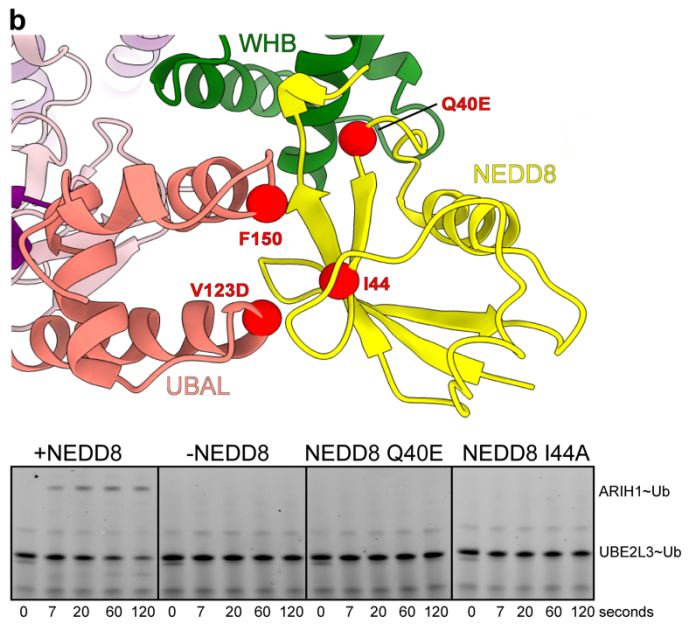
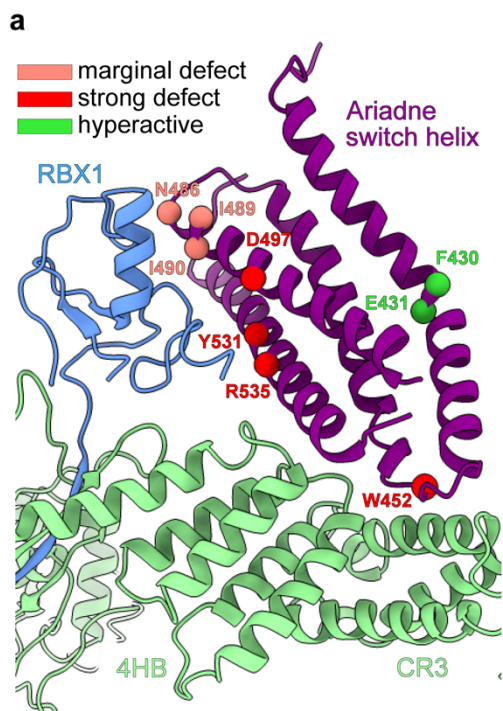


**Supplementary Figure 10- Cryo-EM map quality analysis.** **a**, Angular orientation assignments of final reconstructions for complex representing transition state 1, generated using our TS1 ABP: UBE2L3~ubiquitin~ARIH1-NEDD8-CUL1-RBX1-SKP1-SKP2-CKSHS1-p27-Cyclin A-CDK2. **b**, Fourier shell correlation curve (FSC) displaying an overall resolution of 3.83 Å with the FSC= 0.143 criterion. **c**, Cryo-EM map coloured by local resolution in Å as estimated by ResMap. **d**, Model shown in EM density. Left - RBX1's RING domain and ARIH1's Ariadne domain interaction with visible side chain density. Middle - ARIH1 RBR catalytic region/ubiquitin binding site. Right -ubiquitin transferase module. **e**, Angular orientation assignments of final reconstructions for complex representing transition state 2, generated using our TS2 p27 ABP: ARIH1\*~ubiquitin~p27-CUL1-RBX1-SKP1-SKP2-CKSHS1. **f**, Fourier shell correlation curve (FSC) displaying an overall resolution of 3.91 Å with the FSC= 0.143 criterion. **g**, Cryo-EM map coloured by local resolution in Å as estimated by ResMap. **h**, Model shown in EM density, representing highest, medium, and lowest resolution areas of the map. Left - RBX1's RING domain and ARIH1's Ariadne domain interaction with visible side chain density. Middle – CUL1 scaffold. Right – ubiquitin transferase module. After the ubiquitin transferase module was modeled and refined for the structure representing transition state 1, it was wholesale docked into the lower resolution density for this region in the cryo EM maps representing transition state 2. Figure adapted from [2].

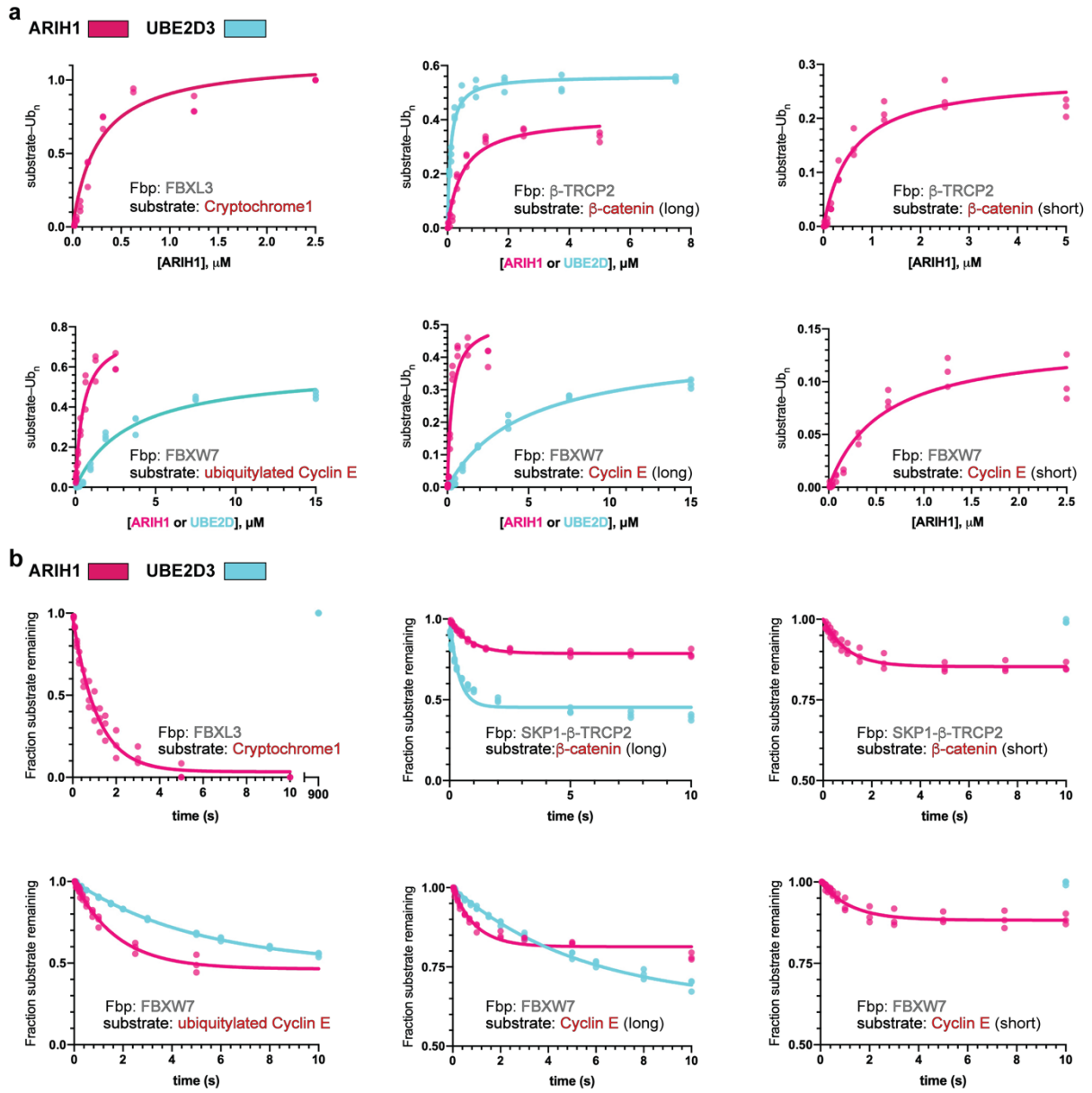


## Supplementary Figure 11- Extraordinary structural rearrangements of CUL1-RBX1 and insights into catalytic RBR conformations

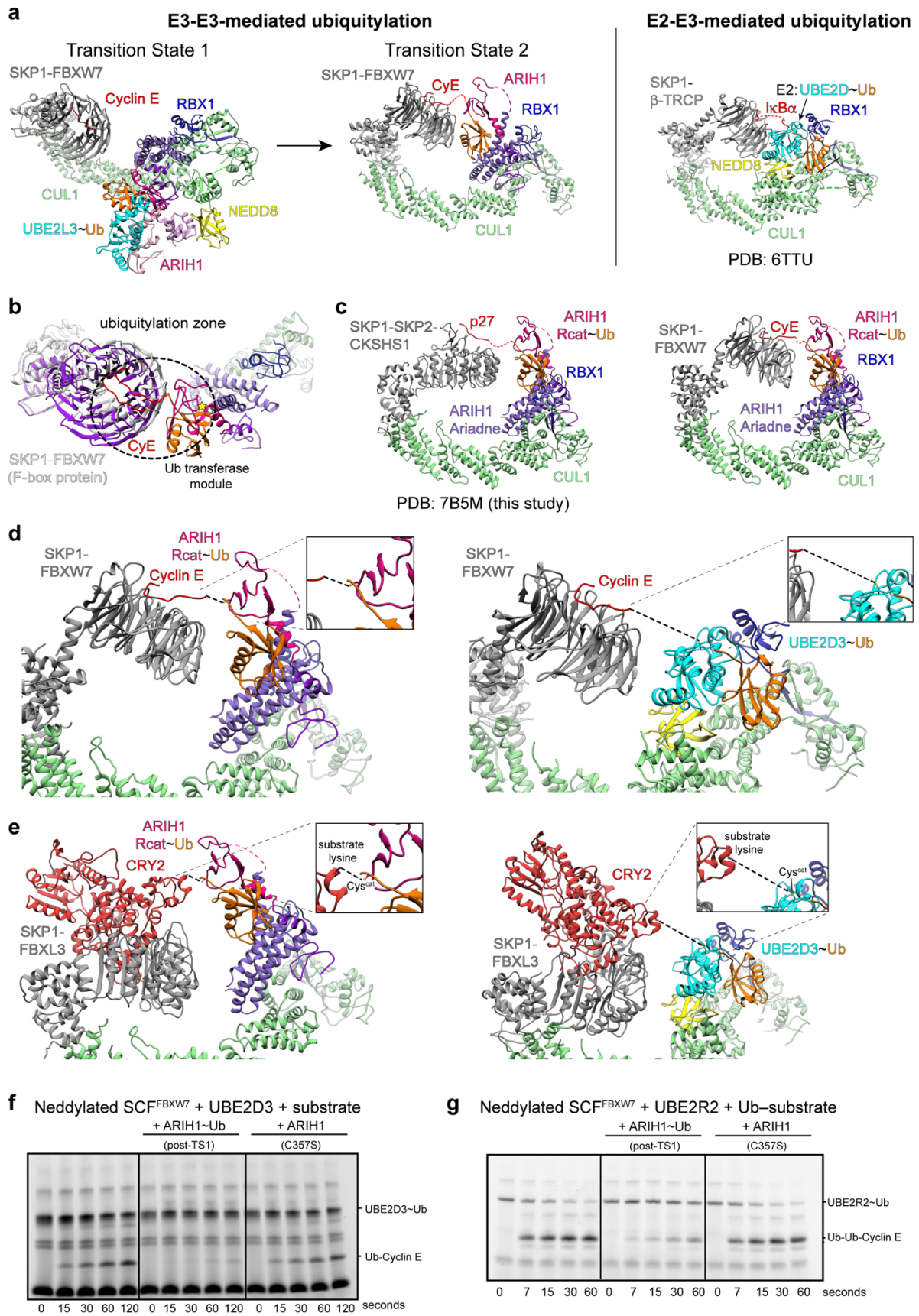
**a**, Side-by-side comparison of E3-E3-catalyzed substrate ubiquitylation, via the two transition states (left), versus conventional E2-E3 mechanism (right). Structures on left represent neddylated SCF<sup>FBXW7</sup>-dependent ubiquitin transfer from UBE2L3 to ARIH1 (transition state 1) and from ARIH1 to Cyclin E substrate (transition state 2) based on EM data shown in Figure 17 and 22. **4a,b** Structure on right shows neddylated SCF<sup>β-TRCP</sup>-dependent ubiquitin transfer from the E2 UBE2D to IκBα[110] (PDB: 6TTU). The structures are aligned over CUL1. In the E3-E3 mechanism, ubiquitin linked to ARIH1's Rcat domain is projected toward the substrate irrespective of F-box protein identity. However, in the E2-E3 mechanism, optimally-positioned UBE2D specifically contacts β-TRCP, explaining the remarkable catalytic efficiency of neddylated SCF<sup>β-TRCP</sup> with the conventional mechanism[110]. **b**, Close-ups showing a common RBX1 RING surface binding to ARIH1 Ariadne domain in the E3-E3act superdomain and binding to the E2 UBE2D[110] (PDB: 6TTU). Structures on left align CUL1-RBX1-ARIH1 and CUL1-RBX1-UBE2D over RBX1, and on right over CUL1. The structures explain results of prior competitive binding experiments[9]. **c**, Close-ups comparing relative orientations of ARIH1 Ariadne domain, Ub-guided helix and Rcat domain for transition state 1 (pink) and in the autoinhibited conformation[104-106] (PDB:5TTE, grey). In addition to reorientation of the Rcat domain, the Ub-guided helix formed in transition states 1 and 2 is remodeled from an autoinhibitory element in the absence of the E3-E3 superassembly. **d**, Close-ups comparing relative orientations of NEDD8 and the isopeptide-linked WHB domain of CUL1 in transition state 1 (yellow-green) with the "activation module" activating conventional UBE2D-dependent ubiquitylation of an SCF<sup>β-TRCP</sup> substrate[110] (PDB:6TTU, grey, left), or during neddylation[155] (PDB:4P5O, grey, middle), or captured by crystal packing in a structure of neddylated CUL5-RBX1 that revealed orientational flexibility of neddylated CUL WHB and RBX RING domains[156] (PDB:3DQV, grey, right). NEDD8 is superimposed across the different structures. **e**, Relative to CUL1 scaffold, NEDD8 (yellow)-linked CUL WHB domain (dark green) position in transition state 1 compared to positions of these domains from structures shown in **d**. After superimposing the CUL-RBX C/R domains, positions of NEDD8 are shown in light yellow and of its linked CUL1 WHB domain in light green from structure representing UBE2D-dependent ubiquitylation of an SCF<sup>β-TRCP</sup> substrate (PDB:6TTU, left), or during neddylation (PDB:4P5O, middle), or captured by crystal packing in a structure of neddylated CUL5-RBX1 that revealed orientational flexibility of neddylated CUL WHB and RBX RING domains (PDB:3DQV, right). Dotted lines show regions of structures connected but not modeled due to lack of density. **f**, In context of transient E3-E3 assembly, neddylated SCF-activated UBE2L3~ubiquitin~ARIH1 transition state 1 adopts the canonical activated RBR configuration. Shown side-by-side are corresponding regions of structures with RBR E3s HOIP[141] (PDB: 5EDV, middle), and Parkin[157] (PDB:6N13, right). Note that the structure of HOIP is represented as a monomer, although it is a domain-swapped dimer in the crystal. A HOIP Ub-guided helix was previously noted to promote ubiquitin transfer from an E2 to this RBR E3[141]. This concept could possibly apply in Parkin as well. Figure adapted from [2].



**Supplementary Figure 12- Structural basis for mutational effects on neddylation of SCF-ARIH1-catalyzed ubiquitylation.** **a**, Close-up of E3-E3act domain with spheres showing locations of strongly defective (red), marginally defective (salmon), and hyperactive (green) mutations identified by prior ARIH1 Ala scanning mutagenesis[9,104]. Defective mutants map to key CUL1- and RBX1-binding residues, while hyperactive mutants map to the site of activating bend-to-kink within the switch helix. **b**, Close-up of NEDD8–CUL1-ARIH1 interactions in transition state 1, showing locations of strongly defective mutants as red spheres. Mutants in ARIH1 UBAL domain (V123D, or F150A) at interface with NEDD8 were described previously[9]. Shown below is a representative SDS-PAGE gel of experiments testing effects of mutating NEDD8 side at the interface with ARIH1 or with CUL1 in the context of neddylation of CUL1-RBX1-activated ubiquitin transfer from UBE2L3 to ARIH1. **c** and **d**, Close-ups of catalytic elements for transition state 1 (ubiquitin transfer from E2 UBE2L3 to ARIH1 Cys<sup>cat</sup>, yellow star). Red spheres show sites of strongly defective mutants identified previously[9], or tested based on the structure representing transition state 1. SDS-PAGE gel shows neddylation of CUL1-RBX1-activated ubiquitin transfer from UBE2L3 to ARIH1, testing effects of ARIH1 mutants in binding sites for the UBE2L3-linked ubiquitin (K257/H260/L261 in the RTI-helix and W336/I337 in the Ub-guided helix leading to the Rcat domain). Due to their drastic remodeling for transition state 1, these regions were not examined in the prior ARIH1 Ala scanning mutagenesis study[9]. **e**, Close-up of catalytic elements for transition state 2, ubiquitin transfer from ARIH1 to SCF-bound substrate. Spheres indicate sites of mutation defective in achieving substrate targeting configuration, assayed by reaction with TS2 ABP shown on right. Sites of blue mutations map to region in switch helix extension contributing to ARIH1 autoinhibition and substrate targeting, and accordingly lead to accumulation of ARIH1~ubiquitin in assays monitoring fluorescent ubiquitin transfer from UBE2L3 to ARIH1 to a neddylation of SCF substrate (top right). Figure adapted from [2].



**Supplementary Figure 13- Quantitative kinetics show ARIH1 ubiquitylates chemically and spatially diverse SCF-bound substrates whereas UBE2D3 activity is far more specialized.** **a**, Plot of the velocities of substrate ubiquitylation as a function of ARIH1 or UBE2D3 concentration. Data were fit to the Michaelis-Menten model (GraphPad Prism software) to estimate the  $K_m$  of ubiquitin carrying enzymes for the SCF-substrate complex. Notice that SCF complexes containing either  $\beta$ -TRCP2 or FBXW7 substrate receptors and b-catenin (long) or Cyclin E (long) peptide substrates can accommodate either ubiquitin carrying enzyme since the Lys acceptor position is sufficient to reach the active sites. Similarly, both ARIH1 and UBE2D3 can poly-ubiquitylate a substrate that contains a single ubiquitin (bottom left panel). However, only ARIH1 can ubiquitylate substrates when the distance between the Lys acceptor and the substrate receptor binding site is shortened or where the position of Lys acceptor is rigid such as in Cryptochrome 1 (CRY1). **b**, pre-steady state kinetics of substrate ubiquitylation are consistent with specialized UBE2D3 activity with  $\beta$ -TRCP2 substrate receptor and  $\beta$ -Catenin (long) peptide and the far more generalized function of ARIH1. Notice that the UBE2D3-catalyzed conversion of b-Catenin (long) substrate to ubiquitylated product is more rapid in comparison with ARIH1 and results in the greater substrate turnover (top middle panel). However, the rate of ARIH1 ubiquitin transfer to Cyclin E (long) is more rapid than UBE2D3, and ARIH1 also displays rapid kinetics with CRY1 as well as b-catenin and Cyclin E (short) substrates, whereas UBE2D3 activity is absent over the length of the time-course for these substrates. In all cases, triplicate data points from independent experiments performed with identical samples are shown. Figure adapted from [2].



**Supplementary Data Figure 14- Comparison of E3-E3 or conventional UBE2D (E3-E2) ubiquitylation mechanisms.**

**a**, Side-by-side comparison of E3-E3-catalyzed substrate ubiquitylation, via the two transition states (left), versus conventional E3-E2 mechanism (right). Structures on left represent neddylated SCF<sup>FBXW7</sup>-dependent ubiquitin transfer from UBE2L3 to ARIH1 (Transition State 1) and from ARIH1 to Cyclin E substrate (Transition State 2). Structure on right shows neddylated SCF<sup>β-TRCP</sup>-dependent ubiquitin transfer from the E2 UBE2D to IκBα[110] (PDB: 6TTU). The structures are aligned over CUL1. In the E3-E3 mechanism, ubiquitin linked to ARIH1's Rcat domain is projected toward the substrate irrespective of F-box protein identity. However, in the E3-E2 mechanism, optimally-positioned UBE2D specifically contacts β-TRCP, explaining the remarkable catalytic efficiency of neddylated SCF<sup>β-TRCP</sup> with the conventional mechanism[110]. **b**, ARIH1~ubiquitin active site faces F-box protein-bound substrate within a confined zone. Structures from two different EM classes are shown (Figure 24b). After superimposing CUL1-RBX1-ARIH1~ubiquitin from both classes, the substrate (red)-bound F-box protein in one is shown in purple (conformation 1) and the other in grey (conformation 2). **c**, E3-E3 catalytic configuration is generalizable for substrates recruited to structurally diverse Fbps: p27 recruited to SKP1-SKP2-CKSHS1 (left) and Cyclin E recruited to SKP1-FBXW7 (right). **d**, Structural modeling and comparison of E3-E3 versus E3-E2-mediated ubiquitylation with Cyclin E as a substrate. The structure on the left corresponds to SKP1-FBXW7-Cyclin E (PDB: 2OVQ), fitted into map corresponding to conformation 1, with neddylated CUL1-RBX1-activated ARIH1~ubiquitin~cyclin E substrate from the refined structure representing TS2 for SCF<sup>SKP2</sup>. Proximity of the ubiquitin transferase domain to the substrate phosphodegron explains how ARIH1 efficiently ubiquitylates a “short Cyclin E” substrate, with only four residues between the phosphodegron and acceptor lysine. On the right is a model E3-E2-mediated ubiquitylation of Cyclin E by SCF<sup>FBXW7</sup>. The model was generated by aligning the SKP1-F-box portion of SKP1-FBXW7-Cyclin E (PDB: 2OVQ) in place of the corresponding region showing UBE2D-mediated ubiquitylation of a substrate of neddylated SCF<sup>β-TRCP</sup> (PDB: 6TTU), which shows the distance separating UBE2D's Cys<sup>cat</sup> and the Cyclin E substrate acceptor. This rationalizes the inefficient ubiquitylation of the short Cyclin E peptide substrate by the conventional E3-E2 mechanism. **e**, As in **d**, but modeled with SKP1-FBXL3-CRY2[72] (PDB: 4I6J) based on the F-boxes. **f**, Competition assay testing whether a neddylated SCF can mediate conventional UBE2D-catalyzed ubiquitylation if occupied by ARIH1. SDS-PAGE gels monitor neddylated SCF<sup>FBXW7</sup>-dependent transfer of fluorescent ubiquitin from UBE2D3 to Cyclin E peptide substrate. Ubiquitylation is severely hindered upon addition of the stable proxy for the E3-E3 post-TS1 intermediate (ARIH1~ubiquitin, generated by ARIH1 reaction with UbVME) to the reaction, but not when ARIH1 is added on its own (right). The results are rationalized by the same portions of RBX1 and NEDD8 binding ARIH1 and UBE2D. Here, a catalytically inactive version of ARIH1 was added to prevent any potential spurious activity of ARIH1. **g**, SDS-PAGE gels monitor neddylated SCF<sup>FBXW7</sup>-dependent transfer of fluorescent ubiquitin from UBE2R2 to ubiquitin-linked Cyclin E substrate, testing competition upon adding the stable proxy for the E3-E3 post-TS1 intermediate (ARIH1~ubiquitin) to the reaction, or ARIH1 on its own (right). Figure adapted from [2].

**Supplementary Data Table 1 – Cryo-EM data collection, refinement and validation- Table adapted from [2].**

	Pre-TS1	TS1	TS1	post-TS1	TS2	TS2	TS2	
Intermediate ABP	none	TS1 ABP	TS1 ABP	Ub-VME	TS2 CyE ABP	TS2 CyE ABP	TS2 p27 ABP	
Substrate Receptor	FBXW7 <sup>263-C</sup>	SKP2	FBXW7 <sup>263-C</sup>	FBXW7 <sup>263-C</sup>	FBXW7 <sup>263-C</sup>	FBXW7 <sup>263-C</sup>	SKP2	
ARIH1	WT	WT	WT	WT	90-C WT	90-C*	90-C*	
NEDD8	yes	yes	yes	yes	no	yes	no	
additional	isopeptide-linked UBE2L3~ Ub Cyclin E peptide	Cyclin A <sup>170-C</sup> , CDK2 CKSHS1 <sup>5-73</sup> , p27 <sup>22-106</sup> p27 phosphopeptide EMD-12037 (composite) EMD-12038 (consensus) EMD-12048 (focused1 CyA/CDK) EMD-12041 (focused2 catalytic) EMD-12050 (focused3 Cullin)	Cyclin E phosphopep.	Cyclin E phosphopep.				CKSHS1 <sup>5-73</sup>
	EMD-12004		EMD-12036	EMD-12005	EMD-12006	EMD-12039	EMD-12040	
<b>Data collection and processing</b>								
Microscope	Krios	Krios	Arctica	Glacios	Krios	Krios	Krios	
Magnification	105,000	105,000	73,000	22,000	130,000	130,000	105,000	
Voltage (kV)	300	300	200	200	300	300	200	
Electron exposure(e <sup>-</sup> /Å <sup>2</sup> )	70	70	60	70	69	69	79	
Defocus range (µm)	-0.8 ~ -3.3	-0.8 ~ -3.3	-1.5 ~ -3.5	-0.8 ~ -3.3	-1.2 ~ -3.3	-1.2 ~ -3.3	-1.2 ~ -3.3	
Pixel size (Å)	0.851	1.09	1.997	1.181	0.851	0.851	1.09	
Symmetry	C1	C1	C1	C1	C1	C1	C1	
Initial particle images (no.)	2,651,495	5,467,024	651,656	723,348	2,525,317	2,568,237	2,709,623	
Final particle images (no.)	122,649	623,409	130,116		462,256	151,246	759,489	
Map resolution (Å)	4.5	3.8	9.6		3.6	4.4	3.9	
FSC threshold	(0.143)	(0.143)	(0.143)		(0.143)	(0.143)	(0.143)	
<b>Refinement</b>								
PDB code:		composite 7B5L	focused1 7B5R	focused2 7B5N	focused3 7B5S		7B5M	
Initial model used (PDB code)		1LDJ 5UDH 2AST 6TTU 1H27	1H27 1LDJ	5UDH 1LDJ 6TTU	1LDJ5 UDH		1LDJ 5UDH	
Model resolution (Å)		3.6	3.6	3.8	3.6		4.0	
FSC threshold		(0.143)	(0.143)	(0.143)	(0.143)		(0.143)	
<b>Model composition</b>								
Non-hydr. Atoms		21532	11606	9965	7671		12859	
Protein residues		2654	1430	1229	931		1594	
Ligands		9 ZN		9 ZN,1 SDF	5 ZN		5 ZN	
<b>B factors (Å<sup>2</sup>)</b>								
Protein		134.15	136.68	63.66	68.70		98.29	
Ligand		158.66		99.15	122.41		201.47	
<b>R.m.s. deviations</b>								
Bond lengths (Å)		0.006	0.010	0.007	0.006		0.012	
Bond angles (°)		0.752	1.002	0.794	0.772		1.132	
<b>Validation</b>								
MolProbity score		2.23	2.50	2.16	2.01		2.80	
Clashscore		15.19	22.55	13.26	9.73		33.10	
Poor rotamers (%)								
<b>Ramachandran plot</b>								
Favored (%)		90.26	85.56	90.65	91.58		78.55	
Allowed (%)		9.74	14.30	9.35	8.42		21.19	
Disallowed (%)		0.00	0.14	0.00	0.00		0.26	

**Supplementary Data Table 2** – Estimates of  $K_m$  and  $k_{obs}$  for substrate ubiquitylation. Table adapted from [2].

Substrate	E3 or E2	SCF	$K_m$ ( $10^{-9}$ M)	$k_{obs}$ ( $sec^{-1}$ )	$\frac{k_{obs}}{K_m}$ ( $M^{-1}sec^{-1}$ )
Cyclin E	ARIH1	FBXW7	288 ± 68	0.25 ± 0.026	8.7x10 <sup>5</sup>
Cyclin E	UBE2D3	FBXW7	4789 ± 529	0.08 ± 0.002	1.7x10 <sup>4</sup>
ubiquitylated Cyclin E	ARIH1	FBXW7	489 ± 82	0.39 ± 0.008	8.0x10 <sup>5</sup>
ubiquitylated Cyclin E	UBE2D3	FBXW7	3416 ± 545	0.13 ± 0.002	3.8x10 <sup>4</sup>
Cyclin E short	ARIH1	FBXW7	568 ± 137	0.12 ± 0.009	2.1x10 <sup>5</sup>
Cyclin E short	UBE2D3	FBXW7	NA	NA	NA
β-catenin	ARIH1	β-TRCP2	499 ± 88	0.41 ± 0.012	8.2x10 <sup>5</sup>
β-catenin	UBE2D3	β-TRCP2	100 ± 9	2.2 ± 0.29	2.2x10 <sup>7</sup>
β-catenin short	ARIH1	β-TRCP2	590 ± 103	0.24 ± 0.007	4.1x10 <sup>5</sup>
β-catenin short	UBE2D3	β-TRCP2	NA	NA	NA
CRY1	ARIH1	FBXL3	265 ± 60	0.90 ± 0.069	3.4x10 <sup>6</sup>
CRY1	UBE2D3	FBXL3	NA	NA	NA